UNIVERSITÀ
DEGLI STUDI
FIRENZE

PhD in
Atomic and Molecular Photonics

CYCLE XXXIII

COORDINATOR Prof. Francesco S. Cataliotti

Brain-wide activation mapping at cellular resolution during learning and retrieval of aversive memory

Academic Discipline (SSD) FIS/03

Doctoral Candidate
Alessandra Franceschini

(signature)

Supervisor
Dr. Ludovico Silvestri

(signature)

Coordinator
Prof. Francesco Saverio Cataliotti

(signature)

Years 2017/2020

Ai momenti che mi hanno permesso di crescere.
A chi per me ha trovato tempo e parole.
A chi non smette di trovarne.

Contents

Summary

The neuronal and molecular mechanisms underlying behavioral responses triggered by fear have received wide interest in the last few years, and various preclinical studies have addressed potential treatments for fear-related disorders. The central histaminergic system is an important modulator of memory related to adverse events and the integrity of the brain histamine system is necessary for the consolidation of this type of memory. Therefore, the use of antihistaminic drugs could be useful for the treatments of conditions such as obsessive-compulsive disorders, post-traumatic stress disorders and generalized anxiety.

In this context, it is essential to understand the neuronal circuits involved in behavioral responses associated with adverse events. During my PhD, I developed a pipeline for mapping neuronal activation at micron resolution, combining transgenic approach, clearing protocol, high-resolution imaging, atlas registration, and automated 3D image analysis. The combination of high-resolution imaging and 3D analysis for processing sub-cellular information became the key point of this pipeline, enabling high performance.

This pipeline was validated using a classical paradigm, as step-through passive inhibitory avoidance, to analyze neuronal activation patterns across the entire brain of male and female mice, at selected time points. This approach highlighted a strong sexual dimorphism, during fear learning and recall, which was not evident from the behavioral task. Further, it identified brain regions whose degree of activity correlated to specific behavioral features. Finally, micron-scale 3D resolution was exploited to investigate histaminergic subpopulations elicited by aversive events.

The combination of behavioral, transgenic, optical and computational methods presented here represents an important tool to quantitatively characterize the neuronal pathways involved in fear memories.

Part I

Introduction

Chapter 1
Motivation: the challenge of memory engram

Quid dicam de thesauro rerum omnium, memoria? Quae nisi custos inventis cogitatisque rebus et verbis adhibeatur, intellegimus omnia, etiam si praeclarissima fuerint in oratore, peritura[1].

As early as in the 55 BC, in a passage by Cicero's De Oratore, memory was recognized as the keeper of all thoughts. Indeed, memory preserves our identity, as it determines who we are. Suffice it to say that everything we lived, goes on building a stratification of our character. The role of our memory is to maintain information over time, drawing on past experiences in order to use them in the present. Over the centuries, memory has probably become one of the most studied scientific themes. At the end of 1800, during his classroom lessons William James, an American philosopher, and psychologist, asked his students: "Of some [experiences] no memory survives the instance of their passage. Of others, it is confined to a few moments, hours, or days. Others, again, leave vestiges that are indestructible, and by means of which they may be recalled as long as life endures. How can we explain these differences?" This question continues to guide current memory research (James, 1891). More than one hundred years later, several theories and discoveries about the mnemonic processes

[1] Cicero, De orat. I, 18: "What need to speak of that universal treasure-house the memory? Unless this faculty be placed in charge of the ideas and phrases which have been thought out and well weighed, even though as conceived by the orator they were of the highest excellence, we know that they will all be wasted".

"Che dovrei dire del tesoro di tutte le cose, la memoria? E se non la si accoglie come custode per pensieri e parole, comprendo che tutto, anche se sarà stato eccellente, finirà".

are available, but we are still trying to understand the mechanisms and the involvement of different neuronal circuits in multiple memory phases. Indeed, yet today we are not able to answer the question proposed by Dr. James. Many attempts have been made to understand which neurons are involved in a precise memory phase, trying to localize the physical trace of a memory, or engram in the brain. From Lashley, the first person who tried to find the location of memory, the struggles in localizing the engram have led it to be called elusive (Franz & Lashley, 1917; Josselyn et al., 2015).

The difficulty in finding the engram was due to the technical limitations that prevent the observation of widely distributed neuronal ensembles. The physical location of memory within the brain is likely to be dependent on the respective system mediating the encoding of this memory (Gerrig & Zimbardo, 2005). In this blurred landscape, memory relates not only to molecular changes inside the cells but especially to circuitries and networks involved. For this reason, studies focused on single regions, although definitely interesting, are likely to be limited. Indeed, a certain region may act differently inside the same brain because during memory processes every region collaborates with others in order to produce a response. Thus, a fundamental obstacle to overcome for finding memory engrams is related to the development of new tools and technologies able to capture it.

In my PhD work, I combined novel high-throughput technologies with well-established protocols like behavioral studies, with the aim to investigate an ancient problem as memory (Figure 1.1). In particular, I focused on memory related to strong emotions like fear. The study of fear or aversive memory has always had a huge impact on society since if this strong emotion degenerates into a pathological state, fear could lead to anxiety and stress-related disorders. Indeed, since these pathologies are estimated to have a life-time prevalence of 28% in western populations, fear representation at the brain level has generated a lot of research attention for a long time (“Neurological Disorders: Public Health Challenges,” 2008).

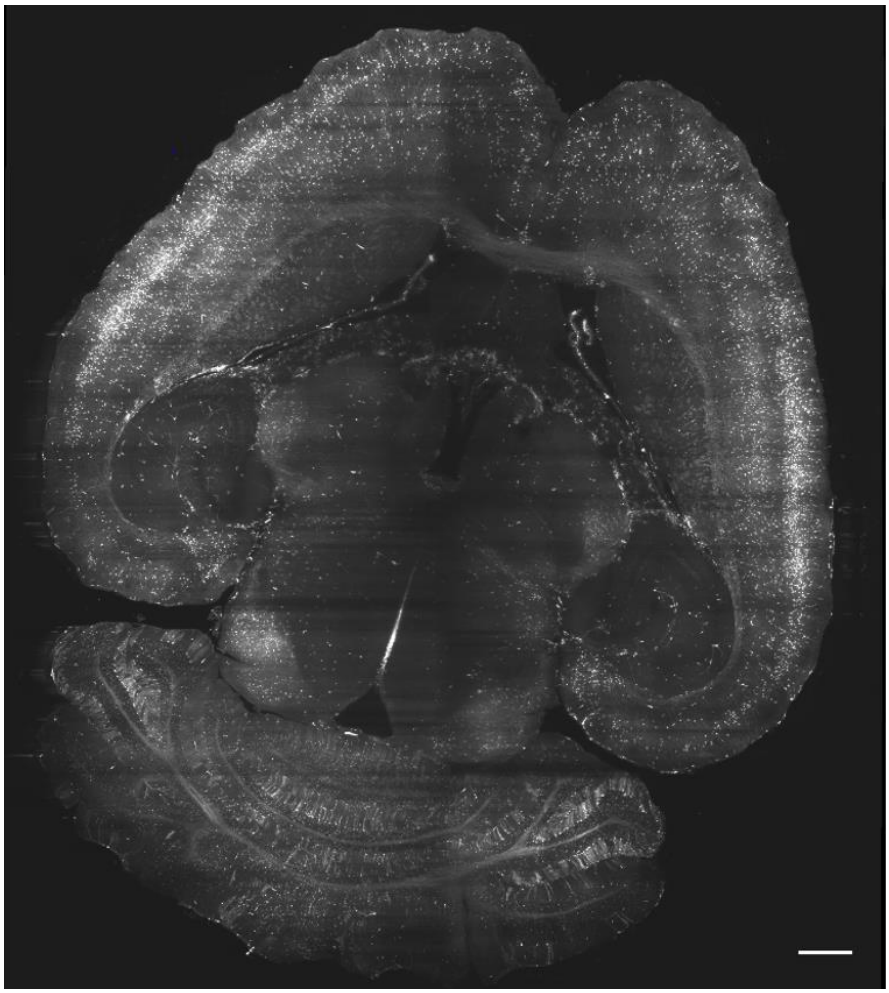

Figure 1.1: **Section of 3D brain reconstruction.** Maximum intensity projection of 80 μm slab from clarified mouse brain imaged with light-sheet microscopy. Every single fluorescent point indicates an activated neuron as a result of behavioral procedures. Scale bar 1 mm.

From a methodological point of view, quantifying neuronal activation patterns during aversive memory phases requires techniques for whole-brain mapping. Indeed, neuronal activation patterns should be studied on the same scale of the structural organization of neuronal networks, i.e., brain-wide. One would ideally need some method to record *electrical activity simultaneously* from *all* the neurons in the brain of a *freely behaving subject*, with *single-cell resolution*. It is immediately apparent that no technique with such capabilities exists, and even if we relax some of the requirements in italics, whole-brain mapping still sounds like a formidable task for state-of-the-art technologies. Traditional functional imaging methods used to reveal large-scale neuronal activity, like functional magnetic resonance imaging (fMRI) or electroencephalography (EEG), lack the proper spatial resolution to record single-cell activity (Logothetis, 2008; Michel and Brunet, 2019). On the other hand, single-cell electrophysiology cannot scale to more than a handful of neurons (Perin and Markram, 2013).

Over the last decade, *in vivo* optical methods have demonstrated the ability to work across different scales (Carrillo-Reid et al., 2017; Yang and Yuste, 2017; Sancataldo et al., 2019), allowing registration of membrane potential or intracellular calcium in hundreds or even thousands of neurons simultaneously (Ahrens et al., 2013; Prevedel et al., 2014; Nöbauer et al., 2017). However, these techniques still suffer several limitations:

1. There is a practical trade-off between spatial resolution and field of view (FOV). For instance, calcium imaging of the entire mouse cortex can be achieved only at coarse resolution (Vanni et al., 2017), while single-cell recordings are limited to a smaller spatial area (Prevedel et al., 2014).
2. Light scattering by nervous tissue limits imaging penetration to less than a mm (Helmchen and Denk, 2005). Thus, in rodents, *in vivo* optical imaging is limited to the cortex (unless endoscopic approaches are used (Dombeck et al., 2010)). Whole-brain imaging has been achieved hitherto only in small organisms like

the nematode *C. Elegans* or the larva of *Danio Rerio* (zebrafish) (Ahrens et al., 2013; Prevedel et al., 2014).

3. Optical microscopes are usually quite sophisticated and heavy, and thus hardly compatible with freely behaving animals. Simpler systems – with poor resolution – can be used on mice moving freely in their cage (Aharoni et al., 2019). However, when single-cell resolution is sought, the only acceptable compromise is to place a head-fixed animal in a virtual reality environment (Dombeck et al., 2010).

To circumvent these constraints, a radical solution is to tag activated neurons *in vivo* and image them subsequently *ex vivo*. Fixed murine brains can be cleared and labeled using many different protocols. Afterward, a comprehensive yet high-resolution reconstruction of these samples can be obtained using the latest developments in *ex vivo* microscopy. Finally, quantitative data can be extracted from raw images using state-of-the-art algorithms. These inherent advantages have been exploited to quantify brain-wide neuronal activation by targeting neurons expressing immediate early genes (IEGs). These genes are expressed by neurons under sustained activation (Bartel et al., 1989) and are considered a reliable proxy for activity. Indeed, IEGs quantification is a classical method to study neuronal activation in selected brain areas (Morgan et al., 1987; Sagar et al., 1988).

Ex vivo whole-brain mapping of IEGs eventually allows mapping *activated neurons* across *the entire brain* of a *freely behaving subject*, with *single-cell resolution*. In the end, this is not too far from the original challenge we issued a few lines before.

In the following chapters, I will discuss the latest technological developments from multiple fields (including genetics, tissue preparation, optical imaging, and image analysis), concurring to map and manipulate activated neurons across the entire mouse brain in order to figure out better what could be a worthwhile approach to visualize fear memory engrams.

Chapter 2

Memory

Since ever, humans have tried to understand what memory is, how it works and why it disappears. From our birth, we remember and learn an enormous series of information that go to build our memory, influencing our future actions. This is obviously an important part of our lives, and yet it is one of the most elusive and poorly understood fields of neuroscience. Many scientists have sought to understand the neurobiological basis of *memory,* but currently, its neuronal and cellular mechanisms are still not explicit.

Memory is defined as the faculty of the brain to encode, store, and retrieve when needed data or information of a learned experience (Iván Izquierdo et al., 1999; Milner, 1998). Although in the past it seemed that engram has to be placed in a particular brain region, today this hypothesis is surpassed. It is a complex process that involves different pathways in the whole brain and multiple systems.

Many researchers have aimed to classify memory in many subtypes. Initially, in 1968 Richard Atkinson and Richard Shiffrin have proposed a classification outlined on time-scale, dividing memory into three separate stages: sensory, short-term (STM), and long-term memory (LTM) (Atkinson, R.C. & Shiffrin, 1968). From 1968 up to now, this classification is still the most persuasive. Generally, sensory memory allows individuals to record initial information that comes in through all senses. The other two types are described on the basis of their duration. STM lasts minutes or few hours, and it could become LTM (defined in days, weeks, or even years) through a process called consolidation that begins immediately after the acquisition phase (Iván Izquierdo et al., 1999; McGaugh, 2000a). Compared with the others, LTM is the most investigated type

of memory and it is currently described as: declarative (or explicit) and procedural (or implicit) memory. The former answers the question “what? where? who? when?” and is based on conscious memory of facts and events, exploiting semantic and episodic recollections. The structures most involved are medial temporal lobe and diencephalic brain structures. The latter answers to “how?” and it refers to unconscious memories such as skills, and it depends mainly on basal ganglia, cerebellum, and neocortex (Gabrieli, 1998). Every type of memory is described by its formation, storage, retrieval and extinction. The initial step of its building is characterized by the acquisition of information related to a particular trace, coming from external stimuli (sensory input from outside) or from internal representations (cognition and emotion). After the first phase, information is processed in different ways, and a part is stored for a short time, whereas the other part for a long one (Iván Izquierdo et al., 1999). Thus, after the acquisition, most inputs are wiped out from our mind and consequently forgotten. Moreover, as time passes, even the most consolidated memories may disappear in a process called forgetting. Ordinarily, long-lasting memories are correlated to powerful emotions, since they play a privileged role in our lives. Indeed, in most cases, we are not able to store memories of what we live, because we filter only events relevant for cognition, emotionally salient, or derived from strong sensory inputs (Cahill & McGaugh, 1998). The reason is for preventing information overload when the brain system tries to learn and store some memories (Iván Izquierdo, Bevilaqua, & Cammarota, 2006).

2.1 Fear memory

An example of memory with a strong emotional component is fear memory. Fear memory is a particular type of memory linked to fear, induced by a real or imaged threat that could disappear once the same threat is finished. There are some cases where this fear-related state of mind can be sustained for a long time, becoming a pathological condition (Ivan Izquierdo et al., 2016). Therefore, the study of neuronal

mechanisms that underlie this emotion, could lead to increasing knowledge about fear circuitry and therefore it could help many treatments of fear-related pathologies, as post-traumatic stress disorders (PTSD), generalized anxiety, obsessive-compulsive disorder (OCD), and phobias (Singewald et al., 2015). An important component of this memory is the association of a neutral stimulus with a dangerous one (Ivan Izquierdo et al., 2016; Silva et al., 2016). In the past century, fear memory was largely investigated, and it became the best-studied form of memory since it has strong survival value. Indeed, its lack could be dangerous and potentially lethal. Frequently in literature, the term *aversive memory* could be used as a synonym for *fear memory*, especially in neuroscience when it comes to fear-motivated learning or conditioning.

The knowledge and representation of circuitry involved in various phases of fear memory have captured the attention of many researchers. It was hypothesized that these circuits are represented by three levels of organization (Silva et al., 2016). The first one is composed of all sensorial inputs coming from outside (acoustic, visual, nociceptive, and olfactory inputs). The second one integrates information from outside into a functional unit that is generally identified with the amygdala and hippocampus (Figure 2.1). Moreover, numerous studies on animal models argue that these brain regions, together with the cortex are the key to the formation and storage of fear memory (Ivan Izquierdo et al., 2016; Silva et al., 2016). The last unit is depicted as "output unit", adapting responses to circumstances (freezing or escape). In 1963 it was already known that the periacqueductal gray (PAG) was the final output for all types of defensive responses (Hunsperger, 1963; Johansen et al., 2010). An impairment or a pharmacological inactivation of this region reduces the expression of defensive behaviors, including freezing (Johansen et al., 2011; Silva et al., 2016)

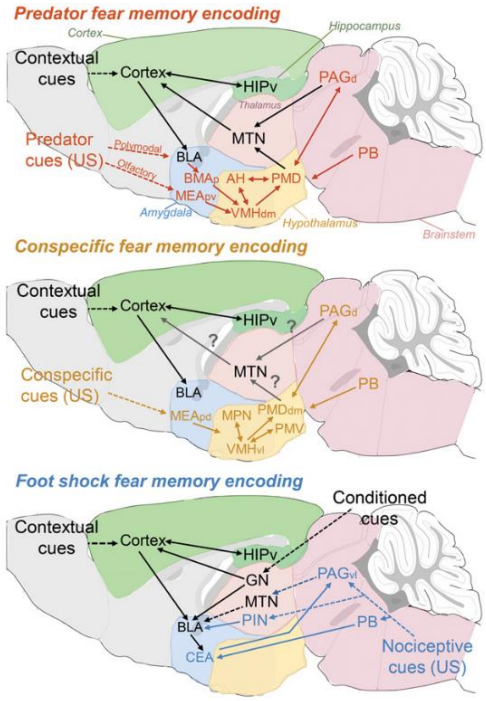

Figure 2.1: Hypothetical circuits mediating memorization of fear to different classes of threats (Silva et al., 2016).

2.2 Most used paradigm to evaluate fear memory in rodents

Much of what know about how the brain processes fear has been learned from animal models, since threat detection is an innate process, conserved among many species (J. E. LeDoux & Hofmann, 2018; Panksepp, 1989; Paradiso, 1998; Raber et al., 2019). Of course, we are not sure that what we feel in a precise condition is necessary identical to what animals feel in the same condition (Ivan Izquierdo et al., 2016; J. LeDoux, 2012; J. E. LeDoux, 2014; Panksepp, 1989). The principal limitation in the use of animal models is the lack of verbal or symbolic representation. This could create a methodological barrier to study fearful feelings in animals, but other responses relative to behavior exist as report or index of fear conditioning (e.g. freezing behavior) (Adolphs, 2013; Ivan Izquierdo et al., 2016; J. LeDoux, 2012).

The most direct way to study fear emotion in animals is by the use of associative mechanisms. Pavlov was the first to describe associative learning. Since 1927, the pavlovian fear conditioning become a very used paradigm in order to assess fear memory on animal models. Fear conditioning occurs when an innocuous conditioned stimulus (CS) (such as the environmental context and auditory or visual stimuli) is contingently paired with an aversive unconditioned stimulus (US) (as a mild foot-shock) (Rescorla, 1968; Watson & Rayner, 1920). Through the CS–US association, the CS comes to elicit various conditioned responses (CRs) that share similar characteristics to innate fear responses. The standard CR is identified with freezing behavior that causes muscular immobility and the absence of movements (Ivan Izquierdo et al., 2016). In the last century, the most used paradigms for fear conditioning are contextual/cued fear conditioning (CFC) and passive inhibitory avoidance (IA) (Gold, 1986; Iván Izquierdo, Bevilaqua, Rossato, et al., 2006; Ivan Izquierdo & Medina, 1997). Contextual fear conditioning is the most basic of the pavlovian fear conditioning. In this task the CS is

the context (cage) while in the cued fear conditioning, a CS (that could be an auditory or visual stimulus) is added to the context. Regarding IA, the term passive means that animals do not need to perform movements to avoid the foot-shock, at the same time, this does not mean inactive because subjects are not refrained from moving in any way. As this task is based on CS-US association, rodents learn to avoid the "unsafe" compartment in which they receive the shock, even though the same compartment has some features most desirable for rodents. There are two ways to perform this test, using the step-through IA or the step-down IA. Both have become classic and give the same results (Ivan Izquierdo et al., 2016). For step-through, rodents are placed on a platform in a brightly-illuminated compartment and they are free to access to the dark compartment where they will receive a mild foot-shock. Instead, For the step-down, animals have to descend from a start platform to an electrified grid where they will receive the same foot-shock. Upon re-exposure, the latency to go into the dark section is considered a direct measurement of memory (Bryan et al., 2009). IA is a form of fear-learning where rodents learn to choose between different behaviors, following as innate mechanism. Just like a child that burns his finger.

Like many other brain function, fear learning and consolidation are modulated by a variety of neurotransmitters. Among all neurological modulation system involved in aversive memory, recent interest has been also aroused by the histaminergic one (De Almeida & Izquierdo, 1986). In the following section, I am going to review the role of histamine as modulator and regulator of memory.

Chapter 3

Brain Histaminergic system

3.1 History of histamine research

At the beginning of the XX century, Sir Henry Dale and his co-workers, in their laboratory in London, identified histamine for the first time. By studying the effects of ergot extracts, they discovered the existence of a new compound and carried out experiments to explore its biological activity. They found that histamine plays several roles in the body: from the stimulant effect on smooth muscle, the induction of vasodilatation and the resulting fall of blood pressure, to the onset of a shock-like syndrome when injected into animals (Dale & Laidlaw, 1910). In 1920, Leon Popielsky recognized that histamine also has a stimulant effect on the acid secretion of dog stomach (Popielski, 1920). At the same time, Lewis described the classical "triple response" to this compound, observing its role in allergy and anaphylaxis. The first description of histamine in the brain, predominantly in the gray matter, was reported by Kwiatkowski (Kwiatkowski, 1943) and White (White, 1959), demonstrating its formation and catabolism at the central level. The observation of side effects of antihistamine drugs as sedation and somnolence have suggested a central role for histamine as a "waking substance" (Monnier et al., 1967). In the '60, by the use of o-phtalaldehyde fluorimetric assay, other biogenic amines (dopamine, norepinephrine and serotonin) became visible to neuroscientists who were able to detect them inside the brain (Carlsson et al., 1961). The failure to demonstrate histamine localization using this technique, in spite of the previous demonstration of its presence in the central nervous system (CNS), led to the negligence of this compound (H. L. Haas et al., 2008;

Parsons & Ganellin, 2006). The reason of this failure is due to the cross-reaction of histamine with spermidine, a polyamine compound found in ribosomes and living tissues. Histamine research flourished again in the '80s when Panula and Watanabe separately developed antibodies able to label histaminergic neurons. They found that all histaminergic neurons are located in the tuberomamillary nucleus (TMN), and project across the entire encephalon (P. Panula et al., 1984; Watanabe et al., 1984). Many studies about histamine affirmed that it regulates many brain functions. Nowadays, its involvement in learning and memory is widely recognized, suggesting a hypothetic use of histaminergic drugs for the treatment of many mental illnesses (Benetti et al., 2015).

3.2 Histamine in the nervous system

Histamine (derived from the Greek ἱστός, tissue) is an endogenous amine found in a variety of tissues. Within the CNS, it acts as a modulatory neurotransmitter, mediating several physiological and pathological processes like sleep-wake regulation, circadian-feeding rhythms, and learning and memory (H. L. Haas et al., 2008; H. Haas & Panula, 2003; Pertti Panula & Nuutinen, 2013). Although histamine is released in blood after mast cell activation, it is not able to penetrate the blood-brain barrier, thus its brain level must be maintained by ex-novo synthesis. Indeed, its concentration is regulated by many enzymes. Histamine is synthesized in a one-step reaction, through decarboxylation of L-histidine by a specific enzyme, histidine decarboxylase (HDC) (Green et al., 1987). HDC is the sole member of the histamine synthesis pathway, and it controls the synthesis of this neurotransmitter according to the bioavailability of the precursor L-histidine. Once formed, histamine is stored in vesicles by the vesicular monoamine transporter VMAT2 and mainly released from axonal varicosities. Its metabolism occurs rapidly in two alternative ways: its primary degradative enzymes, histamine-N-methyltransferase (HNMT), or its secondary, diamine oxidase (DAO) (Schwelberger et al., 2013; Shimshek et al., 2002; Weihe & Eiden, 2000). In brain tissue,

the predominant pathway to inactivate histamine is provided by the methylation through HNMT, followed by oxidation with monoamine oxidase (MAO-B) (Leurs et al., 2012). Both metabolic reactions lead to inactive products, unable to bind histaminergic receptors, and to trigger a signal transduction pathway.

3.2.1 The tuberomamillary nucleus (TMN)

Starting from Panula's and Watanabe's studies in 1984, it was found that TMN, which is located in the posterior hypothalamus, is the sole source of histaminergic fibers projecting through ascending and descending pathways in the entire brain (Blandina et al., 2012; H. L. Haas et al., 2008; H. Haas & Panula, 2003; Leurs et al., 2012; P. Panula et al., 1984; Watanabe et al., 1984). The highest densities of histaminergic fibers are found in hypothalamic nuclei, medial septum, nucleus of the diagonal band, and ventral tegmental area. Substantial innervation is also found in the hippocampus and thalamus. Moderate densities are found in the cerebral cortex, amygdala, striatum, and substantia nigra. Most areas of the brainstem, as well as the retina, cerebellum, and spinal cord, contain only a small number of fibers (Inagaki et al., 1988; P. Panula et al., 1990). The histaminergic system is phylogenetically well preserved in all vertebrates, including humans, and all the studies performed up to now proved that histaminergic neurons are localized in this nucleus (H. L. Haas et al., 2008; Leurs et al., 2012). The human TMN contains approximately 64000 histaminergic cells whereas, in the mouse, Parmentier has estimated the number of 2500-3500 neurons (H. L. Haas et al., 2008; Parmentier et al., 2002). For the rat, more studies have been carried out, and almost 4500 histaminergic neurons were found in the nucleus, subdivided into 5 clusters (E1-E5) (Figure 3.1). Net subdivisions are bridged by scattered neurons in line with the concept of one continuous cell group that becomes dispersed during development (Watanabe et al., 1984). In addition to histamine, other transmitters are found

inside TMN, like GABA, galanin, proenkephalin A-derived peptides, and thyrotropin-releasing hormone (Pertti Panula & Nuutinen, 2013). Everything we have learned about this nucleus and its relative function is far from clear. Various researchers have tried to understand whether histaminergic neurons inside the TMN can be divided into different subpopulations that project in specific brain regions and consequently with a specific physiological role (Blandina et al., 2012). In spite of the absence of systematic studies about TMN cytoarchitecture, the hypothesis about the subdivision of the nucleus in many function units, is the most affirmed.

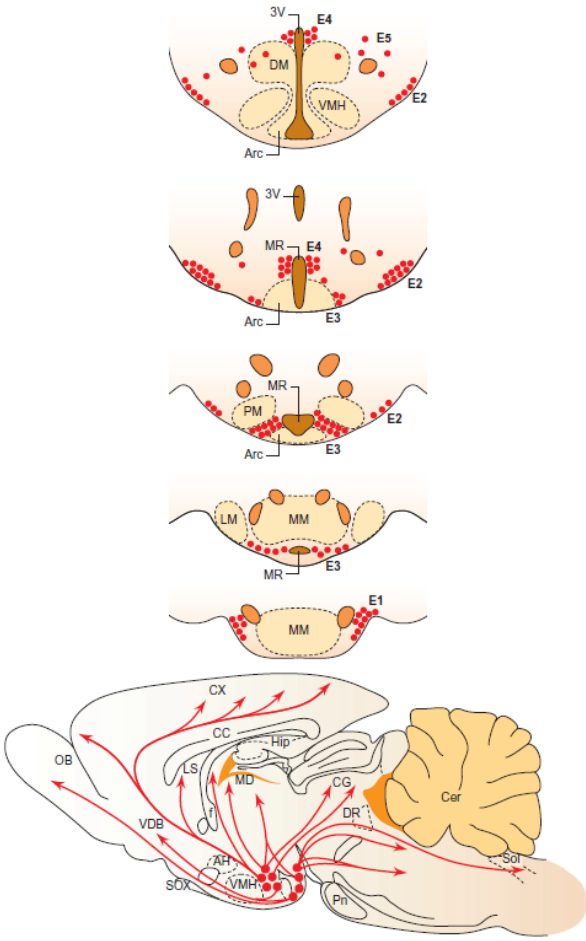

Figure 3.1: **The brain histaminergic system of a rat**. Top Coronal sections of TMN and its 5 clusters (E1-E5). Arc, arcuate nucleus; DM, dorsomedial nucleus; LM, lateral mamillary nucleus; MM, medial mamillary nucleus; MR, mamillary recess; PM, premamillary nucleus; 3V, third ventricle; VMH, ventromedial hypothalamic nucleus. Bottom A sagittal view illustrating the major ascending and descending fiber projections. AH, anterior hypothalamus; CC, corpus callosum; Cer, cerebellum; CG, central gray; CX, cerebral cortex; DR, dorsal raphe; f, fornix; Hip, hippocampus; LS, lateral septum; MD, mediodorsal thalamus; OB, olfactory bulb; Pn, pontine nuclei; Sol, nucleus of solitary tract; SOX, supraoptic decussation; VDB, vertical limb of the diagonal band; VMH, ventromedial hypothalamic nucleus (Leurs et al., 2012).

3.2.2 Histaminergic receptors

Histamine regulates its function through four metabotropic receptors: H1-, H2-, H3R are expressed in the brain while H4R is mainly present in peripheral tissue (bone marrow and leukocytes). All metabotropic histamine receptors (H1R-H4R) belong to the rhodopsin-like family of G protein-coupled receptors (GPCR) (Hayashi et al., 1984; Hill et al., 1997; Leurs et al., 2005). These receptors differ in their signal transduction pathways, distribution, functionality, and pharmacological properties of their agonists and antagonists (Table 1). H1R and H2R are located in neuronal and glial cells and are expressed postsynaptically in all parts of the brain. They regulate excitability and plasticity of postsynaptic neurons. H3R was thought to be an autoreceptor implicated in the regulation of histamine, but following studies have proved that it also works as a heteroreceptor in non-histaminergic neurons, controlling the release of various neurotransmitters (H. L. Haas et al., 2008). At TMN level, H3R is more expressed compared with other receptors, and is localized on somata, dendrites, axons of histaminergic neurons. (H. Haas & Panula, 2003; Pertti Panula & Nuutinen, 2013; Schlicker et al., 1988; Yamamoto et al., 1997).

Properties	H1R	H2R	H3R	H4R
Chromosome gene locus	3p25	5q35.2	20q13.33	18q11.2
Protein (amino acids)	487	359	445	390
G protein isoforms	$G_{q/11}$	$G\alpha_s$	$G_{i/o}$	$G_{i/o}$
Constitutive activity	+	+	++*	?
Signal transduction	PLC IP_3, DAG Ca^{2+}, PKC AMPK, NF-κB	AC cAMP, PKA CREB	AC ↓ cAMP ↓ MAPK Akt/GSK3	AC ↓ cAMP ↓ MAPK
Effector pathways	TRPC IK_{leak} ↓	I_h (HCN2) I_{AHP} ↓	I_{Ca} ↓	Cytoskeleton
Cellular function	Postsynaptic excitability and plasticity†	Postsynaptic excitability and plasticity	Presynaptic transmitter release‡ and plasticity	?
Systemic function	Behavioral state and reinforcement (novelty, arousal) Working memory Feeding rhythms Energy metabolism Endocrine control	Learning and memory (consolidation)	Numerous CNS functions,‡ cognition, emotion, learning, and memory Blood-brain barrier control	Chemotaxis
Pathophysiology	Disorders of sleep, mood, memory, eating, and addiction Pain and neuroinflammation	Schizophrenia Pain and neuroinflammation	Disorders of sleep, mood, memory, eating, and addiction pain and neuroinflammation	?

Table 1: Properties of different histamine receptors in CNS (H. L. Haas et al., 2008)

3.4 Histaminergic brain function: learning and memory

Behavioural studies suggest that the central histaminergic system has an important role as regulator of learning and memory (Alvarez, 2009; H. Haas & Panula, 2003; Passani et al., 2017). The first insight about the role of histamine in memory formation was in 1986 with a study by Almeida and Izquierdo (De Almeida & Izquierdo, 1986). They administrated histamine directly into later ventricles (LVs) of rats and observing an enhanced IA memory consolidation. Starting from these results, the relationship between histamine and memory processing, particularly fear-related memories, has been investigated. One of many hypothesis is based on the anatomical connection between the TMN and the septum/diagonal band nucleus, that in turns is connected to

the hippocampus, a structure critically involved in fear memory consolidation and retrieval (Wouterlood et al., 1988). Although many studies about histamine and the regulation of memory consolidation have been recently published, the big picture is still unclear. Starting from results obtained by Almeida and Izquierdo, many researchers have tried to inject histaminergic agonists or antagonists in various brain areas. Most reported that this amine facilitates consolidation while a small part affirms the opposite, depending on the behavioural task and the injection site (Álvarez & Ruarte, 2004; Baldi et al., 2005; Benetti et al., 2012; Benetti & Izquierdo, 2013; Cacabelos & Alvarez, 1991; Cangioll et al., 2002; Charlier & Tirelli, 2011; da Silva et al., 2006; Foley et al., 2009; Frisch et al., 1999; Giovannini et al., 2003; Kida et al., 2002; M. Beatrice Passani et al., 2001; Spieler et al., 1999). Recent data, obtained with a classic paradigm as inhibitory avoidance, have shown what Almeida and Izquierdo have already discovered, highlighting the importance of the integrity of the central histaminergic system for memory consolidation (Benetti et al., 2015; Fabbri et al., 2016). The litmus test was performed administrating α-fluoro-methylhistidine (α-FMH), a suicide inhibitor of histidine decarboxylase that blocks cerebral histamine synthesis in LVs of rats. This administration causes amnesia and impairs the consolidation of memory (Benetti et al., 2015; Passani et al., 2017; Provensi et al., 2020). In 2017 Benetti et al. found that depletion of endogenous histamine damaged long-term (LTM) but not short-term memory (STM). A further application of exogenous histamine into basolateral amygdala (BLA) and CA1, was able to restore LTM at different time points, based on site injection. In memory processing, damages of a specific brain region are compensated by recruiting alternative circuitry. In the same way, the histaminergic system comprises parallel, coordinated pathways that provide compensatory plasticity when CA1 or BLA are compromised, trying to replace the function of the damaged region (Benetti et al., 2015).

Studying learning and memory and their relative circuitries is an arduous challenge. Indeed, the role of many different brain regions have been investigated. From a

methodological point of view, whole-brain mapping of histaminergic activated neurons is the most appropriate way to study memory and the relative histaminergic circuits. The next chapter will describe the latest technological developments concurring to map activated neurons across the entire mouse brain.

Chapter 4

Tagging neuron activation following sensory and behavioral stimuli

The first step to map activated neurons across the whole brain is to tag them with a label allowing visualization through an optical microscope. Different methods have been proposed during the years, ranging from classical immunohistochemistry (IHC) to sophisticated transgenic or viral approaches. All these different techniques share a common principle: the use of immediate early genes (IEGs). In this section, we first recall the basic features of IEGs and then describe in detail the various methods that could be used to tag neurons according to the expression of one of these genes.

4.1 IEGs-based approaches as useful tools to access activated neurons

Nowadays, the discovery of IEGs has enabled us to reconstruct functional maps with single-cell resolution. IEGs, such as *c-fos*, *Arc* and *Egr1* (also known as *ZiF268),* are a class of genes that is activated transiently and rapidly in response to a wide variety of cellular stimuli (Hunt et al., 1988; Sagar et al., 1988; Kaczmarek and Nikolajew, 1990; Hughes et al., 1992; Pinaud, 2004; Terleph and Tremere, 2006; Bahrami and Drabløs, 2016). At the brain level, the expression of all IEGs is induced by neuronal activity through depolarization (Greenberg et al., 1986; Morgan et al., 1987; Bartel et al., 1989; Sheng and Greenberg, 1990; Smeyne et al., 1992). In this way, the rise of intracellular

Ca^{2+} levels activate second messenger pathways that, in turn, stimulate transcriptional factors. Within few minutes, these factors trigger the expression of the relative genes. For that reason, for a long time, they have been used as an indirect marker to measure neuronal activity. In addition to their rapid induction, IEG proteins have a relatively short life due to their fast transcription that is interrupted with the end of external stimulation. Thus, in a few hours, the expression levels of these proteins return to their baseline (Sheng and Greenberg, 1990).

Starting from these characteristic features of IEGs, a series of IEGs-based tools have been developed either in the form of transgenic mice or viral vectors (Reijmers et al., 2007; Guenthner et al., 2013; Kawashima et al., 2013; Sakurai et al., 2016; Sørensen et al., 2016; DeNardo et al., 2019; Hasan et al., 2019). These genetic approaches have been developed to translate neuronal activity into gene expression by making it possible the visualization of behavioral-relevant cells and also the access to the same neurons in living animals or ex-vivo tissue slices. Most of these strategies pave the way to cell manipulation with chemogenetic or optogenetic tools, giving to researchers the possibility to activate, inactivate and record neuronal activity using electrophysiology or genetically encoded calcium indicators (Barth et al., 2004; Wang et al., 2006).

Before describing in detail the mechanisms, advantages and disadvantages of each genetic approach, it is worth adding few general considerations. IEGs transcripts or proteins are present in neurons for a limited time after the stimulus that elicited the activity of a specific brain circuit. Therefore, any protocol aimed at mapping the presence of IEGs must be performed within a limited time window after the behavioral test. If proteins or transcripts have to be mapped directly, e.g. with IHC, this means that the animal must be sacrificed after the stimulus, preventing further behavioral tests. Genetic approaches, driving recombination in the presence of IEGs, have been developed to overcome this limitation allowing access to activated cells for a period much longer than the IEG timescale.

The time window of IEG expression also defines the maximum temporal resolution of the method, i.e. the capability to distinguish neurons activated by the stimulus of interest from those activated by subsequent or previous stimuli. When using transgenic or viral strategies in combination with some drug, the pharmacokinetics of the drug itself must also be taken into account, as it will often extend the time window beyond the natural half-life of IEG proteins (Guenthner et al.; Sheng and Greenberg, 1990; Reijmers et al., 2007). This loss of temporal resolution leads to the labeling of more neurons than those activated in the behavior of interest. These "false positives", usually referred to as "background", effectively reduce the capability of the method to find statistically significant variations in the number of activated neurons between different areas or subjects.

On the contrary, "false negatives" can appear when the method fails either to tag activated cells or to maintain labelling after the recombination event (as in the case of genetic methods). In both cases, a fraction of IEG-positive neurons is missing, again reducing statistical power. The main reasons for the insufficient labelling of activated cells are limited efficiency of the recombination mechanisms in selected cell types, or also the limited penetration of exogenous dyes (e.g. in IHC).

Here below, we describe in detail the existing methods able to tag activated neurons, providing useful information for researchers. Figure 4.1 summarizes them with schematic illustrations, whilst Table 2 recapitulates the main features of each method.

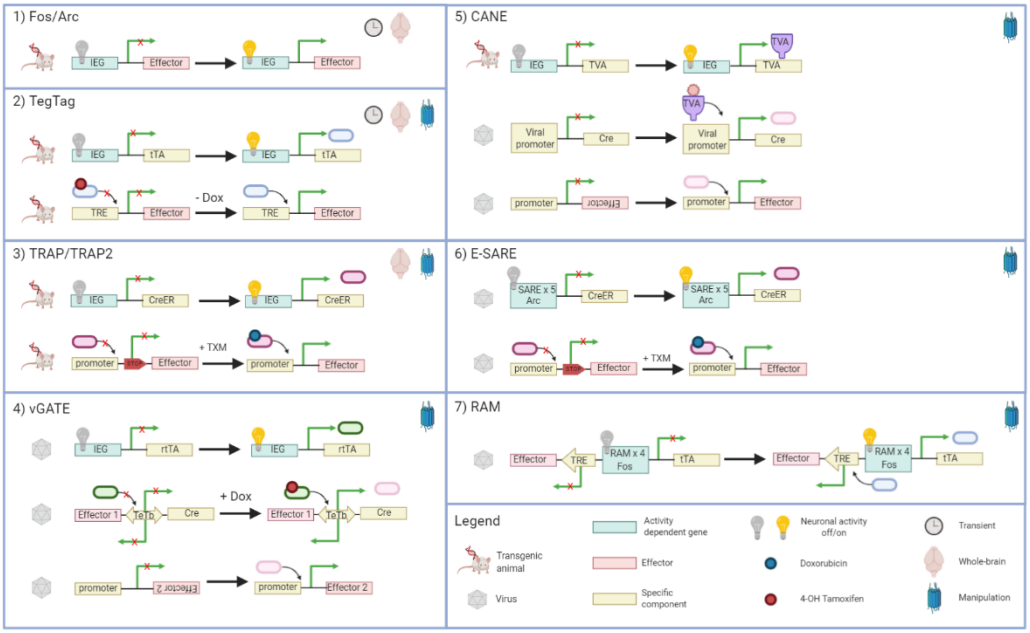

Figure 4.1: **Diagram of IEGs-based approaches for neuron tagging**. For each method information about the characteristic of the final effect are described. In particular: the duration time (transient or not), the location (whole-brain or not), and if the method can be coupled with optogenetic and chemogenetic tools (manipulation). Abbreviations lists: tetracycline responsive element (TRE); doxycycline (Dox); artificial transcription factor (tTA); 4-hydroxytamoxifen (TXM); tamoxifen-inducible recombinase (CreER); reverse tetracycline transactivator (rtTA); bidirectional Tet promoter (TeTb). Image from (Franceschini et al., 2020)

	IHC	Fos-GFP Arc-dVenus	TetTag	TRAP	TRAP2	CANE	vGATE	E-SARE	RAM
Whole-brain cell counts	X	X	X	X	X				
Projection mapping of activated cells				X	X	X	X	X	X
Tran-synaptic tagging				X	X	X			
Optogenetic or chemogenetic manipulation of activated cells			X	X	X	X	X	X	X
Subsequent behavioural test				X	X	X	X	X	X
Cell-type specificity							X		

Table 2: Summary of the main features of each IEG tagging method. Table from (Franceschini et al., 2020)

Immunohistochemistry (IHC)

The immunohistochemical staining has been considered the "gold standard" for the reconstruction of whole-brain activity maps at the cellular scale. Leveraging the fact that IEG-synthesis is induced by neuronal activity, the first way to visualize the activity at the brain level was obtained by the immunostaining of *c-fos* (Morgan et al., 1987; Sagar et al., 1988). Despite the large number of genetic approaches developed in the last years, IHC still remains the reference method to map IEG-expressing cells. It has been coupled with many clearing techniques, such as iDISCO, CLARITY, CUBIC, for the 3D reconstruction of brain-wide activated circuits (Susaki et al., 2014; Tomer et al., 2014; Renier et al., 2016). However, there are some limitations concerning this method. After the stimulus, when IEGs arrive at the

transcription peak, animals have to be sacrificed, so it is not possible to carry out other studies on the same animal.

Moreover, it is often interesting to understand whether a neuronal ensemble, activated with a stimulus, could be reactivated with a distinct one, and the traditional IHC does not allow this type of investigation. In order to solve this latter problem, *cellular compartment analysis of temporal activity by fluorescent in situ hybridization* (catFISH) has been developed. This technique exploits different compartmentalization of mRNA into the nucleus and the cytoplasmic region (Guzowski and Worley, 2001). However, starting from the previous method, a new double- labelling technique is applied in order to study two sequential stimuli separated by an appropriate interval. Thus, the *tyramide-amplified ICH-FISH* (TAI-FISH) exploits different compartmentalization of IEG protein and the relative mRNA, in this way the first stimulus is visualized by IEG cytoplasmic protein while the second with the mRNA in the nucleus (Xiu et al., 2014).

Fos-GFP, Arc-dVenus

As mentioned above, IEGs offer genetic access to neurons activated in response to specific stimuli; therefore, strains of transgenic or knock-in mice have been developed to directly link IEG transcription to some type of reporter. Genes coding for fluorescent proteins, LacZ markers or luciferase, are inserted under the control of the IEG-promoters (Smeyne et al., 1992; Barth et al., 2004; Wang et al., 2006; Xie et al., 2014; Kim et al., 2015b; Vousden et al., 2015). This approach has been first proven in transgenic mice in which *Fos* promoter drove transcription of the β-galactosidase; neurons activated in response to light pulse stimulation during the dark cycle were then identified as Fos-LacZ positive through a blue pigment (Smeyne et al., 1992).

More recently, several transgenic models have used fluorescent proteins as reporters in an activity-dependent manner (Barth et al., 2004; Wang et al., 2006; Xie et al., 2014; Kim et al., 2015b; Vousden et al., 2015). For example, *Fos-GFP* mice have been used to map the neurons stimulated during social or parenting behaviors (Kim et al., 2015b) while different activation patterns involved in recalling contextual and tone fear memories at whole brain-level were explored with the *Arc-dVenus* strain (Vousden et al., 2015). The half-life of the fluorescent proteins is similar to endogenous IEGs ones, leading to fluorescent peaks in a short time, about 1-2 hours, and lasts approximately 6-8 hours. This temporary access to neurons prevents manipulation of the same activated cells later in time. Still, GFP-expressing cells may be targeted in vivo for electrophysiological recording right after the behavioral experiment (Barth et al., 2004). *Fos-GFP* and *Arc-dVenus* have been included inside a pipeline that demonstrated, for the first time, the possibility to detect neural activity on a brain-wide scale, using automated whole brain imaging (Kim et al., 2015b; Vousden et al., 2015).

TetTag

More complex strategies limit the expression of an IEG-linked effector to some kind of pharmacological treatment. One of the first approaches demonstrated in this sense is *TetTag*, that uses *Fos* promoter to drive the expression of a doxycycline-repressible tetracycline transactivator (tTA) (Reijmers et al., 2007). This strategy has been developed to understand whether neurons activated during fear learning are reactivated during fear memory recall (Reijmers et al., 2007). This inducible expression system, called *Tet-Off*, exploits the "switch-off" mode in the presence of the doxycycline antibiotic (DOX). The *TetTag* strategy needs two transgenes: the first requires the tTA,

an artificial transcription factor while the second, a tetracycline responsive element (TRE) that is a synthetic promoter. TRE needs to bind to tTA for the expression of any genes. During the resting state, tTA is usually bound to DOX and consequently unable to link to the TRE sequence. Therefore, in presence of a stimulus and of a diet lacking in DOX at the same time, the *Fos* promoter stimulates the synthesis of tTA, which now is able to bind TRE for the effector expression, achieving neuronal labelling. Due to the slow metabolism of DOX, the time window becomes very wide and leads to high levels of neuronal background (Shockett and Schatz, 1996; Reijmers et al., 2007). Moreover, this method does not allow to permanently access to activate neurons because TRE-conditional effectors last only few days (Reijmers et al., 2007).

Finally, for the manipulation of behavioral-responsive ensembles in many paradigms this technique can be coupled with optogenetic and chemogenetic tools, using some rhodopsins and excitatory human M3 muscarinic (hM3Dq) receptors directly as effectors (Koya et al., 2009; Garner et al., 2012; Liu et al., 2012; Ramirez et al., 2013, 2015; Cowansage et al., 2014; Redondo et al., 2014).

TRAP

Targeted recombination in active populations (TRAP) is another drug-dependent approach, such as *TetTag.* However, compared to the latter, TRAP shows a better temporal resolution and permanent genetic access to neurons, making activated cells permanently fluorescent (Guenthner et al., 2013). Like the previous one, also this strategy needs two transgenes: the first expressing a tamoxifen-inducible recombinase $CreER^{T2}$ in an activity-dependent way, i.e. under the control of *Arc* and *Fos* promoter (ArcTRAP and FosTRAP) (Feil et al.,

1997). The second exploits the Cre-Lox recombination under a ubiquitous promoter for the reporter expression.

$CreER^{T2}$ is expressed in active cells but is not effective unless in presence of tamoxifen (TMX). When present inside cells, TMX binds the ER site allowing $CreER^{T2}$ to move from the cytoplasm to the nucleus, driving the expression of a reporter *(i.e. fluorescent protein*) by the removal of loxP-stop-loxP sequence (Guenthner et al., 2013). The time window for "*cell TRAPing*" is provided by the lifetime of TMX and, therefore, by its metabolism and excretion. Due to the long lifetime of TMX, *Guenthner et al.* have decided to use its metabolic form, 4-hydroxytamoxifene (4-TMX), limiting the time window to a period < 12h (Guenthner et al., 2013). As a result, only neurons that are activated around drug administration can be TRAPed.

This genetic tool has facilitated previously impossible experiments, enabling the manipulation of neural ensembles activated during a specific task later in time, even days after (Ye et al., 2016; Ishii et al., 2017; Kim and Cho, 2017; Girasole et al., 2018). Moreover, this method has allowed whole-brain reconstructions and it is often coupled with clearing approaches. Besides the many progresses made in this field, TRAP has some limitations: the first is caused by the *Arc* and *Fos* haploinsufficiency that provokes the disruption of their endogenous expression; the second is about stochastic labelling mainly due to random reporter expression.

TRAP2

Recently, *TRAP* has been improved with a new version, called *TRAP2* (DeNardo et al., 2019). The mechanism is the same as *TRAP* with few but essential developments. *TRAP2* is further optimized with an improved Cre (iCre) to enhance the effector expression (Shimshek et al., 2002). It preservers the Fos

endogenous expression, allowgin keeping transgenic animals in homozygosis. Therefore, this capability of maintaining Fos endogenous expression also improves the penetration in many brain regions. Using *TRAP2* tool*, Luo's group* has studied fear memory retrieval in the prelimbic cortex.

CANE

Sukurai et al. have developed a "lock-and-key strategy" for *capturing activated neuronal ensembles with engineered mice and viruses (CANE)* (Sakurai et al., 2016). In *CANE* system, a destabilized targeting avian leukosis (dsTVA) receptor, not present in mice, is knocked-in to endogenous Fos locus. In presence of external stimuli, Fos and dsTVA are co-translated in the same neuron so that all Fos^+ cells have on their membrane the avian receptors. Before any external stimulation, rabi/lentiviruses coated with a surface glycoprotein (EnvA), a typical ligand of TVA, are delivered into the brain and infect Fos^+ neurons in the injection area. After transfection, the virus genome is inserted into the neuron and allows the effector expression (Sakurai et al., 2016).

CANE leads to a more precise temporal and spatial resolution compared to previous techniques. Its short time window depends a) on the brief half-life of dsTVA, which mimics the kinetics of the endogenous *Fos*, and b) on tightened limitations of viral vectors transduction. For those reasons, it enables low background and it has been used to study "mild behavior" (*i.e. brief behavioral encounters or brief behavioral events*). Moreover, this double-control mechanism appears to permanently tag the majority of activated cells, leading to high-efficiency. The use of lenti and rabiviruses allows labelling two or more ensembles in the same brain region and also trans-synaptic tracing of activated cells (Sakurai et al., 2016; Rodriguez et al., 2017; Jiang-Xie et al.,

2019; Tschida et al., 2019). CANE is an excellent technology, able to reconstruct efferent and afferent connections, but it cannot be used for whole-brain labelling because viral infection is limited to the injection site. Moreover, virus delivery requires stereotaxic surgery and anesthesia, which could alter behavior and neuronal response.

vGATE

The most recent genetic approach, which uses a mixture of three viruses, is called *virus-delivered genetic activity-induced tagging of cell ensembles* (vGATE). This multi-level strategy has been used to investigated fear memory engrams and especially to manipulate hypothalamic oxytocin neurons with the aim of understanding the role of this sub-population in fear response (Hasan et al., 2019). The authors used a system composed of three adeno-associated viruses (AAV). The first one drives the expression of a reverse tetracycline transactivator (rtTA) under the *Fos* promoter. In order to have a permanent tagging of Fos^+ neurons, a Tet operator sequence has been integrated upstream of *Fos* promoter, able to sustain an extensive induction of rtTA in presence of DOX through an autoregulatory expression loop. The second virus contains a bidirectional Tet promoter, that in presence of the DOX stimulates the expression of a fluorescent protein and simultaneously activates the Cre recombinase. The last virus uses a cell-type-specific promoter that, under a Cre recombinase, expresses Channelrhodopsin-2 (ChR2) to optically manipulate neuronal activity (Hasan et al., 2019).
Contrary to *TetTag,* this IEG-based method exploits a Tet-On system, i.e., DOX "switch-on" mode. By the intraperitoneal DOX injection, the transcriptional activator is expressed, providing a better-controlled time window, which

depends only on the drug metabolism and viral transduction, avoiding the integration of the DOX in the feed.

The great advantage of the vGATE is the lack of use of transgenic mice; in this case, there is the possibility to switch to other species. For instance, *Hasan et al.* have applied this tool to rats for their study. Moreover, the last virus contains a cell-type-specific promoter, and consequently, a specific neuron subpopulation may be manipulated and visualized. The use of viruses has its own limitations yet: it cannot be used for systemic tagging due to the local nature of viral injection; furthermore, as in always complex stereotaxic surgery, the potential effects of any brain injury on animal behaviour could not be overlooked.

E-SARE

Recently, many researchers focused on endogenous promoters, modifying their genomic sequences to have better control of the transcription of IEGs induced by neuronal activity. Therefore, viral strategies using engineered promoters have expanded the horizon of IEG-based methods to improve the specificity and efficiency of activated neurons, increasing reporter expression level more than 20-fold. Kawashima et al. have introduced the *synaptic activity-responsive elements* (SARE), which regulate *Arc* expression throughout the cooperation of three activity-dependent transcription factors (CREB, MEF2, and SRF) to induce a strong transcription (Kawashima et al., 2009). Exploiting their study based on the SARE enhancer element of the Arc promoter, the same authors have constructed a new synthetic promoter called “E-SARE” that is composed of five tandem repeats of SARE sequence fused into an *Arc* minimal promoter (Kawashima et al., 2013). This genetic tool has been used to tag neurons activated by different visual orientation stimuli.

In order to obtain a reliable circuitry map and to manipulate permanently tagged neuronal ensembles, E-SARE has been coupled to an inducible Cre sequence. The combination of the E-SARE upstream of the $CreER^{T2}$ allows to have a tightly-controlled time resolution (Kawashima et al., 2013). This system can be packed into AAV vectors or lentivirus without the use of transgenic animals, consequently, the great advantage is the potential "switching" to larger mammalian species.

RAM

RAM *Robust activity marking* system is another method, such as E-SARE, that exploits a synthetic promoter to investigate activity-dependent cells. This strategy has been used to label and manipulate neuronal ensembles in the hippocampus of animals subjected to contextual fear conditions (CFC) and in the amygdala following tone-fear conditioning (TCF) (Sørensen et al., 2016). The RAM promoter (P_{RAM}) is composed of four repeats of an enhancer module, which is composed by the AP-1 site and the neuronal-specific activity-dependent gene Npas4 binding motif, upstream of *Fos* minimal promoter (Sørensen et al., 2016). Related to existing IEG-genetic tools that do not take advantage of synthetic promoters, RAM has been developed to reduce background levels, meaning that it only responds to neuronal activity with a robust signal and to precisely control the time of its activation. P_{RAM} has been combined with an improved version of a Tet-Off system with a destabilized version of tTA (d2tTA) for many reasons: best activation time and tight time-window that leads to lower basal expression. Moreover, the P_{RAM} small dimension allows to pack the entire DNA sequence into a single virus, bypassing transgenic animals and using it in other species like rats or flies,

thanks to high conservation of the sequence used (Sørensen et al., 2016). Finally, to show the versatility of this method, a Cre-dependent RAM has been developed to study cell-type specific ensembles activated by a specific stimulus (Sørensen et al., 2016).

4.2 Different approaches, not based on IEG, to tag activated neurons

IEG based approaches have been generally used to tag neurons activated during behavioral experiences. Still, these methods cannot be used to study "mild" behaviors or behaviors that produce neuronal activity less sustained in time. The reason lies in the fact that these IEGs share some limitations, which are mainly caused by the long time-window, ranging from hours to days, and high-level background. For that reason, photoactivable approaches have been developed to overcome the problems related to IEG's nature, using calcium as indicator for neuronal activity and light instead of drugs, as tool for a more rapid temporal resolution and better control of non-specific reporter expression, significantly lowering the background. FLARE (Wang et al., 2017) and Cal-Light (Lee et al., 2017) are the first Ca^{2+}-and-light-gated tools that exploit a transcriptional readout while CaMPARI (Fosque et al., 2015) is another Ca^{2+}-and-light-gated tool that uses fluorescent protein photoconversion.

Chapter 5

Tissue clearing protocols as fitting tools to image three-dimensional (3D) brain volume

Once neurons are activated and labelled in response to behavioral stimuli, brain samples can be analyzed with optical microscopy. However, given the opaque nature of biological specimens, the full volume of the brain cannot be directly reconstructed in 3D. From standard histology to more recent techniques, methods based on serial sectioning are able to reconstruct the 3D volume (for more details, see Section 4). These methods are based on mechanical operations that lead to sample disruption. Indeed, the brain cutting could cause compression, stretching, or accidental incision, which often make the volumetric reconstruction hard. Although these approaches are widely used, the most straightforward way to preserve the 3D structure is to make specimens transparent through tissue clearing methods. The transparency provides direct optical access to bulky specimens, allowing to overcome sample sectioning. In general, keeping brains intact rather than exploring smaller parts is important to achieve a better comprehension of neuronal mechanisms. It is evident that virus injections, generally used to tag neuronal projections of neuronal subgroups activated by a particular stimulus, or used to select specific subpopulations,

Scattering: diffusion of light in random directions, without absorption by the sample. It is caused by microscopic variations of the refractive index.

Refractive index (RI): the ratio between the speed of light in the vacuum and in a given material. The higher the RI, the slower the speed of light in the medium.

could be scarcely evaluated by two-dimensional (2D) sections. Neuronal projections are extended in every possible direction; therefore, brain cutting can result in loss of information about connections between regions or about the virus pathway.

As mentioned above, a relevant problem to rapidly image large volumes of tissue is associated with the milky aspect of the brain due to its heterogeneous composition. This heterogeneity leads to light scattering, with light rays diffused in random directions by the microscopic components of the sample. This diffusion of light hinders brain imaging. Indeed, light is scattered as a result of the mismatch between the refractive indices (RIs) of different tissue components (Figure 5.1). Possible solutions to overcome this problem consist of limiting the scattering effects by reducing optical inhomogeneities within the sample (Tuchin, 1997; Richardson and Lichtman, 2015). Thus, the clearing protocols work minimizing the mismatch between macromolecules and the surrounding medium. Generally, the "dry" part of biological tissue (proteins and lipids) has a high RI (ranging from 1.4 to 1.6), while the surrounding medium is mainly composed of water, which has a RI of 1.33 (Jacques, 2013). The first approach to achieve the transparency of the brain is related to the removal of lipids that are the primary source of scattering in the fixed sample. By eliminating lipids from the sample, "dry" RI is reduced, and the surrounding medium is replaced with a solution that has the same RI of the delipidated tissue. The other approach consists of directly acting on the surrounding medium, immerging the brain in solutions able to increase the RI of the medium to homogenize it with the components of our tissue. In conclusion, the clearing approaches operate in two ways: on the brain components or on the surrounding medium. Depending on the clearing approach researchers use, the final RI for cleared brain or other tissues ranges from 1.33 (water RI) to 1.6 (lipid RI).

In this section, we review all of the existing clearing methods. Different classifications have been proposed (Richardson and Lichtman, 2015; Silvestri et al., 2016; Tainaka et al., 2016). Still, we try to gather them into three groups: (1) hydrophobic- reagent or

organic solvent-based clearing methods, (2) hydrophilic-reagent or water-based clearing methods, and finally (3) hydrogel-based clearing methods.

It is worth emphasizing that in this review, we are focused on the brain, but clearing methods can be applied to many other organs.)

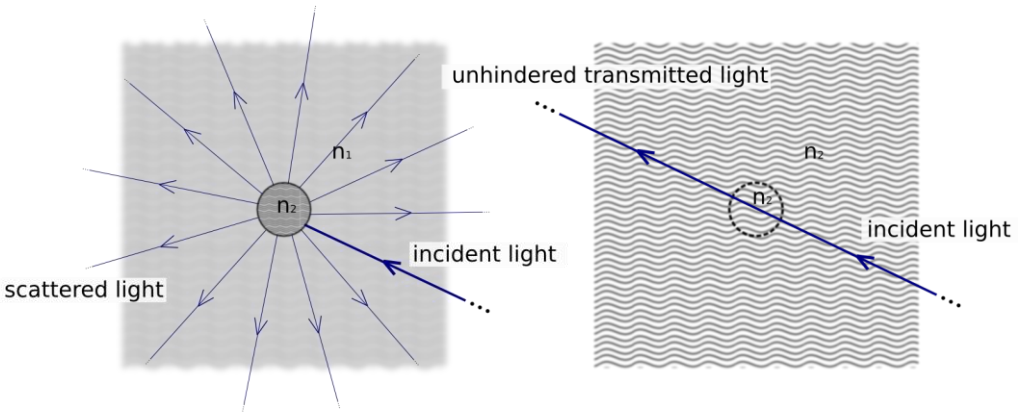

***Figure 5*.1: Physical principle underlying tissue clearing.** In normal tissue (left) cellular components have a refractive index n_2 significantly larger than that of the surrounding medium (water, n_1). This inhomogeneity results in scattering of light and thus opaqueness of the sample. Clearing methods try to match refractive indices (right), so that tissue appears as a homogeneous optical medium where light can travel unhindered. Image from (Franceschini et al., 2020).

5.1 Hydrophobic-reagent or organic solvent-based clearing methods

More than a century ago, Spalteholz described, for the first time, a clearing approach for fixed tissue using organic solvents (Spalteholz, 1914). He replaced water with a high-RI mixture, composed of benzyl benzoate and methyl salicylate, and observed that biological tissue became almost entirely transparent. In general, hydrophobic-reagent methods involve organic solvents with high-RI and provide remarkable transparency of large samples (*i.e* brain) in a quick time (1-2 days), perfect for a whole-brain pipeline. Due to their rapid "brain-transparentizing" capability, this class is the most used among clearing techniques (Costantini et al., 2019). Since tissues are mainly composed of water, the main principle of this method is based on dehydration and RI matching. The first step consists of water removal by organic solvent as alcohols or ethers, which are also able to solvate a small fraction of lipids. Dehydration usually leads to sample shrinkage and hardening. Whereas, agents used in the second step, have the function to match the high-RI of water-free tissues and also to remove the remaining lipids.

PRACTICAL STEPS TO MAKE BRAIN TRANSPARENT

- Tissue clearing methods are usually referred to ex-vivo applications. Therefore, brains or other organs are subjected to *fixation* step. Alcohol, paraformaldehyde (PFA), hydrogel and glutaraldehyde are chemicals generally used to preserve intracellular protein during this protocol. An excessive fixation could cause autofluorescence problems inside the brain.

- The quickest way to homogenize the RI, provides lipid removal since lipids are constituted by higher-RI inside the cell and are the main source of tissue inhomogenity. On the clearing side, delipidation allows passive diffusion to exchange water with a different RI medium.

- Autofluorescence and pigments could cause respectively a low signal to noise ratio and light absorption, denying high transparency. Accordingly, a chemical treatment could solve this problem.

This general scheme, composed of dehydration and RI matching, has been later used by Dodt, replacing methyl salicylate with benzyl alcohol. BABB (the acronym of agents used) has been created from this change (Dodt et al., 2007). A relevant limitation of organic solvent-based clearing methods is related to the dehydration step, which often leads to fluorescent protein quenching. For that reason, this method is not suitable for the endogenous reporters as GFP or tdTomato. Thus, using this type of clearing on transgenic or transfected mice is discouraged. The introduction of tetrahydrofuran (THF) and dibenzyl ether (DBE), respectively, as dehydrated and RI matching agent, has developed 3DISCO techniques and has improved fluorescence preservation, that lasts for few days (Becker et al., 2012; Ertürk et al., 2012). This has been possible by the elimination of peroxides generating from THF and DBE before usage of these solvents. Other improvements have allowed the developed many variants of DISCO-based techniques. *Renier et al.*, using iDISCO, overcame the problem related to fluorescence quenching, combining clearing with whole-mount IHC, with the aim to direct an antibody against the different fluorescent proteins (Renier et al., 2014). Anyway, they have also used a combination of phosphate-buffer saline (PBS) and dimethyl sulfoxide (DMSO) also to preserve GFP expression for a few days. These techniques make tissue highly transparent, and they allow permanent preservation of

specimens, owing to their hardening. Moreover, organic solvent-based techniques are extremely rapid. To understand their speed, just think that an entire brain is cleared in only a few days. However, the use of many toxic and dangerous agents, the scarce availability of appropriate immersion lenses for imaging, the fluorescent protein quenching, have induced researchers to develop alternative approaches.

5.2 Hydrophilic-reagent or water-based clearing methods

The extensive use of endogenous fluorescent reporters, as GFP or tdTomato protein, has driven the development of new clearing protocols replacing organic solvents with water-soluble reagents. These hydrophilic clearing methods exploit two different approaches: passive immersion in high-RI aqueous solution, and delipidation with hyperhydrating reagents. The former approach is based on a direct immersion of the sample in a high-RI solution to clear the sample gradually. In detail, saturated sugar solutions that are prepared with elevated concentration of sucrose or fructose are used in SeeDB and FRUIT techniques, respectively (Ke et al., 2013; Hou et al., 2015). The practical drawbacks of using high-sugar concentration are the high viscosity that limits sample manipulation and could introduce air bubbles, the potential precipitation at room temperature, and browning coloration at more elevated temperatures. The sugar viscosity causes slow penetration inside the sample, thereby extending clearing time up to months. This problem can be overcome using different water-based reagents with low viscosity as 2,2'- thiodiethanol (TDE) and FocusClear (Chiang et al., 2002; Staudt et al., 2007; Aoyagi et al., 2015; Costantini et al., 2015). The use of this latter is limited by its expensive cost.

On the other side, hyperhydrating reagents operate increasing osmotic pressure and water flux inside the cell. The water entrance tries to maintain an aqueous environment for fluorescence preservation, while the simultaneous use of detergents for lipid

removal lowers the tissue RI. Hyperhydrating reagents are also used to hydrate and often partially denature proteins, the other major tissue component, further reducing the overall RI closer to that of water. Miyawaki group has discovered the clearing ability of urea, thereby developing *Scale* approach (Hama et al., 2011). Urea is able to simultaneously penetrate and to break protein folded regions, requiring water to adjust RI. *Scale*, which involves urea, glycerol, and a detergent (Triton-X), was the first technique taking advantage of hyperhydrating reagents. In general, these protocols produce abundant hydration that leads to an optimal "specimen-transparentizing" but causes sample swelling. Therefore, in the *ScaleS* method, the substitution of glycerol with sorbitol was used to avoid the deformation and expansion of the sample (Hama et al., 2015). Although hydrophilic methods have overcome fluorescence preservation problems relative to the use of organic reagents, they require lengthy incubation times (from days to months) to clear only small portions of tissue. Starting from the ingredients of *Scale* solution, Ueda group has developed an alternative approach called CUBIC. The aim was to clear entire organs and to accelerate clearing process without losing safety and preservation of protein function, typical of this clearing class (Susaki et al., 2014; Tainaka et al., 2014). They have screened many chemical agents and find that a series of amino alcohols have both decolourization and delipidation function. Therefore, a mixture of selected amino alcohols, together with Triton-X and urea, have included in CUBIC protocol. High concentrations of Triton-X maximize lipid removal, but also damages some protein epitopes. To allow whole-mount immunostaining, CUBIC protocols found an optimal concentration of detergent that permeabilize membranes while preserving epitopes useful for antibody labeling. New CUBIC versions are extended even in the expansion microscopy (ExM) field (CUBIC-X) (Murakami et al., 2018). ExM is a method able to improve the resolution of light microscopy by physically expanding biological samples (Chen et al., 2015). This approach allows to reconstruct full details of small structures (i.e., synaptic connections). In conclusion, another strategy that exploits hyperhydrating reagents is *Clear*^{T} that uses a solution composed

of water and formamide. Starting from *Clear*^{T}, various methods were proposed as *Clear*^{T2} and RTF (Kuwajima et al., 2013; Yu et al., 2018).

5.3 Tissue transformation-based clearing methods

In the last years, new clearing approaches based on tissue transformation have been developed to combine the advantages of the abovementioned techniques. In 2013, Deisseroth group was the first to introduce a hydrogel-based clearing method, called CLARITY (Chung et al., 2013). The basic idea behind CLARITY is to transform a biological tissue, in our case brain, into a hydrogel-tissue hybrid. The hydrogel, which is mainly composed of acrylamide monomers, has the function of stabilizing dispersed proteins and nucleic acid by covalent bonds. Moreover, this hybrid construct has to support and preserve tissue architecture after lipid removal. In general, for every tissue, lipids have a structural function, but, as we have explained before, they are the primary source of scattering. Thus, their elimination facilitates achieving brain transparency. The removal of all lipids from the tissue using a high concentration of detergent (in this case, sodium dodecyl sulfate (SDS)) is a process that takes a long time, typically many weeks for an entire murine brain. To reduce the incubation time of the sample an electrophoretic field could be applied to accelerate the diffusion of the ionic detergent.

Furthermore, the large gel meshes allow macromolecule penetration, like antibodies or fluorescent dyes, and the hydrogel itself increases the preservation of epitopes. For this reason, CLARITY can often be coupled with immunostaining techniques for the imaging of large tissue. Passive diffusion of probes requires longer incubation times, and the application of stochastic electric field has thereby sped up their diffusion (Kim et al., 2015a). During the years, many variants of CLARITY have been implemented. Researchers have looked for alternative methods in which passive diffusion of detergent has been preferred to electrophoretic transport. Also, the index-matching solution Focus Clear has been replaced with cheaper ones. Thus, PACT, PARS,

CLARITY/TDE, CLARITY/glycerol are developed (Tomer et al., 2014; Yang et al., 2014; Costantini et al., 2015). Harsh conditions applied in the clearing process could cause troubles for protein antigenicity, fluorescence reporters, and tissue architecture. Chung lab has addressed these limitations by promoting two different techniques. SWITCH protects protein antigenicity for a rapid tissue clearing and unlimited rounds of antibody labeling (Murray et al., 2015) while SHIELD uses epoxides as chemical compounds able to create intra e intermolecular crosslinking in order to preserve fluorescence and probe binding capability (Park et al., 2019). Moreover, these hydrogel-based clearing approaches have demonstrated useful for super-resolution imaging, reconstructing details of neuronal projections, or even synaptic contacts (Ku et al., 2016). MAP technique exploits the idea of brain expansion, using a hydrogel that is isotropically expanded. However, in contrast to classic ExM, this approach avoids protein digestion, then the entire proteome is preserved. Although the elevated cost and long process, these hydrogel-based methods are commonly applied over the whole brain or other organs with much more safety than organic solvent ones.

Chapter 6

Quantifying neuronal activation across the entire murine brain

After tagging activated neurons and preparing samples for imaging, murine brains have to be reconstructed in 3D with some high-throughput optical microscope. In this section, we review imaging methods used for whole-brain activation mapping, together with the software tools necessary to extract quantitative information from raw data.

6.1 Imaging

Three-dimensional optical imaging of biological tissue is traditionally achieved using confocal (Conchello and Lichtman, 2005) or two-photon microscopy (Zipfel et al., 2003). These methods afford three-dimensional resolution (which is also known as 'optical sectioning') either by removing out of focus fluorescence with a spatial filter (confocal microscopy), or by restricting fluorescence excitation to the focus of the objective lens (two-photon microscopy). However, standard implementations of both techniques are not suitable for whole-brain reconstruction for two reasons. First, they are point-scanning methods, meaning that the image is reconstructed point-by-point. This approach is inherently slow, with typical volumetric imaging rates in the order of $10^{-4} \div 10^{-3}$ mm^3/s. Considering that a mouse brain is about 1 cm^3, this means that 10 to 100 days are needed to fully reconstruct one full murine encephalon. Second, optical sectioning in two-photon or confocal microscopy is proportional to the numerical

aperture (NA) of the imaging objective, i.e. the angle of emitted light that is collected by the lens. Typically, NA is inversely proportional to the objective working distance, i.e. the distance between the first lens and the focal plane. Thus, high-NA objectives, which are needed to achieve proper 3D resolution in confocal or two-photon microscopy, usually have limited working distances that cannot encompass the entire murine brain.

Optical sectioning: the ability of the microscope to distinguish light emitted from different planes, and thus providing real 3D resolution.

Numerical aperture (NA): is given by $n \sin \alpha$, n being the refractive index of the imaging medium and α the semi-aperture angle of the objective lens. Quantifies the amount of light gathered by the microscope, as well as the spatial resolution. In confocal and two-photon microscopies, it is also proportional to the optical sectioning of the apparatus.

Working distance: the distance between the first lens of the objective and the focal plane. It

To overcome these limitations several approaches have been developed during the years. Serial two-photon tomography (STP) incorporates a vibratome inside a standard two-photon microscope, reconstructing the volume by a continuous sequence of cutting and imaging operations (Figure 6.1a) (Ragan et al., 2012). In this way, only the sample layers closer to the vibratome cut are imaged, allowing the use of standard high-NA objectives with limited working distance. To reduce reconstruction times, a sampling strategy is usually adopted, acquiring 1 optical section (1 to 2 µm thick) every 50 or 100 µm. STP has been exploited to study neuronal activation in Fos-GFP and Arc-dVenus transgenic mice (Kim et al., 2015b; Vousden et al., 2015).

Speed-up of confocal microscopy can be obtained by parallel scanning. Spinning-disk approaches exploit multiple pinholes arranged on a rotating disk to image multiple spots simultaneously, increasing the volumetric imaging rate to 10^{-1} mm^3/s (Wilson, 2010). Seiriki and co-authors developed block-face serial microscopy tomography

(FAST), a spinning-disk confocal system coupled with a vibratome (Figure 6.1a) that can image entire mouse brains with micron resolution in 2.5 hours (Seiriki et al., 2017). The authors reported the use of FAST to map fluorescent neurons in Arc-dVenus mice during acute vs. chronic restraint stress (Seiriki et al., 2017).

Sectioning methods, like FAST and STP, are in general used without any tissue clearing since the microscope does not need to penetrate deep inside the sample. In addition, the specimen needs to be sufficiently stiff to be adequately cut by the vibratome, a requirement incompatible with most clearing protocols. On the one hand, avoiding tissue clearing simplifies and speeds up experimental procedures. On the other hand, this prevents exogenous staining of samples, limiting the application of these methods to animal models providing intrinsic fluorescence.

The technique of choice in combination with whole-brain clearing is light-sheet microscopy (LSM) (Dodt et al., 2007; Keller and Dodt, 2012; Ueda et al., 2020). In this method, the sample is illuminated from the side with a thin sheet of light, and fluorescence is collected along an axis perpendicular to the illumination plane (Figure 6.1a). In this way, optical sectioning is achieved in a plane-scanning rather than a point-scanning approach. LSM is thus considerably faster than confocal or two-photon microscopy: a whole mouse brain can be reconstructed in a time ranging from hours to minutes, depending on the resolution. Indeed, a key advantage of LSM is its flexibility: the resolution of the system can be modulated from tens of microns – sufficient to discriminate cell bodies when neuronal processes are not labeled – to less than one micron – allowing distinguishing axons and dendrites. Low-resolution LSM has the merits of a simple optical layout, and the reasonable size of the generated datasets; for these reasons, several groups were able to use it to study neuronal activation in large behavioral cohorts (Susaki et al., 2014; Renier et al., 2016; Tatsuki et al., 2016; Ye et al., 2016). However, when labeling of active neurons includes small processes, a sub-cellular resolution is needed to distinguish cell bodies from bundles of axons or

dendrites. For instance, Ye et al. used low-resolution LSM on TRAP mice and were forced to exclude several brain regions from their analysis (Ye et al., 2016). High-resolution LSM can instead produce a quantitative mapping of neuronal activation independently of the labeling strategy used. The challenges, in this case, are represented by the size of the datasets produced (usually exceeding one TeraByte per brain) and the need for more complex optical systems. Indeed, high-resolution imaging through several millimeters of tissue introduces optical artefacts even with the best possible clearing. For instance, specimen induced defocus needs to be corrected automatically to produce sharp images (Tomer et al., 2014; Silvestri et al., 2017; Matsumoto et al., 2019). Another issue that has to be addressed is the presence of shadowing artefacts introduced by adsorbing or scattering objects in the sample. Different methods have been proposed in this respect, including the use of non-Gaussian laser beams (Fahrbach and Rohrbach, 2012; Müllenbroich et al., 2018b, 2018a) and axial sweeping of the excitation light sheet (Chakraborty et al., 2019; Voigt et al., 2019). Anyhow, whatever optical improvement must rely on a good optical clearing, which is an essential prerequisite for the use of high-resolution LSM. The group of Hiroki Ueda has pioneered IEG mapping at subcellular resolution, demonstrating the potential of this approach to quantify neuronal activation across the entire murine brains without excluding any areas (Murakami et al., 2018; Matsumoto et al., 2019; Susaki et al., 2020).

Whatever the microscopy method used to image brain samples, the next step is to transform the raw images – which are just a matrix of gray values – into semantically relevant information. This process involves two different phases that could be performed in parallel: cell detection (Figure 6.1b) and atlas registration (Figure 6.1c).

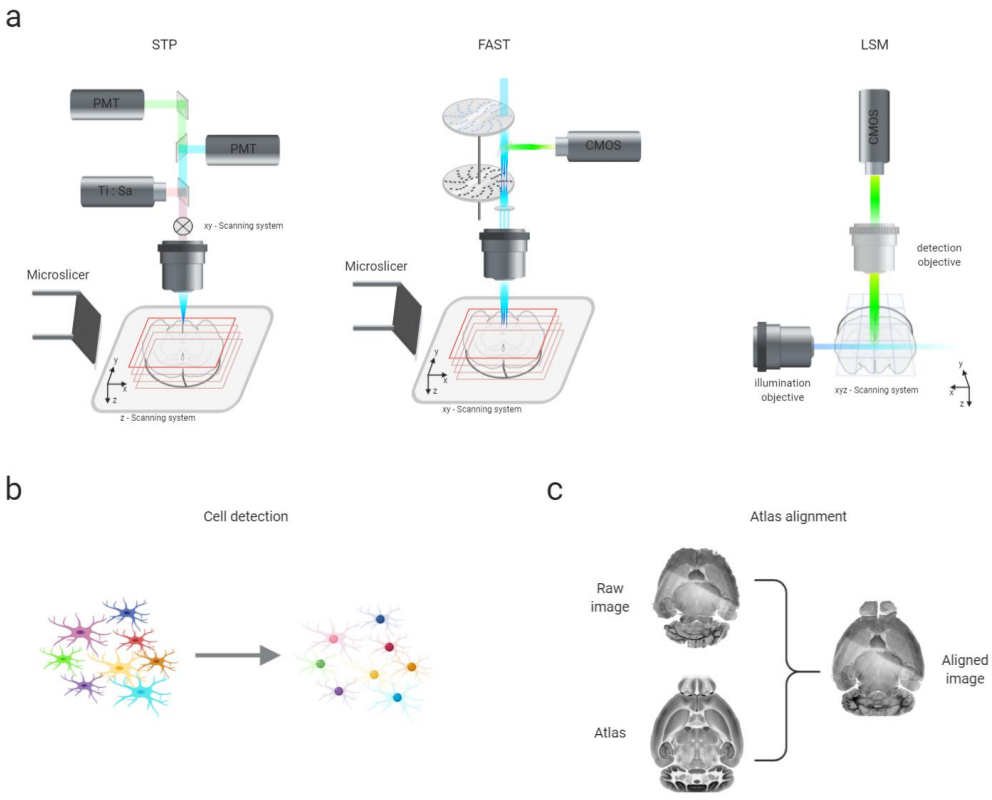

***Figure 6.1*: Representation of the three steps necessary to obtain neuronal quantification across the entire murine brain.** a) Scheme of advanced imaging approaches for whole-brain reconstruction: serial two-photon tomography (STP), block-face serial microscopy tomography (FAST), and light-sheet microscopy (LSM); b) Cell detection; c) Atlas alignment. Image from (Franceschini et al., 2020).

6.2 Cell detection

Automatic detection or segmentation of labeled cells is a well-known problem in biomedical image analysis, and many different methods have been developed during the years (Acciai et al., 2016; Magliaro et al., 2019). However, whole-brain images present some peculiar challenges that need to be faced. First, datasets are usually extensive, ranging from tens of GigaBytes to tens of TeraBytes for a single sample. Thus, algorithms must be fast and scalable. Second, in LSM images, the contrast is very heterogeneous between deep and superficial brain regions since excitation and fluorescence cross variable thicknesses of biological tissue. Third, when the entire neuron is filled with the fluorescent label (e.g. when using transgenic strategies), an additional problem is represented by the presence of bright axons or dendrites, which may confound the detection algorithm.

Standard pipelines for cell detection use a combination of filters to homogenize contrast and highlight spherical objects, followed by adaptive thresholding of the images and then some operations/filters on binary data to refine segmentation. Such pipelines are highly parametrical: estimation of parameters is usually done on a small training set of manually annotated images. Sometimes, different sets of parameters are estimated for different brain areas to improve accuracy (Seiriki et al., 2017). Standard image processing pipelines are effective when labeling is confined to cell bodies, as in anti-c-fos IHC (Renier et al., 2016), or when imaging quality is highly homogeneous, as in STP (Ragan et al., 2012) or FAST (Seiriki et al., 2017). Their use in LSM images of transgenic animals has been sometimes reported, but on a subset of brain regions (Ye et al., 2016), or on the whole brain but without a clear evaluation of the accuracy of the results (Menegas et al., 2015; DeNardo et al., 2019).

Machine learning approaches can be used to cope with complex or inhomogeneous images. In these methods, a model for classification of pixels or image transformation

is trained using example data ("ground truth") provided by the user. As a general principle, the performances of the model increase with its complexity (the number of hidden parameters). However, more complex models require more ground truth for successful training. Thus, in practice, a trade-off between performances and manual annotation has to be found.

Ilastik (Berg et al., 2019) is a popular image processing tool implementing simpler models – a random forest classifier based on a set of user-defined image features. This software allows real-time training and testing, together with a user-friendly environment suitable also for researchers with limited background in computer science. Menegas and co-workers reported its use in whole-brain LSM images, albeit not for an application related to IEG mapping (Menegas et al., 2015).

More sophisticated models, like the multi-layered neural network used in the emerging field of deep learning (Gupta et al., 2019), have the potential to process images with human-level (or even super-human) performances. They are an established standard in the analysis of natural images, and their application to whole-brain image analysis have been reported (Kim et al., 2015b; Kirst et al., 2020; Todorov et al., 2020). Even if they are extremely powerful, their use is still quite limited in the field, probably because they need large human-annotated training datasets. In this respect, strategies to speed up labeling, e.g. by pinpointing the position of the neuronal soma rather than segmenting the neuronal volume, are promising to generate annotations much faster (Frasconi et al., 2014; Silvestri et al., 2015).

6.3 Spatial registration to reference atlas

Detected cells must then be assigned to a specific brain region to allow precise quantification of which areas are elicited during a specific behavior. Albeit anatomy experts can directly draw major regions on the collected images (Seiriki et al., 2017), the standard choice is to refer to standard atlases, like the classic Franklin and Paxinos (Paxinos and Franklin, 2004) or the more recent one from the Allen Institute for Brain Science (Jones et al., 2009). This latter is the average of more than 1'000 whole-brain images obtained with STP, and is associated with a 3D parcellation operated by a group of expert neuroanatomist. By registering, i.e. aligning, a sample image to the atlas template (or vice versa), detected cells can be directly assigned to a specific brain region.

Image registration is performed by finding the best transformation mapping one image into the other and is thus defined by the transformation itself, a quality metric, and an optimization strategy. Inter-sample differences are usually quite significant, both because of biological variability (Scholz et al., 2016) and of the deformation introduced by chemical clearing (Kutten et al., 2016). Global affine transformations, which are composed of translation, rotation, global (anisotropic) scaling, and shear, are usually not enough to match samples and reference. Conversely, non-linear local transformations, like B-spline (Klein et al., 2010; Fürth et al., 2018) or symmetric diffeomorphisms (Avants et al., 2011; Kutten et al., 2016), can recover sample deformations and provide reliable mapping onto the atlas.

The parameters of any transformation are obtained by maximizing some measure of registration quality. The most commonly used are cross-correlation – which works nicely for images sharing the same type of labeling – and mutual information – which performs well when the datasets are based on different stains. Coupling the quality metrics of choice with a suitable optimization algorithm, it is then possible to find the

best transformation mapping the sample to the atlas or vice versa. The most commonly 3D registration tools used in the field are probably Elastix (Klein et al., 2010) and ANTs (Advanced Normalization Tools) (Avants et al., 2011), and they have also been incorporated in larger projects like ClearMap (Renier et al., 2016) or CUBIC-X (Murakami et al., 2018).

In practice, registration is performed on images at coarse resolution, typically 25 µm pixel size or worse. To facilitate the process, a reference channel containing either tissue autofluorescence (Kim et al., 2015b; Menegas et al., 2015; Renier et al., 2016; Ye et al., 2016) or some kind of nuclear staining (e.g. propidium iodide (Murakami et al., 2018)) is used rather than the channel related to labeled cells. Several authors also suggested to first perform a mutual registration of all the samples into an 'average brain', followed by semi-manual registration of this latter to the reference atlas (Vousden et al., 2015; Ye et al., 2016; Murakami et al., 2018). Finally, it is worth noting that direct 3D registration is often quite challenging, especially for cleared samples that underwent severe deformations. Some groups proposed hybrid strategies, where a first 3D coarse alignment is followed by 2D accurate registration slice-by-slice (Tainaka et al., 2014; Fürth et al., 2018; Murakami et al., 2018).

Part II

Methods

Chapter 7

Methods

This chapter explains the innovative techniques used to perform the fear memory engram.

7.1 Animals

Male and female FosTRAP mice (B6.129(Cg)-Fos$^{tm1.1(cre/ERT2)Luo}$/J × B6.Cg-Gt(ROSA)26Sor$^{tm9(CAG-tdTomato)Hze}$/J) were used for this work (Guenthner et al., 2013). They were housed in groups, giving the opportunity to behave as 'social animals'. Mice received food and water ad libitum and were maintained in a room under controlled light and dark cycle (12/12 h; light starts at 7:00 AM), temperature (22 ± 2 °C), and humidity (55 ± 10 %). Adult mice (aged between 3 months and 6 months) were divided in four groups: homecage (n=5 males, n=5 females), training (n=5 males, n=5 females), test 24h (hours) (n=5 males, n=5 females) and test 7d (days) (n=5 males, n=5 females). All experimental procedures were approved by the Italian Ministry of Health (Authorization n. 512-2018_FC). Alternatives to in vivo techniques were not available, but all experiments were conducted according to principles of the 3Rs.

7.2 IA task

All mice were trained and tested using the behavioral paradigm, step-through inhibitory avoidance (IA). Behavioral procedures were performed in a sound-

attenuated room, during the light cycle. The day before the experiment, mice were placed in this room for the habituation. Each mouse was subjected to the task separately, and care was taken to remove any olfactory tracks of previous experiments by cleaning the box. The apparatus consists of an automatic controller and a box (47x18x25(h)cm, Ugo Basile, Comerio, Italy) which is divided into two separate compartments by a sliding door (Figure 7.1). The start compartment is brightly-illuminated while the escape one is dark and connected to the shocker (Figure 7.1).

***Figure 7.1*:** Ugo Basile Step-through instrument. Designed for Mice.

During the training session, every mouse was gently placed in the brightly-illuminated compartment, facing the door and allowing free access to the dark compartment. The apparatus is designed to exploit the natural behavior of mice to go into the darkness. For this reason, they rapidly step through the door and then received a 0.3 mA mild

foot-shock lasting 2 s. Latency was measured using an automated tilting-floor detection mechanism. After the foot-shock, mice were immediately removed from the dark box, and consequently, they received the 4-TMX injection.

The retention test was carried out 24 h or 7 d after the training session. All mice were trained, and a part was tested 24h after training while the other, 7 d after. During the test, trained animals were placed again on the start compartment until they eventually enter into the dark one. The procedure was the same, but mice do not receive any shock during this phase. Five minutes is the maximal latency time given for stepping through, and it is measured by the same automated mechanism. At the end of 300 s, mice, that do not step through, are removed from the apparatus. After removal from the system, all animals received the 4-TMX injection. The latency to step through was considered a direct measurement of memory.

For the control group, mice were left in their cage during the entire behavioral procedure and they received 4-hydroxytamoxifen (4-TMX) injection, simultaneously with other groups.

7.3 Delivery of 4-hydroxytamoxifen

Mice were handled and got used to needle pain with saline solution daily for at least 3 days prior to the 4-TMX injection.

4-TMX (Sigma H6278) was first dissolved in absolute ethanol to give a final concentration of 20 mg/mL. This stock was then mixed with corn oil (Sigma C8267) at 37 °C in order to get an emulsion. The injectable oil formulation at the final concentration of 50 mg/kg was obtained using the Eppendrorf ThermoMixer® C. The emulsion was heated and shaken for 2 hours until the ethanol was entirely evaporated.

At this time, the drug was totally dissolved in corn oil and kept at 37°C. 4-TMX was delivered by intraperitoneal (i.p.) injection through an injection needle 22 gauge.

7.4 Ex-vivo processing and CLARITY

One week after the tamoxifen injection, animals were deeply anesthetized isoflurane (1.5%–2%) and transcardially perfused with 50 mL of ice-cold 0.01 M phosphate buffered saline (PBS) solution (pH 7.6), followed by 75 mL of freshly prepared paraformaldehyde (PFA) 4% (wt/vol, pH 7.6). Brains were extracted and prepared according to the CLARITY/TDE protocol (Chung et al., 2013; Costantini et al., 2015) (Figure 7.2). Immediately after perfusion, brains were post-fixed in PFA overnight at 4°C. The day after, samples were incubated in a hydrogel solution (containing 10% acrylamide (vol/vol), 2.5% bis-acrylamide (vol/vol) and 0.25% VA044 (wt/vol) in PBS) at 4°C for 3 days, allowing a sufficient diffusion of the solution into the tissue. Samples were then degassed, replacing oxygen inside the vials with nitrogen, and incubated in a water bath at 37°C for 3 hours in order to initiate polymerization of the hydrogel. After 3 hours, embedded brains were placed in a clearing solution (containing 4.4 % (wt/vol) sodium dodecyl sulfate (SDS) and 1.2 % (wt/vol) boric acid in ultra-pure water, pH 8.5) at 37°C. Clearing solution was changed every 2-3 days. Specimens were gently shaken throughout the whole clearing period, which typically takes 3-4 weeks. When the samples appeared sufficiently transparent, they were incubated 1 day in PBS with 0.1 Triton-X (PBST, pH 7.6) and 1 day in PBS (pH 7.6), removing the excess SDS. Finally, murine brains optically cleared with serial immersions of mixtures containing 20% and 40% 2-2’ Thiodiethanol (TDE) in PBS, each for 1 day while rotating. The last mixture (40% TDE) was used as index-matching solution for our imaging (Figure 7.2) (Di Giovanna et al., 2019).

PROTOCOL

perfusion and fixation

hydrogel infusion and hybridization (4°C)

passive tissue clearing (37°C)

2,2'-Thiodiethanol (TDE) matching by refractive index

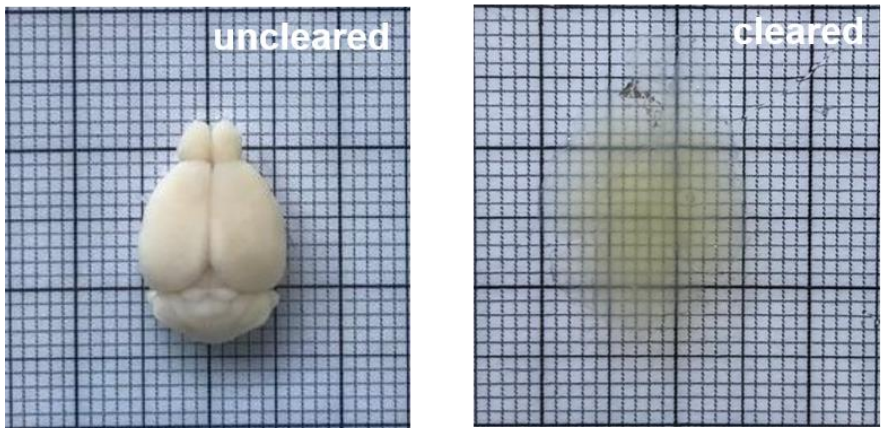

***Figure 7.2*: CLARITY technique**. **Top** Scheme representing CLARITY/TDE protocol used for all brains. **Bottom** On the left a brain sample in PBS before CLARITY process; on the right, the same sample in TDE before imaging.

7.5 Immunohistochemistry

After whole-brain imaging, brains were brought back into a solution containing 20% TDE for 1 day and then washed for 3 days in PBS. A thick section (0.7x0.5x0.5 cm) containing the TMN was isolated through a brain matrix and preincubated in PBST at room temperature (RT) overnight. Then, the section was incubated with HDC (03-16045 Rabbit-histidine decarboxylase, American Research Product) primary antibody (dilution 1:100 in PBST) at 4 °C for 3 days. After a further day-long PBST washing, the section was incubated with an AlexaFluor ®647 (cat. Ab 150079 Goat Anti-rabbit) secondary antibody (dilution 1:200 in PBST) at RT for 2 days. In order to remove antibody excesses, the thick section was washed again in PBST at RT for one more day. Last steps provided for sample fixation in PFA 4% for 10 minutes at 4°C and sample washing in PBS for 3 cycles of 15 minutes at RT. Before imaging with the light-sheet microscope, specimen was optically cleared with a solution containing 40% TDE in PBS.

7.6 Light-sheet fluorescence microscope and imaging

The entire cleared mouse brains, and their respective TMN were imaged using a custom-made confocal light sheet microscope (LSM), described in detail in

[Muellenbroich et al., Neurophotonics 2015] (Figure 7.3). Briefly, a laser beam, at either 561 nm (Jive 50 mW, Cobolt AB, Sweden) or 638 nm (06-MLD 180 mW, Cobolt AB, Sweden) wavelength, was expanded and collimated. The power delivered to the specimen was adjusted using and acousto-optical tunable filter (AOTFnC- 400.650- TN, AA Opto-Electronic, France). The light sheet was then generated using a galvanometric mirror (6220H, Cambridge Technology, United States) followed by a 4f system and an objective lens (Plan Fluor EPI, 10x, 0.3NA, WD 17.5 mm, Nikon, Japan). Fluorescence emission was collected through a specialized immersion objective (XLPLN10XSVMP, 10x, 0.6NA, WD 8 mm, Olympus, Japan), bandpass-filtered by a fluorescence filter (Semrock FF01-609/54 and FF01-676/37 for tdTomato and AlexaFluor, respectively) and focused by a tube lens (180 mm focal length) onto the chip of an sCMOS camera (Orca Flash4.0, Hamamatsu Photonics, Japan). The camera was run in light-sheet mode, allowing confocal line detection. RAPID autofocusing was used to keep images sharp throughout acquisition [Silvestri et al., bioRxiv 2017]. The entire system was controlled with custom software written in LabVIEW (National Instruments, United States) (Figure 7.3).

Optical resolution measured in the plane was 1.35 µm, while along the z axis was 8.6 µm (Di Giovanna et al., 2019). Voxel size in the x,y and z axis was 0.65x0.65x2 pixel. Given the limited field of view of the microscope (approximately 1.3x1.3 mm^2), whole-brain datasets were acquired as a grid of partially overlapping image stacks. Tiles were subsequently aligned using ZetaStitcher (https://lens-biophotonics.github.io/ZetaStitcher/). The microscope allows laser excitation from two opposite directions; for each stack, we used the closer illumination arm in order to reduce the distance traveled by excitation light inside the sample. Likewise, to minimize the fluorescence optical path inside the sample, we adopted a dual-side detection scheme. However, our microscope does not have 2 detection arms. Thus, we imaged the half of the sample closer to the detection objective (Figure 7.4a), then we rotated

the specimen by 180 degrees and imaged the other half, with an overlap of about 1 mm (Figure 7.4b).

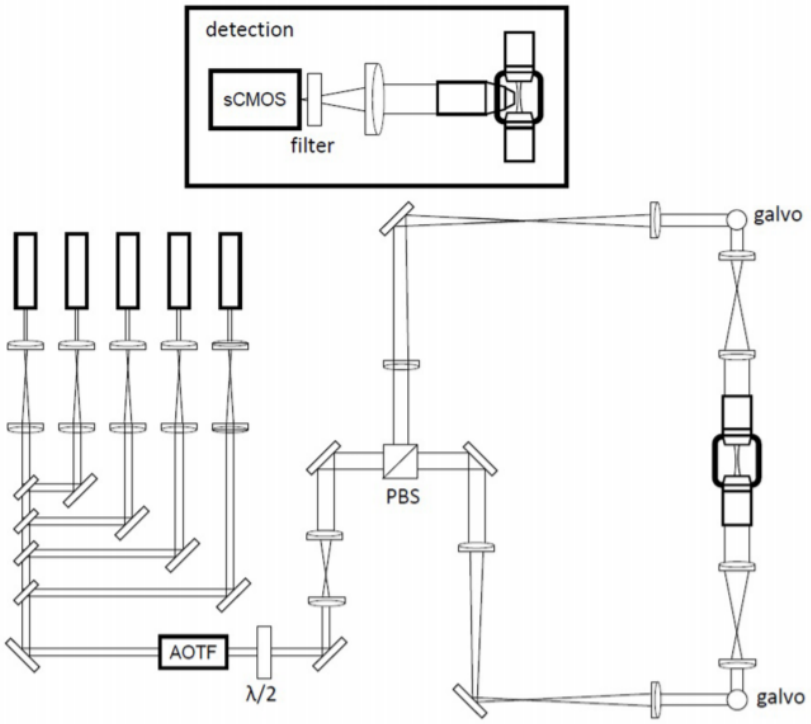

***Figure 7.3*: Schematic representation of our custom-made light-sheet microscope** (Di Giovanna et al., 2019). A battery of five laser lines is multiplexed into a common beam path with long-pass filters. An AOTF (acousto-optical tunable filter) is used as a shutter and for power regulation. Double-sided illumination is generated by rapid scanning of the excitation beam with galvanometric mirrors in two equivalent excitation arms selected by input polarization via a half-wave plate (λ/2) and polarization beam splitter (PBS) combination. The galvanometric mirrors are mounted above periscopes. Inset: detection path in a wide-field configuration using a specialized objective for direct immersion in high-refractive-index (RI) media and a sCMOS (scientific complementary metal oxide semiconductor) camera.

***Figure 7.4*: Schematic representation of two-halves imaging**. The brain half, closer to the objective, was imaged first (A). Then, the sample was rotated and the other half was imaged (B).

7.7 Atlas registration

As a preliminary step, the images of the two brain halves (Figure 7.4) were aligned together and fused in a single whole-brain volume. To this aim, a downsampled version of the two datasets (voxel size 25 µm) were used. Non-linear gamma correction (γ = 0.3) was applied to the downsampled images to enhance the contribution of tissue autofluorescence. Brain halves were spatially registered with Advanced Normalization Tools (ANTs, http://stnava.github.io/ANTs/), using an affine transformation and normalized cross-correlation as similarity metric. After alignment, images were blended together with a custom python script that averaged the two volumes in a user-defined transition area.

The fused volume was then registered to the Allen reference atlas (voxel size 25 µm), again using ANTs. First, an affine transformation was performed for gross alignment

(Figure 7.5). Then, to correct large deformations introduced by sample clearing, three brain regions (olfactory bulbs, hippocampi, cerebellum) were manually segmented using Amira 5.3, producing a binary mask. This mask was aligned to the corresponding one segmented out of the reference Atlas using a diffeomorphic non-linear transformation (SyN) (B. B. Avants et al., 2008) and normalized cross-correlation as metric. This transformation was then applied to the grayscale image. Final SyN registration was performed on the grayscale volume, using mutual information as similarity metric. All image transformations (both affine and SyN) were stored and subsequently applied to the point cloud produced by the cell detection algorithm (paragraph 7.9), to obtain cell counts for each brain region.

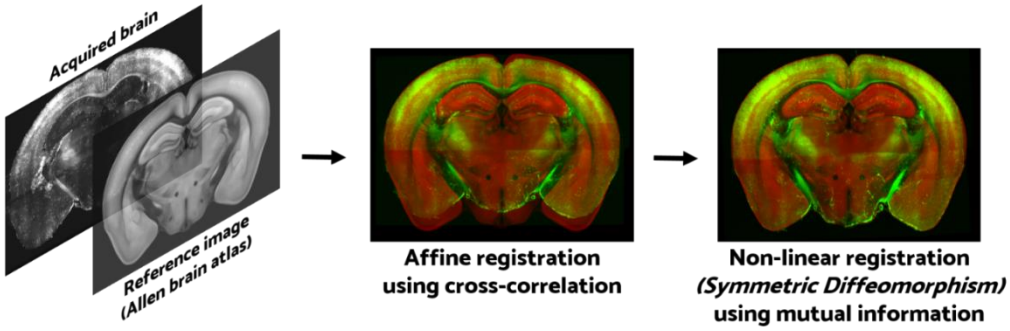

***Figure 7.5*: Light-sheet images aligned to the Reference atlas**. 3D image registration has been performed @ 25µm resolution using Advanced Normalization Tools (ANTs). Reference Atlas images are in red and LSM images are in green.

7.8 Cell detection

Fluorescently activated neurons were localized in the whole-brain images using a modified version of BrainCell Finder[13]. Briefly, patches of the original dataset were fed into a UNet with 4 contraction layers of 3D convolutions with exponentially increasing number of filters and 4 expansion layers of transposed 3D convolutions with decreasing number of filters. UNet training was carried out with binary cross-entropy loss and Adam optimizer. The goal of this network is to transform the original image into an ideal one. In this ideal image, cell bodies are clearly visible, whereas disturbing objects as structures like dendrites and axons are removed. In this way, only small spheres at the location of neuronal bodies were detected. The network was previously trained on a ground-truth dataset where human experts have localized the center of neuronal somata. The training dataset was composed of 221 image stacks for a total volume of about 6.8 mm^3 and 19'166 manually labeled cells. The stacks were not all from the same brain region but are randomly selected from different areas, in order to train the network to recognize the large variability in cell shape that can be found across the sample. The images deconvolved by the network are then processed with a standard blob detection algorithm (Difference of Gaussians, DoG). This algorithm was able to prove center of bright structures, which in this case represent activated neurons. A list of neuronal centers found by the software were compared with human-annotated ground truth on a test set of 57 image stacks for a total volume of about 1.8 mm^3 and 1'786 manually labeled cells. These stacks were also randomly selected from different areas of the brain, in order to increase network performance. If two neuronal centers from the two annotations (automatic and manual) are closer than 10 μm (roughly half of the average diameter of a neuron), they are considered to be the same cell, i.e. a true positive (TP). If a center is present only in the manual annotation, it is considered a false negative (FN), whereas if it is present only in the results of the algorithm, it is considered a false positive (FP). Maximum Bipartite Matching algorithm was used to

quantify TP, FP and FN (Galil, 1983). We evaluated localization performances using precision = TP/(TP+FP), recall = TP/(TP+FN) and F1-score (defined as the harmonic mean of precision and recall). On our test set, we found precision 0.80, recall 0.64 and F1-score 0.71., All annotations of cell positions were performed using Vaa3D (https://github.com/Vaa3D).

7.9 Quantification of histaminergic neurons activated during behavior

For all TMN samples, the two channels (tdTomato and anti-HDC staining) were acquired sequentially using our LSM. They were merged afterward in ImageJ. In the 2-color fused images, neurons that express tdTomato fluorent protein and the fluorophore conjugated to the HDC antibody, were easily detectable. Using an ImageJ plugin ("Name Landmarks and Register"), a quantification of all colocalisations was manually performed in the entire TMN. This tool registers and enumerates in a volume the colocalizations by three numbers (x,y,z). Individual stacks were put together in a point cloud using a custom script written in Python, and visualized using either CloudCompare (https://www.cloudcompare.org) or Paraview (https://www.paraview.org).

7.10 Point Cloud alignment to a Reference Atlas

All point clouds were manually aligned with a Reference Atlas through some points of interest.

Five points of interest were selected in three sequential coronal slices. For each slice, points were always annotated in the same order, from the 1 to 5 using the same imageJ plugin used for colocalizations (Figure 7.6). Then, the same annotations (from 1 to 5) were performed on the same Reference slices. Using a custom script by Python, the Point Cloud was successfully aligned to the Reference Atlas.

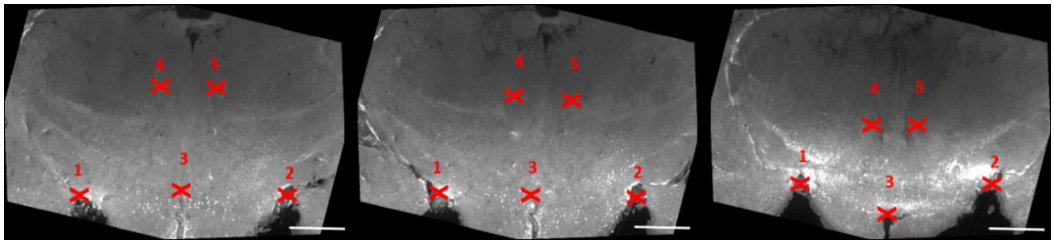

***Figure 7.6*: Protocol for image registration to the Atlas.** Image reveals the annotations of five points necessary for the Atlas Registration. In the picture, three sequential slice of a TRAINING sample, completely labelled with anti-hdc antibody is shown. In each slides, white spots represent histaminergic neurons. Image acquired with LSM. Scale bar 1 mm.

7.11 Statistical analysis

Regional cell counts of animals from different experimental group or sex were compared using Welch t-test (which assumes unequal variances) with false discovery rate (FDR) (Benjamini & Hochberg, 1995) to account for multiple comparisons (stars in red) and without correction for multiple comparisons (stars in black). Simultaneous evaluation of group and gender effects was performed using standard Analysis of Variance (ANOVA). Voxel-based analysis was carried on by generating for each sample a heatmap with voxel size 25 µm where a bright sphere of 200 µm radius was centered around every detected cell. Correlation between step-through latency times and regional counts was calculated using Pearson correlation. Significance level were determined using t-test without correction for multiple comparisons. All statistical analysis was performed using custom scripts in Python.

7.12 Graphics and image visualization

All drawings in this thesis were created using the online software Biorender while brain image stacks were performed and analyzed using the open source image processing program, ImageJ Fiji (https://fiji.sc). 3D renderings of brains were produced using image processing software, Amira 5.3 (Visage Imaging) through the Voltex function. Graphs and data analysis were done with GraphPad Prism 6 (GraphPad Software), OriginPro (OriginLab Corporation), or with custom code written in Python (https://www.python.org).

Part III

Results

Chapter 8

Results I

The purpose of this thesis was the development of a pipeline able to visualize whole-brain activity patterns in order to understand how neuronal circuits are implied in different aversive memory phases (Figure 8.1). The developed method was then applied to quantify neuronal activations in various brain regions, analyzing differences between various experimental classes and focusing on a small nucleus, TMN, known for its involvement in memory functions.

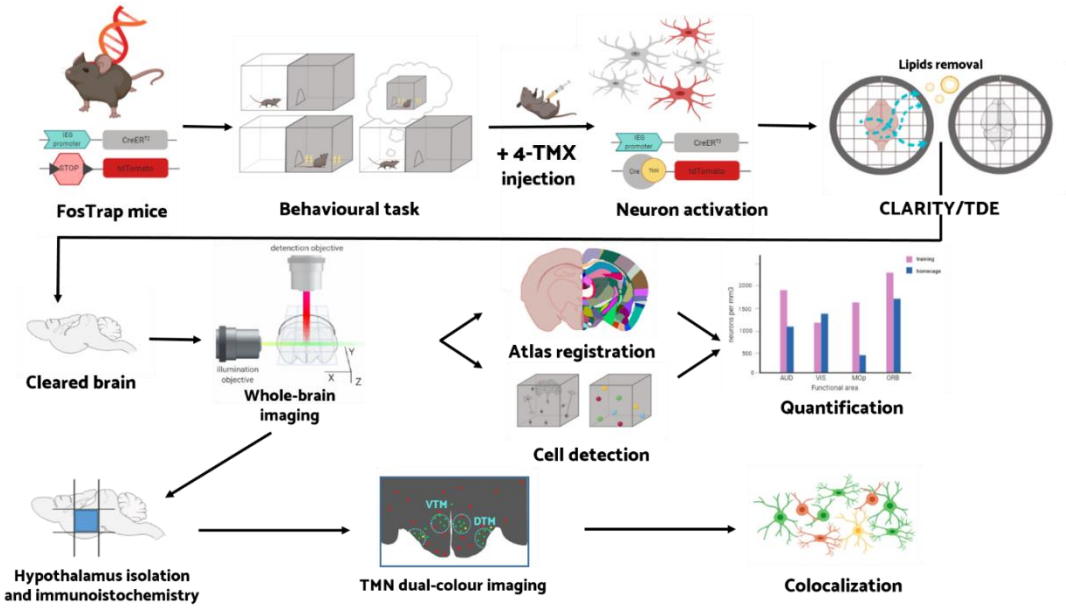

***Figure 8.1*: Experimental pipeline**. Schematic representation of various steps that constituting experimental pipeline developed in this thesis.

8.1 Characterization of a pipeline for the reconstruction of brain-wide maps during different aversive memory phases

Understanding large-scale neuronal patterns involved in learning and retrieval of fear memories requires new techniques based on whole-brain approaches.

Nowadays, there is no unique way of visualizing neuronal activation on a brain-wide scale. Therefore, I developed a pipeline, exploiting existing techniques, and optimizing them to fit our purpose best. Combining FosTrap transgenic strategy, CLARITY/TDE, LSM and data analysis, it was possible to quantify activated neurons during different aversive memory phases. Differently from previous reports (Renier et al., 2016a; Ye et al., 2016) I used high-resolution imaging, enabling going from general to the specific. Starting from the whole brain, then I focused on a small hypothalamic nucleus, the TMN.

Here, I am going to describe in detail every single part of this pipeline that ranges from genetics to imaging and image analysis, ending with the examination of a small nucleus as TMN. Apart from the characterization of this pipeline, the major result was the large-scale reproducibility of this method and the ability to use it in a routine way.

8.1.1 Effects of different shock intensities on fear memory retrieval

The study of fear memory involves the employment of fear learning paradigms, able to create robust memories. In this pipeline, I decided to use step-through IA, one of the most studied forms of fear learning in the past 60 years (Ivan Izquierdo et al., 2016). Step-through IA is a behavioral paradigm, classically used to assess fear memory on small laboratory animals in which the subject learns to associate a particular context

with the occurrence of an aversive event (e.g., an electrical shock). This task (briefly schematized in Figure 8.2) is based on the suppression of the innate preference of rodents for the dark compartment of the test apparatus following exposure to an inescapable shock. In general, the robustness of aversive memory is assessed by the latency time before entering into the dark compartment. Therefore, the shock should be strong enough to create a memory that persists over time. Consequently, the evaluation of shock intensity was my first goal.

In order to carefully design our behavioral task, the first set of experiments was based on a comparison of four different shock intensities, evaluating the impact of those ones on animal retention (Figure 8.3a). Taking scientific literature as benchmark, I evaluated four increasing foot shock values, 0.1 mA, 0.2 mA, 0.3 mA, 0.5 mA (Figure 8.3b) (Baarendse et al., 2008; Burwell et al., 2004; Fendt & Fanselow, 1999).

I tested mice 24h and 7d after training, and found that 0.3 mA value was the most appropriate to our scope because all mice remembered what happened during the training, and there was also inter-individual variability. Meanwhile, 0.1 and 0.2 mA shock intensities have proven to be weak and consequently, they did not have a strong impact on LTM and short long-term memory (SLTM). On the contrary, 0.5 mA value was too high, showing no variability between experimental groups. Therefore, in this case, the foot shock was more comparable to a trauma rather than an aversive event.

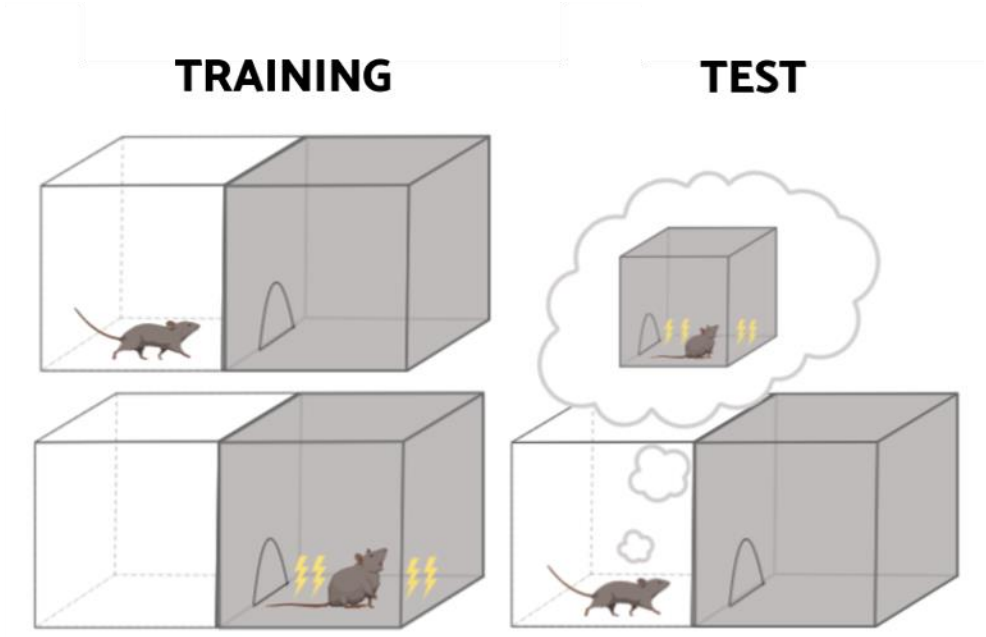

Figure 8.2: **Step-through IA task**. This procedure consists of placing a mouse on a grid in a brightly-illuminated compartment and allowing free access to the dark compartment where it will receive a mild foot shock during the training section. During the test session, upon re-exposure to the same environment, the latency to go into the dark section is considered a direct measurement of memory.

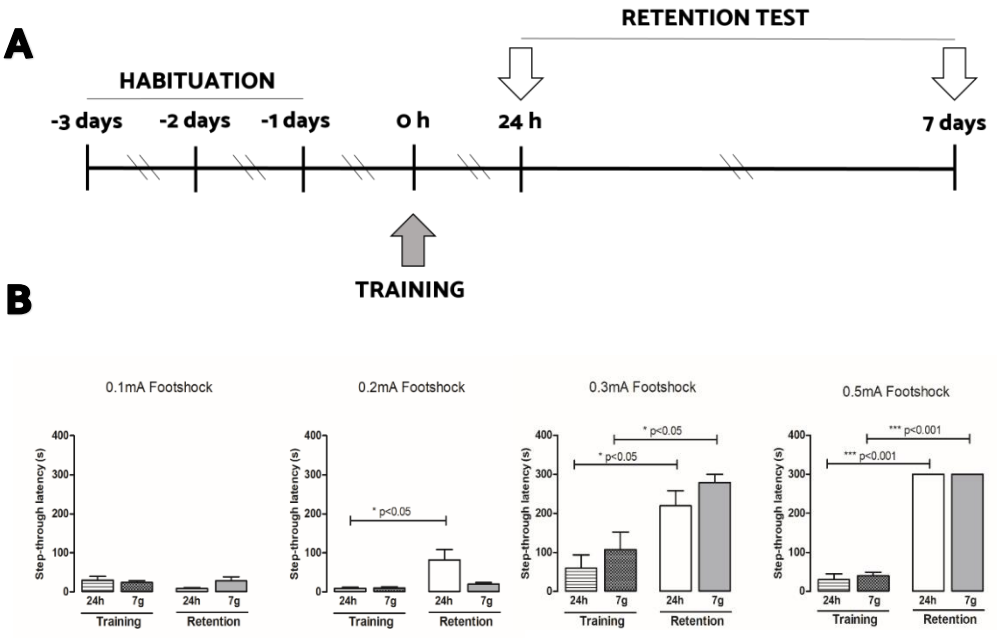

Figure 8.3: **Evaluation of four shock intensities for the optimization of step-through paradigm**. (A) The schematic drawing shows the sequence of procedures. Animals are handled for three days before training. During training session, all mice receive a foot-shock. Test is performed 24h or 7 days after training (B) The comparisons of acquisition and retention latency times are analyzed by 1-way ANOVA, followed by Bonferroni's post-hoc comparisons tests. Data are expressed as means ± SEM of 7 to 10 animals for each group.

8.1.2 Evaluation of short- and long-term memory in FosTRAP mice

Once the shock intensity was determined, to observe how memory varies at different time points in FosTRAP mice, we compared the results of different experimental classes. In particular, the influence of gender on fear memory retrieval was examined.

I chose four experimental groups of both genders in order to study various phases of aversive memory. The first group is called **HOMECAGE**, also known as the control group. This group did not undergo IA and consequently, its brain activations were considered as basal. The second group or **TRAINING** group was chosen to study the formation of fear memory while the remaining classes, **TEST 24H** and **7D** after training were selected to assess different retrieval of SLTM and LTM.

With the aim to investigate gender differences in memory retrieval, I examined the performances of these groups in one-trial step-through IA. No statistically significant difference was found between latency times of male or female animals in the same experimental group (Figure 8.4). Whereas, there is a statistically significant difference between training and test times in both genders, indicating that all mice formed a trace of memory independently from their sex.

Interestingly, observing all latency times, we found animals tested 24h after training show lower latency times comparing with animals tested 7 days later (MALE 123,7+/-95,5 and 174,7+/-125,4 FEMALE 147,2+/-130,4 and 245,9+/-114,7 respectively, mean +/-SEM). Although with our cohort, this trend is not statistically significant, it is nevertheless consistent with the fact that memory well-consolidated are likely more robust and hardly extinguishable (Albo & Gräff, 2018). This view could suggest that memory retention increases with time.

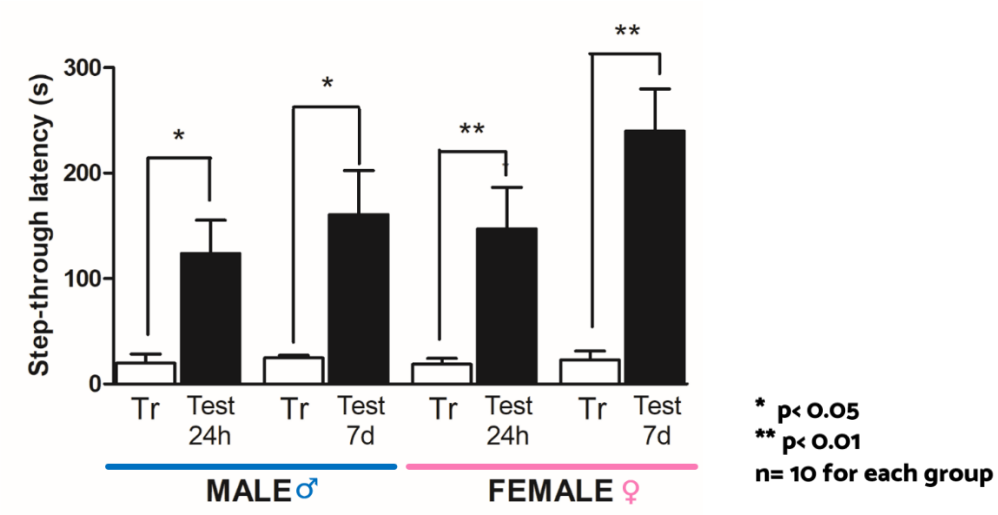

Figure 8.4: **Result of one-trial step-through IA**. The comparisons of acquisition and retention times are analyzed by 2-way ANOVA, followed by Bonferroni's post-hoc comparisons tests

8.1.3 Trials of tamoxifen administration to maximize neuron activations across the entire brain

In my thesis, I used a particular transgenic mouse line, FosTRAP mice (Guenthner et al., 2013). TRAP approach needs a tamoxifen injection for neuronal activation because it uses the Cre-Lox recombination with CreER^{T2}, an inducible variant of Cre recombinase (Figure 8.5). TRAP strategy requires two transgenes: one that expresses CreER^{T2} from an activity-dependent IEG promoter and the other that allows expression of an effector gene, such as tdTomato, in a Cre-dependent manner. Without 4-TMX, CreERT2 is retained into the cytoplasm of active cells, so there is no recombination. In the presence of 4-TMX, cells expressing CreER^{T2} – i.e. activated cells – undergo recombination and therefore express the tdTomato. Due to the transient nature of IEG transcription, CreER^{T2} is present for a limited time window following neuronal activation, and simultaneously the lifetime of 4-TMX is limited by metabolism and

excretion. Therefore, only neurons that are active within a limited time window around drug administration can be TRAPed.

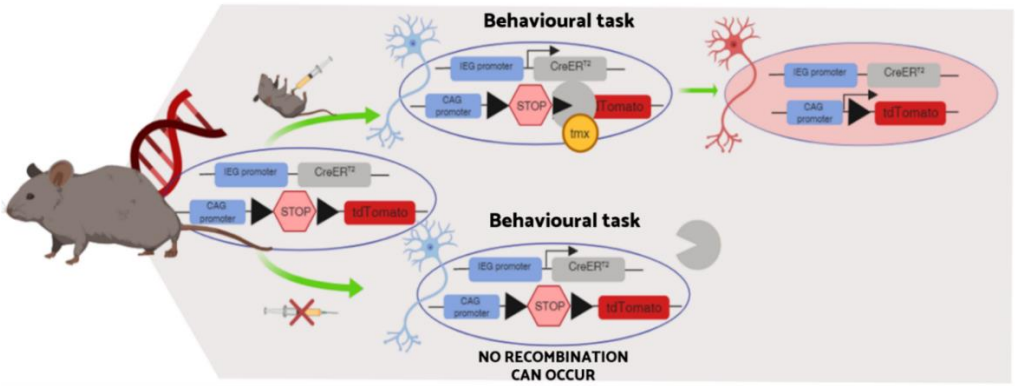

Figure 8.5: **Scheme of TRAP approach**. Figure shows the mechanism of TRAP transgene. Rectangles indicate exons, black triangles represent loxP sites, yellow circle indicates 4-TMX, arrows represent translational start sites and gray pacman is CreER^{T2}. **Up** Figure shows what happens after the 4-TMX injection. **Down** Figure shows what happens in the absence of the 4-TMX injection.

Our aim was to find the fair 4-TMX dose to have the maximal recombination of activated neurons across the entire brain. The 4-TMX is a drug soluble both in water and oil. Generally, the classical protocol consists in dissolving this drug in oil to perform i.p. injections (Guenthner et al., 2013; Ransom et al., 2018). There are also other protocols that solubilize 4-TMX in aqueous solution although these ones are still rarely used (Ye et al., 2016). By using aqueous solution, the injection appears to be less painful for animals and more stable at room temperature. The main problem of aqueous vehicles is linked to the impossibility to solve high drug concentration. Indeed, the

failed solubility could lead to a loss of neuronal recombination. For this reason, oil is preferred as vehicle of high drug concentration as in this case.

To find the appropriate quantity for sound activation, I tested increasing concentration of 4-TMX in corn oil: 10,25,50,75 mg/kg. I found that 50 mg/kg of 4-TMX induced maximal recombination in FosTRAP mice, consistently with previous reports (Guenthner et al., 2013) (Figure 8.6). I also observed that concentrations higher than 50 mg/kg are not well tolerated also in oil vehicle (Guenthner et al., 2013).

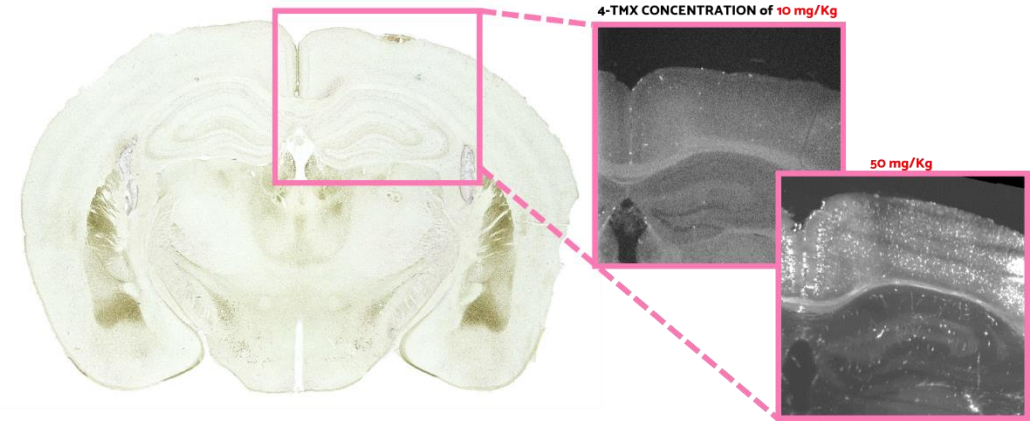

Figure 8.6: **Images that show neuron recombination at two different 4-TMX concentration**. Image illustrating that higher 4-TMX concentration increases the density of TRAPed cell in a portion of cortex and hippocampus. The images on the right were acquired with a wide-field epifluorescence microscopy.

8.1.4 Optimization of clearing, imaging and registration to reference Atlas

3D whole brain reconstructions were achieved optimizing clearing and imaging protocols to visualize neurons activated in various aversive memory phases. Since we use LSM for the acquisition, the transparency of the sample is our first requisite to obtain an entire brain map. For this purpose, I used CLARITY/TDE, a method developed in our lab, to make whole brains transparent (Costantini et al., 2015). Differently from the usual protocol, a 40% TDE solution was exploited to homogenize the RI of the tissue. At this concentration of TDE I found a moderate linear expansion (1.27 ± 0.05) as compared to the original size (Figure 8.7). Moreover, this isotropic change in sample size offered the possibility to investigate small components, such as neuronal processes. The brain expansion, however, was modest and had little impact on data volume generated, which must be kept in consideration when acquiring whole brain volumes (Di Giovanna et al., 2019).

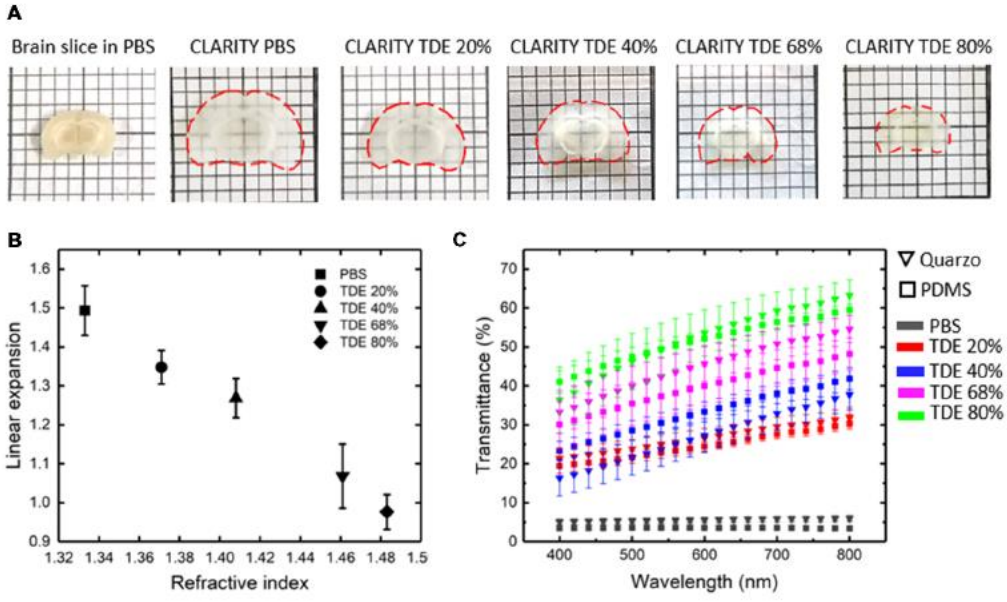

***Figure 8.7*: Sample deformation and transmittance**. (A) Images of a coronal brain slice processed with CLARITY and increasing concentration of TDE. Slice contours are indicated with dashed red lines. (B) Diagram explains that brain expansion is inversely proportional to RIs. These experiments were performed using 1 mm thick slices. These samples were previously cleared and then incubated in different TDE/PBS solutions, (n = 4, SD). (C) The diagram shows that longer wavelengths led to an increase in transmittance. These experiments were performed using 1 mm thick slices, placed inside a Quartz or PDMS cuvette. These samples were previously cleared and then incubated in different TDE/PBS solutions (n = 4, SEM) (Image modified from Di Giovanna et al., 2019).

All cleared brains were then imaged using a custom-made LSM able to reconstruct mesoscopic samples at microscale resolution (Müllenbroich et al., 2015). Due to the large sample size, the image acquisition required two steps. In this way, one half brain at a time was imaged. Indeed, considering the thickness of the cuvettes and the entire sample volume, the working distance of our objective (XLPLN10XSVMP, 10x, 0.6NA, WD 8 mm, Olympus) was unable to encompass the entire murine brain. Moreover, acquiring only half sample, high quality of the image was maintained also when going deep inside the specimen (Figure 7.4).

The entire dataset collected during the imaging was stitched using ZetaStitcher (https://lens-biophotonics.github.io/ZetaStitcher/), a custom-made Python software based on a global optimization algorithm. Furthermore, all brains reconstructed by our LSM were aligned to the Allen Brain Reference Atlas. This alignment was fundamental for a precise neuronal quantification in every brain area. To do that, the two halves of a brain were co-registered by an affine transformation and then fused together. Then,

whole-brain datasets were registered to the reference atlas by an affine transformation. However, due to tissue distortion introduced by clearing, affine registration was insufficient to achieve good alignment with the atlas (Figure 8.8). Thus, an additional co-registration based on non-linear symmetric diffeomorphism (B. B. Avants et al., 2008; Brian B. Avants et al., 2011) was used for final registration to the atlas. Non-linear registration was first performed on a manually binarized image showing masks at the location of olfactory bulbs, hippocampi, and cerebellum, to correct larger deformations, and then to the grayscale image for finer alignment. All 3D image registration steps have been performed using Advanced Normalization Tools (ANTs). By optimizing all these procedures, maps of every experimental class were realized (Figure 8.9).

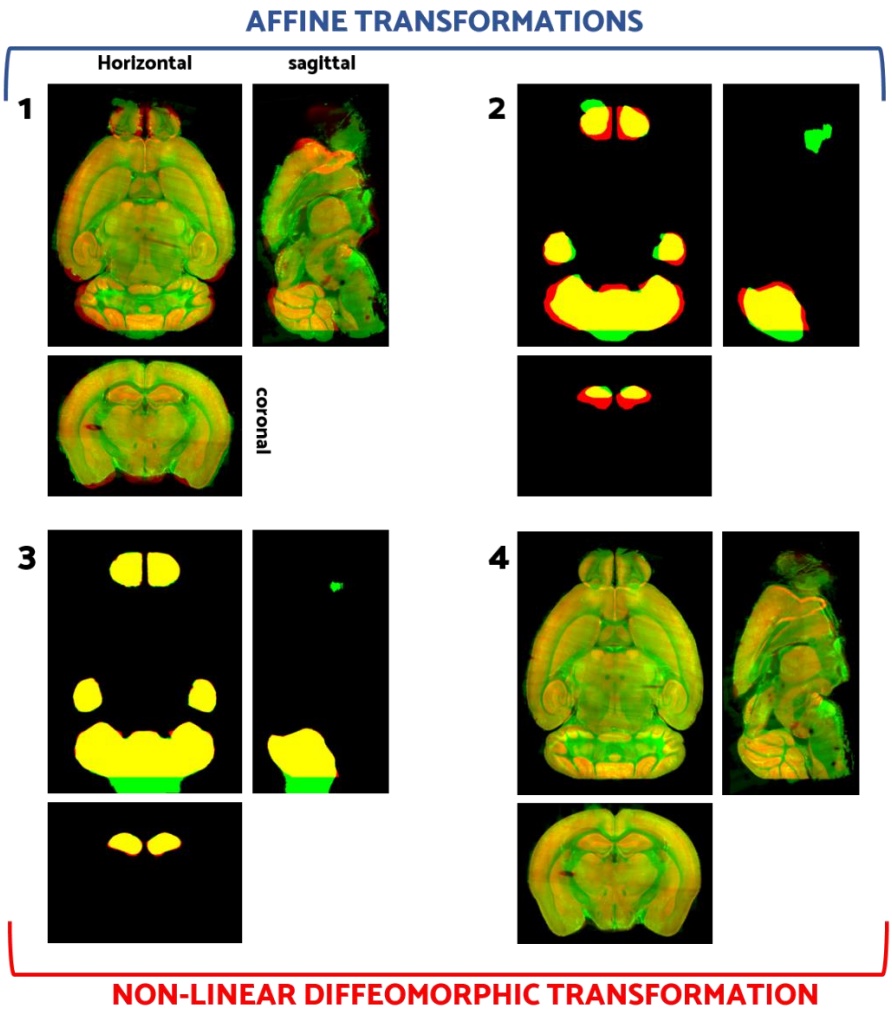

***Figure 8.8*: Atlas registration.** The image that shows four steps necessary for registering whole-brain fluorescence datasets with standard reference. Reference Atlas and relative masks are in red, while LSM images and masks are in green. (1) The first step is a gross registration of LSM datasets with images of Reference Atlas through an affine transformation. (2) From these images, binary masks of 3 main anatomical regions (olfactory bulbs, hippocampi, and cerebellum) are extracted. (3) Large distortions are corrected by running a non-linear registration on these masks. (4) Using alignments calculated from the masks, final non-linear registration between the sample and the atlas is found.

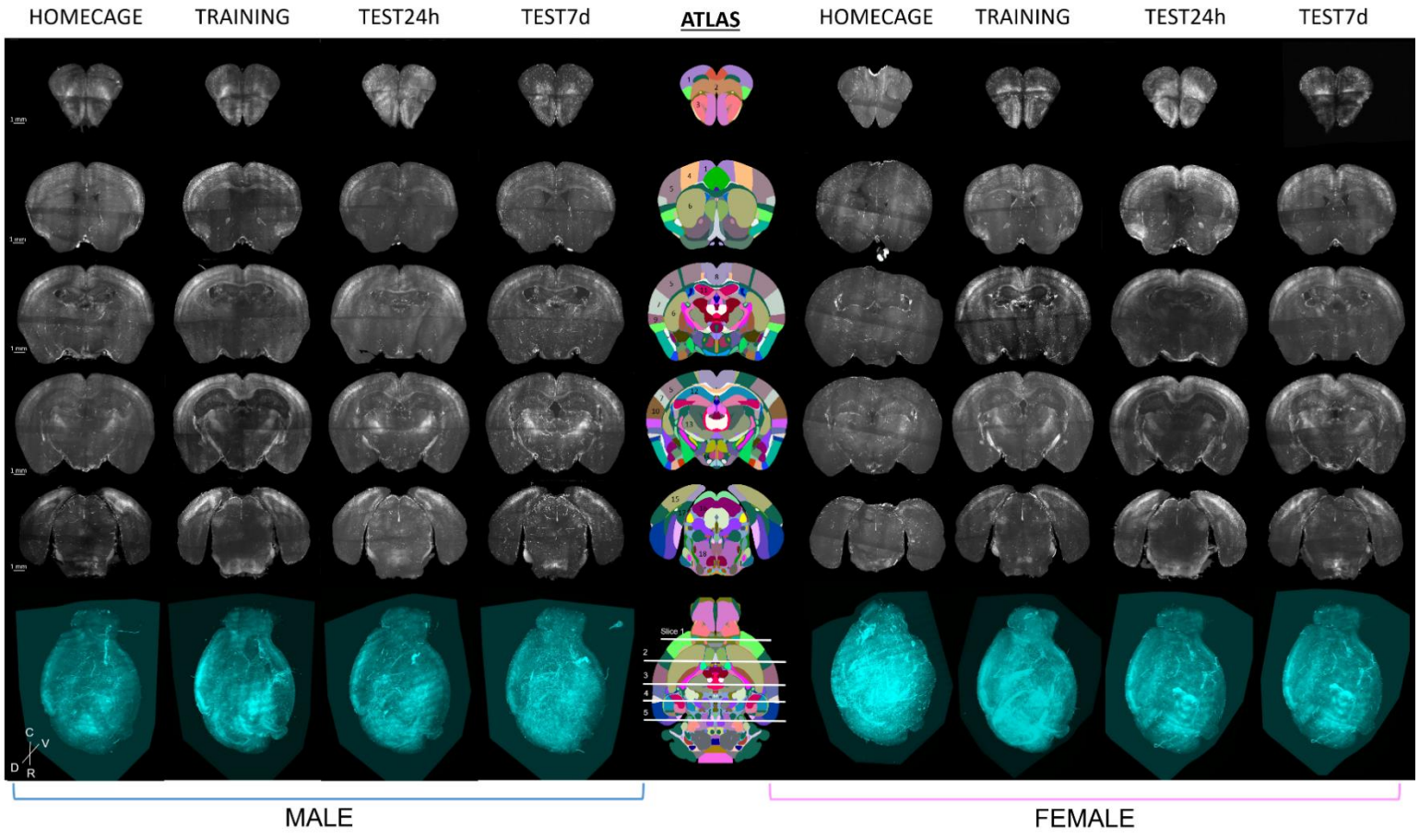
HOMECAGE
TRAINING
TEST24h
TEST7d
ATLAS
HOMECAGE
TRAINING
TEST24h
TEST7d
1 mm
Slice 1
C
V
D
R
MALE
FEMALE

Figure 8.9: **Map reconstruction of every experimental class**. Brains of all experimental classes used in this project were aligned to the Allen Mouse Brain Atlas. The Central column represents the atlas coronal plate to which all sections relate. The last line shows the 3D reconstructions of each brain and the horizontal reference plate cut by five lines. White lines show the exact place where slices are extracted. The numbers on reference coronal slices are referred to: 1 secondary motor area, 2 orbital area, 3 anterior olfactory nucleus, 4 primary motor area, 5 primary somatosensory area, 6 caudoputamen, 7 supplemental somatosensory area, 8 retrospinal area, 9 visceral area, 10 infralimbic area, 11 CA1, CA2, 12 dentate gyrus, 13 ventral group of the dorsal thalamus, 14 hypothalamus, 15 visual area, 16 superior colliculus, motor related, 17 postsubiculum, 18 pontine reticular nucleus, 19 periaqueductal gray. 3D renderings are performed by image processing software Amira.

8.1.5 Development of an automated method for 3D localization of activated neurons in the whole brain

The purpose of this thesis is the identification of fear memory representations, both during its formation and its consolidation. Although the identification of what happens in these phases should be useful in terms of understanding the neural circuits that process innate fear, the most direct method to compare differences and similarities between these phases is by the quantification of activated neurons. The use of FosTrap transgene is beneficial because mice do not need to be sacrificed immediately after the behavioral task, but it implies a big problem for data analysis. As I have just explained in 8.1.3, all activated neurons express the TdTomato fluorescent protein. Differently from c-Fos IHC where labelling is mostly confined to neuron somas, TdTomato protein tags the entire neuron and consequently, it is well visible also in the axons and dendrites (Figure 8.10).

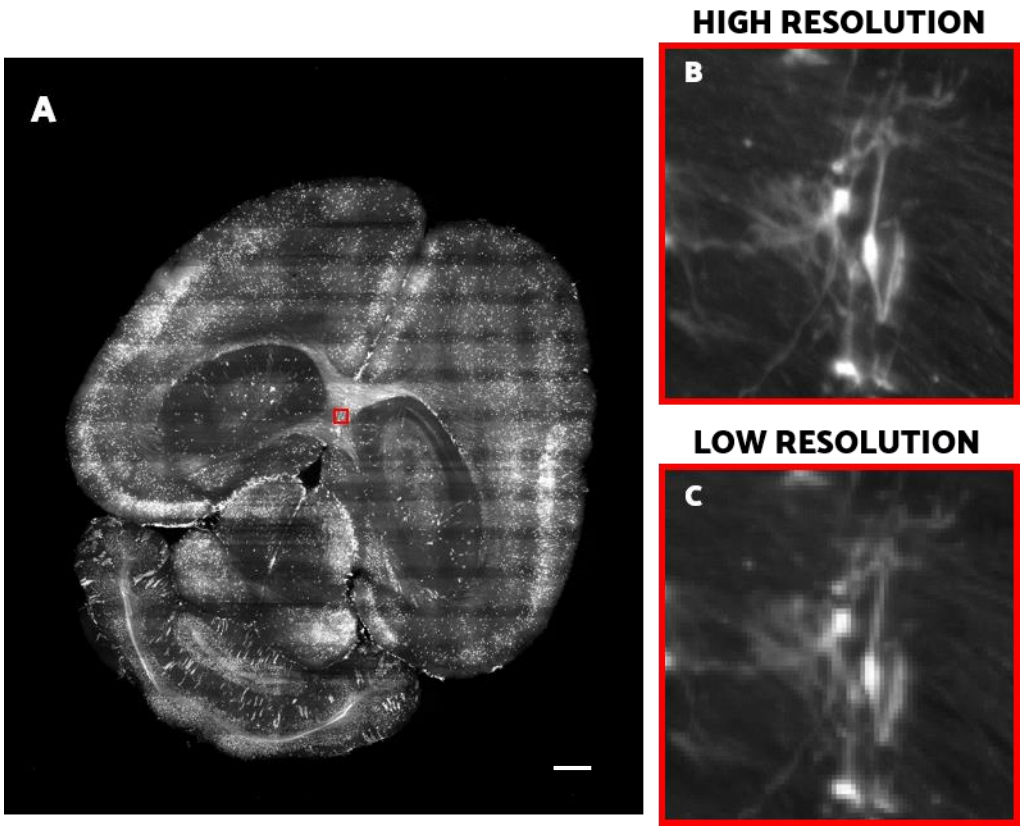

Figure 8.10: (A) Whole-brain image of neuronal activations during fear memory learning. Maximum intensity projection of 100 µm slab from clarified mouse brain imaged with light-sheet microscopy. Scale bar 1 mm. (B) Zoom-in from the red square in A. As can be seen the presence of axons and dendrites makes cell localization challenging. (C) Low resolution view of the same area, shown above in B, proves that high-resolution imaging is necessary to distinguish individual neurons from axons, dendrites and bundles.

In this way, the direct application of methods based on thresholds and blob detectors was complicated. For this reason, the development of a method trained to quantify all neurons activated in the entire brain, was performed. This methods is a deep learning approach, based on a U-net architecture, widely used in the image-analysis field (Ronneberger et al., 2015). The task of our artificial neural network (ANN) was to transform raw images, containing many disturbing objects (like axons, dendrites, and vessels) into ideal images that include only small spheres at the location of neuronal bodies (Figure 8.11). At this point, the use of standard methods for neuronal detection allowed an easy location of activated neurons and saved them as coordinates. The localization performance was obtained with a precision = TP/(TP+FP) equal to 0.80, recall = TP/(TP+FN) 0.64 and F1-score = 0.71. F1 is defined as the harmonic mean of precision and recall, 1/F1 = (1/P + 1/R)/2. Contrary to many algorithms, trained for direct neuron segmentation, the algorithm I used was trained to “clean up” the image, performing what its developers described as “semantic deconvolution” (i.e. a deconvolution based on semantic content) (Frasconi et al., 2014). The main advantage of this approach lies in the fact that ground-truth annotations, which in this case are only locations of neuronal soma centers rather than full volumetric segmentation, can be produced with very high throughput. Indeed, ANN needs a lot of manually annotated examples for its training. In this pipeline, the avoidance of neuron segmentation provides us a rapid way to train the ANN, quickly producing a satisfactorily large ground-truth dataset.

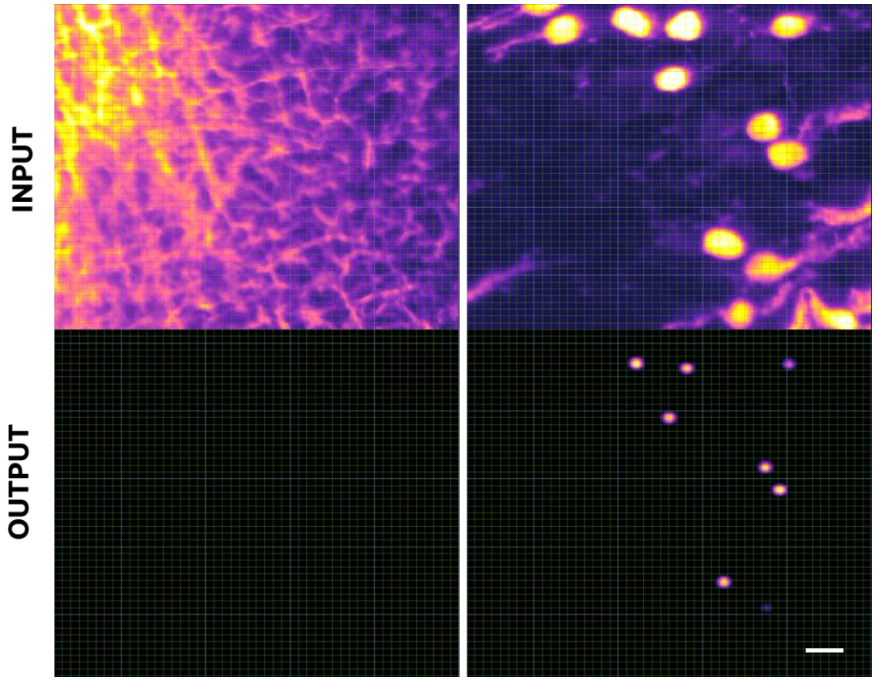

Figure 8.11: **ANN operation**. The image shows the functioning of the ANN. ***Up*** example of images given as INPUT to the ANN. On the left, the image contains a lot of axons and dendrites. On the right, a different image that contains neuronal somas. **Down** transformation applied by the ANN. In the output, only neuronal somas are represented as spheres. Scale bar 30 µm.

8.1.6 Investigation of histaminergic neurons inside TMN that are involved in different aversive memory phases

Different neuromodulator systems are known to be involved in learning and memory (Singewald et al., 2015). Amongst them, the histaminergic system is one of the less studied, despite several reports highlighting its fundamental role in this process (Singewald et al., 2015).

All the histaminergic neurons in the brain are placed in the TMN (Alvarez, 2009; Haas et al., 2008; Leurs et al., 2012; Parmentier et al., 2002; Parsons & Ganellin, 2006; Weihe & Eiden, 2000). These neurons are implied in many physiological roles. Due to the spatial distribution of histaminergic cells inside TMN, the most convincing hypothesis about the relationship between anatomy and function suppose that each TMN sub-population has different roles (Blandina et al., 2012). Our purpose was to elucidate the role of the histaminergic system in the formation and consolidation of fear memory, also analyzing the change in the spatial distribution and in the cell number in response to an aversive stimulus. For this reason, I have developed a method able to detect histaminergic neurons activated during behavior. All histaminergic neurons share the expression of HDC enzyme, necessary for histamine synthesis. Thus, from the FosTRAP brains used in previous experiments, I isolated the brain part that includes TMN and performed whole-mount IHC against HDC. Two-colors imaging – with red channel showing TRAPed neurons (expressing tdTomato) and in green channel, the other HDC-positive cells – revealed that many histaminergic neurons were activated during behavior (Figure 8.12). The scope was to understand different histaminergic pathway involved in fear memory. Moreover, I tried to assess whether the inter- and intra-group variability in the number of histaminergic neurons activated in a precise phase of memory.

I directly quantified all the colocalization from each image. From the x,y,z positions of each annotation, I extrapolated a point cloud per sample. Every TMN point cloud was aligned to Reference Atlas with a manual registration based on landmarks. This step was fundamental because these reconstructions are useless if not correctly aligned to the Atlas (Figure 8.13). This pipeline let us extrapolate the precise number of histaminergic neurons activated during different fear memory phases, understanding the different distribution of these cells inside the TMN.

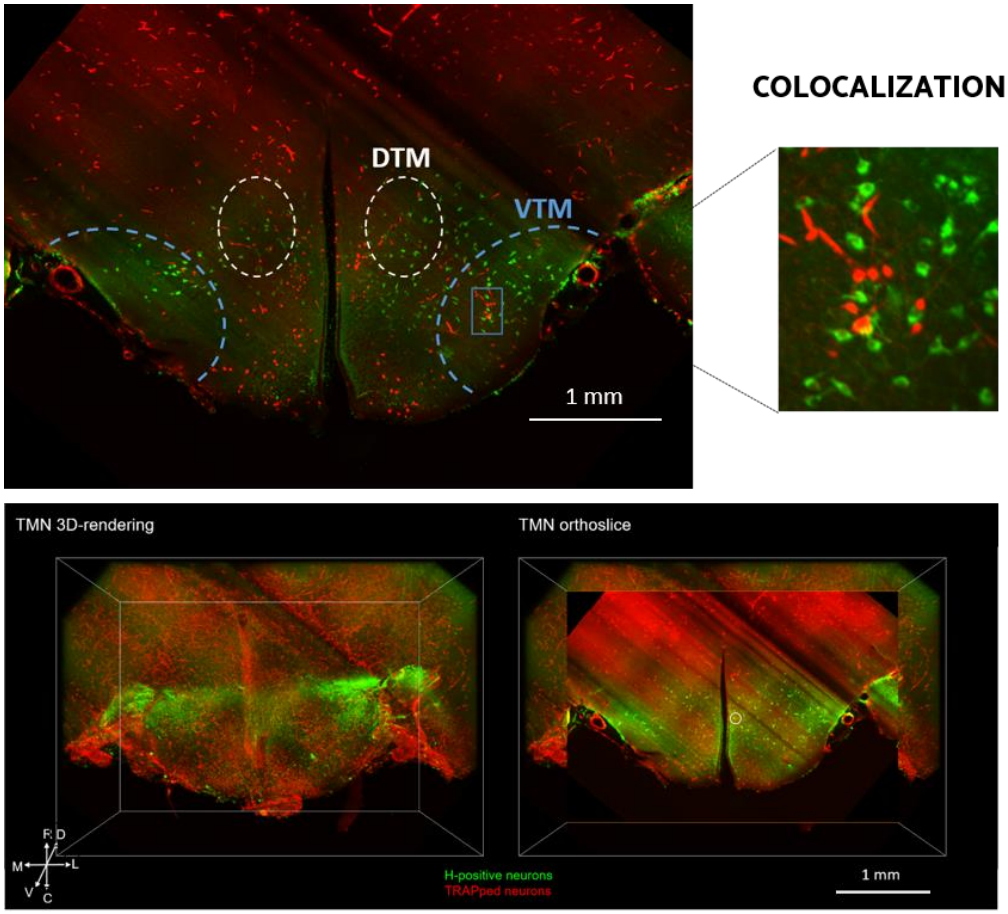

Figure 8.12: **Up**, Overview of TMN stained with an HDC antibody (green channel) and expressing c-fos positive neurons (red channel). TMN MIP of 50 slabs shows its two subdivisions: ventral TMN (VTM) and dorsal (DTM) and a zoom-in a neuron colocalised. **Bottom**, on the *left*, 3D visualization of activated neurons (red channel) inside the TMN, labelled by anti-HDC antibody. The box on the *right* represents a slice taken from the volume.

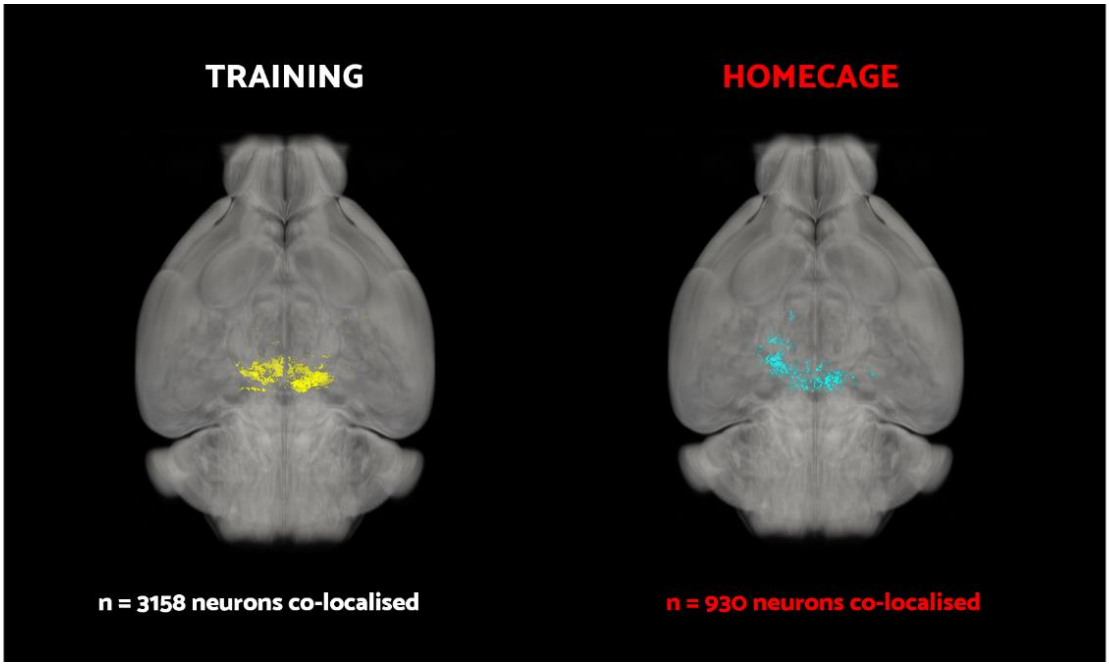

Figure 8.13: Point clouds of histaminergic neurons activated during behavior with the respective count of neurons colocalised. These 3D representations are aligned and registered to Atlas. Here a horizontal view.

Chapter 9

Results II

The above-mentioned pipeline was then applied to quantify all activated neurons across the entire brain. The different activation patterns observed among various experimental classes and genders allowed highlighting the main regions involved in fear memory.

By using the Allen Brain Atlas as the spatial reference, 45 macroareas were selected for the analysis. I focused on larger regions in order to avoid problems related to imperfect image registration. Indeed, the effect of alignment errors on cell counts per area is proportional to the surface to volume ratio, and is thus reduced by considering macroareas instead of small parcellation (e.g. the entire visual cortex instead of V1 layer IV). Here below, a series of diagrams has been reported, showing a different distribution of TRAPed neurons and the relative statistical significances. In detail, I quantified c-Fos$^+$ cells among various experimental classes, also considering sex influence.

9.1 Quantification of c-Fos$^+$ cells across the entire brain revealed an unexpected trend between the experimental classes

Here I applied this quantitative brain-wide mapping pipeline to document the distributions of activated neurons in every selected region. This distribution revealed a strong sexual dimorphism, with two completely opposite trends. This unexpected

outcome demonstrated the capability of our developed whole-brain protocol to assess activation in a comprehensive and unbiased way, revealing significant differences also in unanticipated brain areas.

By examining the following histograms, statistical significances among experimental groups were also observed in regions not necessarily related to fear memory. Before analysing and describing in detail all produced data, it is worth adding an important caveat. Due to the large time window of 4-TMX, some of the observed activation patterns may reflect stimuli induced by the group-housing of mice, especially those involving activation of areas where visual, auditory, olfactory and motor information were processed. The housing conditions were selected in order to avoid side effects on behavior. Indeed, it has been shown that socially deprived mice exhibit increased anxiety and depressive-like behaviors in standard behavioral tasks as the open field test, elevated plus maze, forced swim test, and sucrose preference test (Berry et al., 2012; Garner et al., 2004; Kalueff et al., 2016; Kappel et al., 2017). In order to avoid these anxious-states that could negatively impact our results, I chose a "social environment" for mice. However, the disadvantage that was associated with group-housing conditions was a "background noise" in brain activation maps that did not easily allow to dissect fear memory patterns.

Here below, I present quantifications of c-Fos$^+$ cells as bar plots grouped by classes or sex (Figures 9.1, 9.2, 9.3, 9.4, 9.5, 9.6, 9.7). The activation pattern imaged across the whole-brain showed a growing trend between experimental groups of female mice. Indeed, in almost all areas of female mice, an increase in activated neurons from training to test 7d can be observed (Figure 9.1). For male groups, quantification of c-fos$^+$ cells follows a totally opposite trend compared to that of the females, decreasing from training test 7d (Figure 9.2). In line with the literature, the main hypothesis about this tendency suggested that fear exposure increased stress levels in male mice. The high-stress level could even lower c-Fos levels during memory retrieval (Azevedo et al.,

2020). Another hypothesis related to the reduction of c-fos activations concerns animal welfare. Indeed, an enriched environment and a paired-housing could facilitate fear extinction and memory recovery loss (Lopes et al., 2018; Smith et al., 2016).

Given the opposite trend found in male and female subjects, the comparative analysis of c-fos expression in all mice (without grouping them by sex) did not show any relevant statistical difference among experimental groups (Figure 9.3).

If at the first sight the circuitry involved in the consolidation and retrieval of fear memory differs much from male and female, many areas were involved in both genders, although with opposite trends. Indeed, a strong variation was displayed in the amygdalar and hippocampal region, anterior cingulate area, prelimbic and infralimbic area, retrohippocampal region, striatum-like amygdalar nuclei, and posterior parietal association areas (Alonso et al., 2005; Barros et al., 2000, 2001; Luft et al., 2004; Myskiw et al., 2010; Myskiw & Izquierdo, 2012; Zanatta et al., 1996). A large change in activation was exhibited also in regions as temporal association areas, somatosensory areas, perirhinal area, and retrosplenial cortex. These regions are not directly involved in memory processing but are more related to the sensory aspects of the memory. For example, substantial evidence identified the retrosplenial cortex as a hub for consolidating and/or retrieving contextual and spatial memories (Milczarek et al., 2018; Todd & Bucci, 2015). This region is reciprocally connected with the hippocampus and various parahippocampal cortical regions, suggesting a role in the contribution of hippocampal-dependent memory and also a role in the association between an emotional stimulus and an environment.

Although each activated brain area played a precise function in the consolidation and retrieval of fear memory, it is important to note that memory does not depend on single brain regions but rather on functional connections among these ones (Vetere et al., 2017). Therefore, an approach, like the one demonstrated in this thesis, that allows

the detection of all activated pathways across the entire brain, seems the most suitable to explore fear memory engram.

BRAIN AREA LEGEND

Cortical subplate
EP Endopiriform nucleus
CLA Claustrum
PA posterior amygdalar nucleus
BMA Basomedial amygdalar nucleus
BLA Basolateral amygdalar nucleus
LA lateral amygdalar nucleus

Hippocampus
HIP hippocampal region
RHP retrohippocampal region
Striatum
sAMY Striatum-like amygdalar nuclei
LSX lateral septal complex
STRv striatum ventral region
STRd striatum dorsal region

Pallidum
PALd dorsal pallidum
PALv ventral pallidum
PALm medial pallidum
PALc caudal pallidum

Thalamus
DORsm thalamus, sensory-motor
DORpm thalamus, polymodal association

Cortex
ECT Ectorhinal area
PERI Perirhinal area
TEa Temporal association areas
PTLp Posterior parietal association areas
RSP retrosplenial area
AI agranular insular area
ORB orbital area
ILA infralimbic area
PL prelimbic area
ACA anterior cingulate area
VIS visual area
AUD auditory areas
VISC visceral areas
GU gustatory areas
SS somatosensory areas
MO somatomotor areas
FRP frontal pole

Hypothalamus
ME median eminence
LZ hypothalamic lateral zone
MEZ Hypothalamic medial zone
PVR periventricular region
PVZ periventricular zone
OLF olfactory areas

CB cerebellum

MB midbrain
MY medulla
P pons

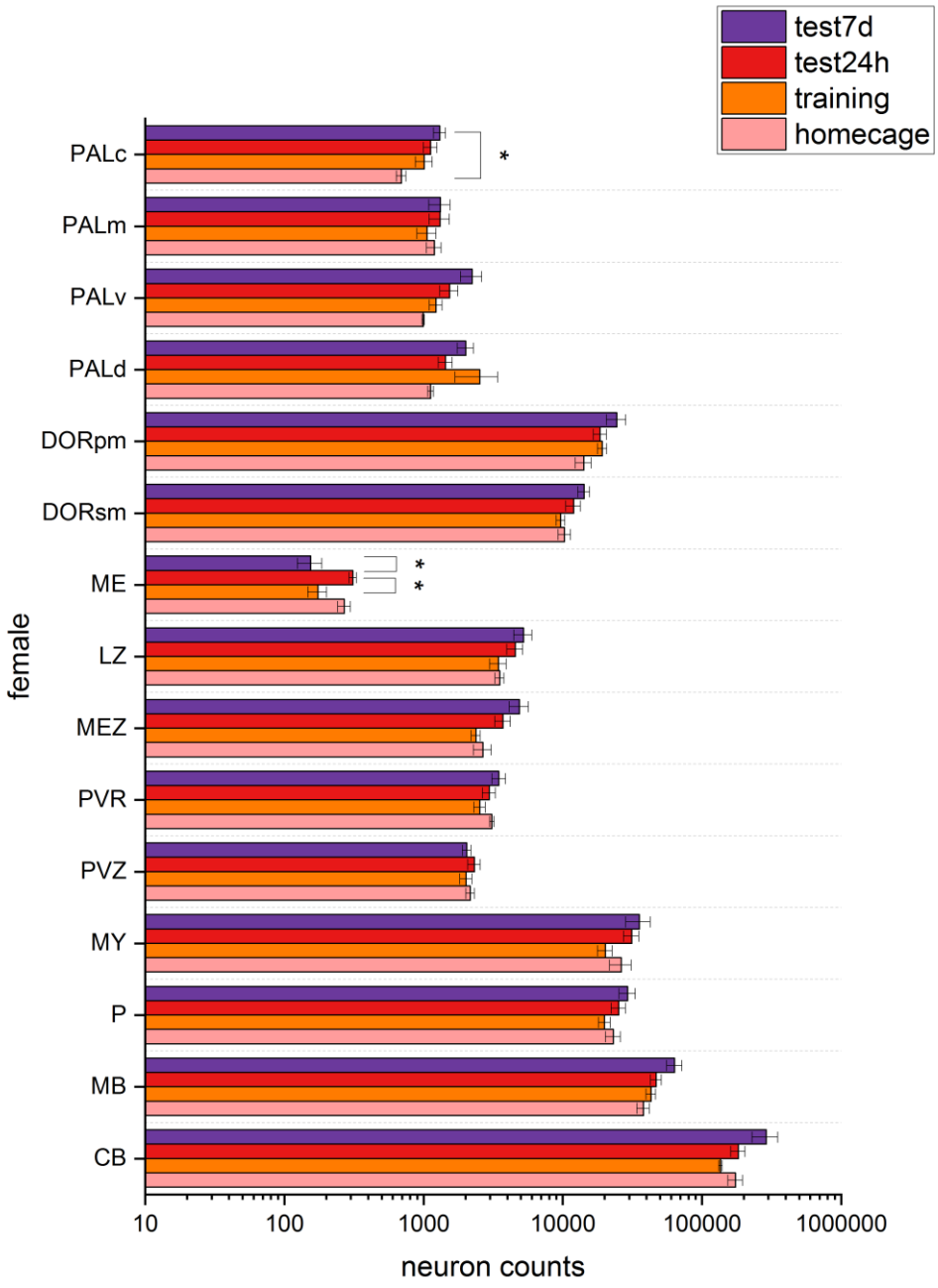

Figure 9.1: Automated quantification of the TRAPed cell between our four experimental classes. Here presented the results from **FEMALE** mice. All brain regions are listed in the legend above.

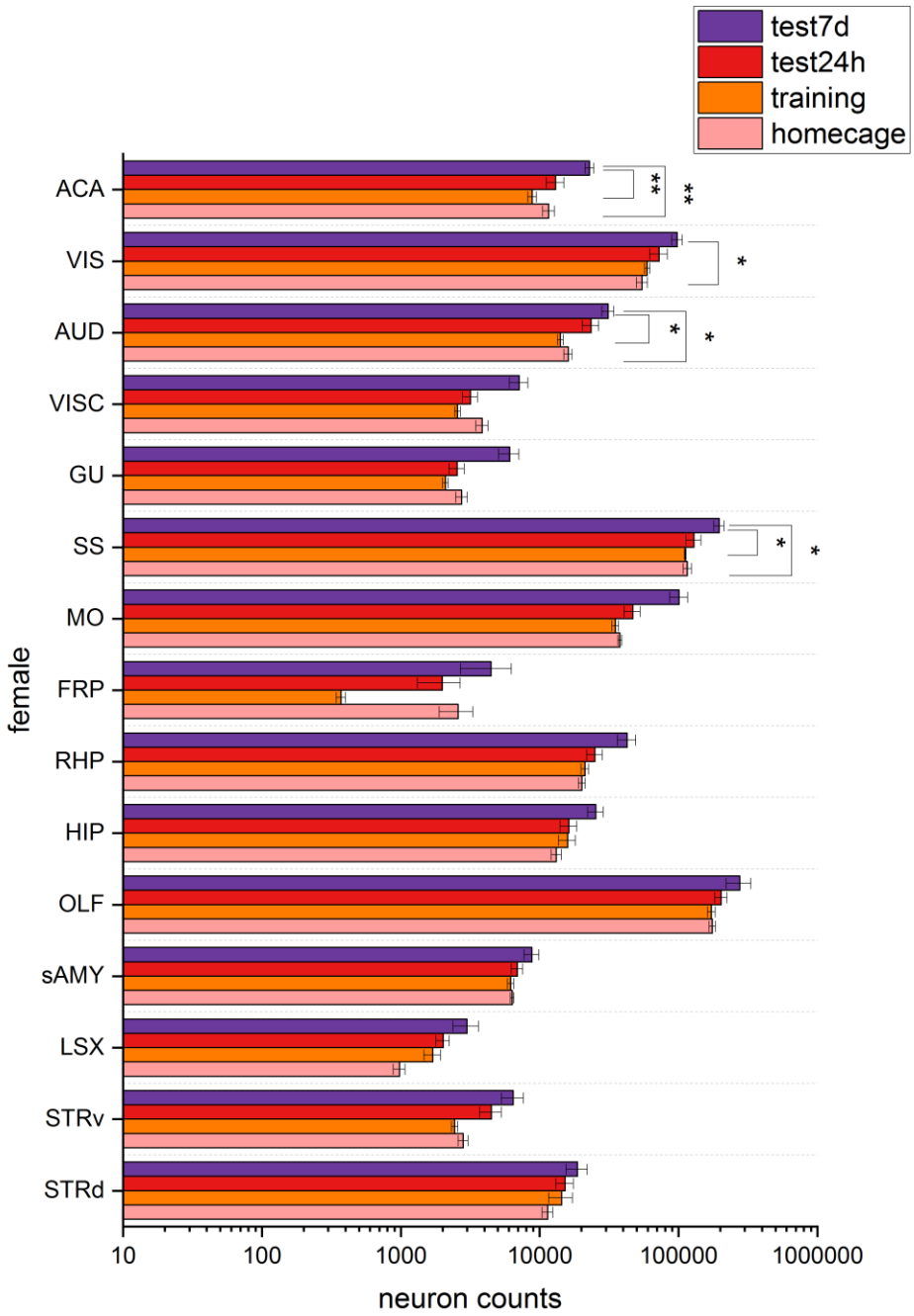

Figure 9.1 (continued): Data are represented as mean ± SEM (***p < 0.01, **p < 0.05, *p < 0.1). FDR approach are used to adjust p values for multiple testing comparison (stars in red)

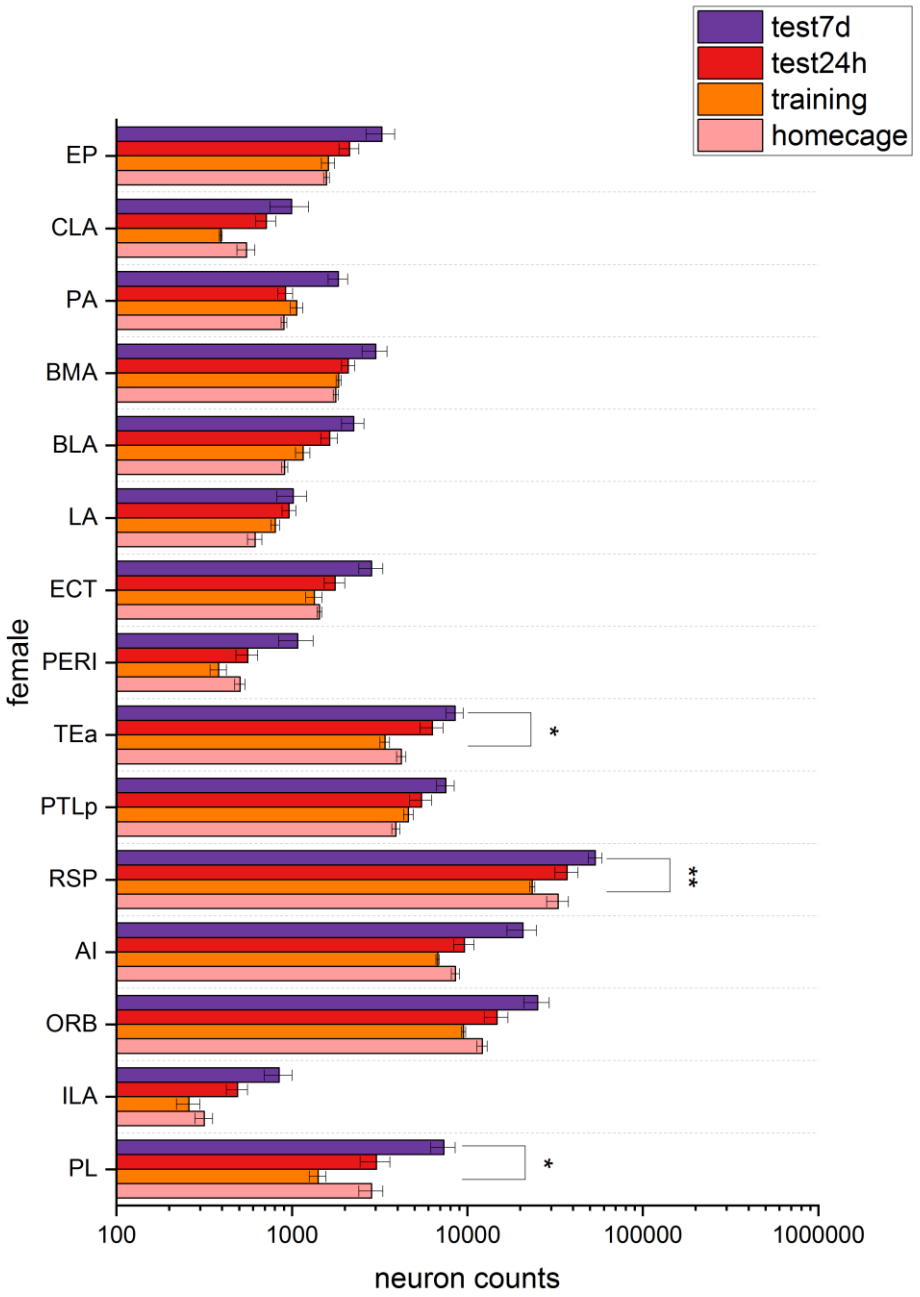

Figure 9.1 (continued)

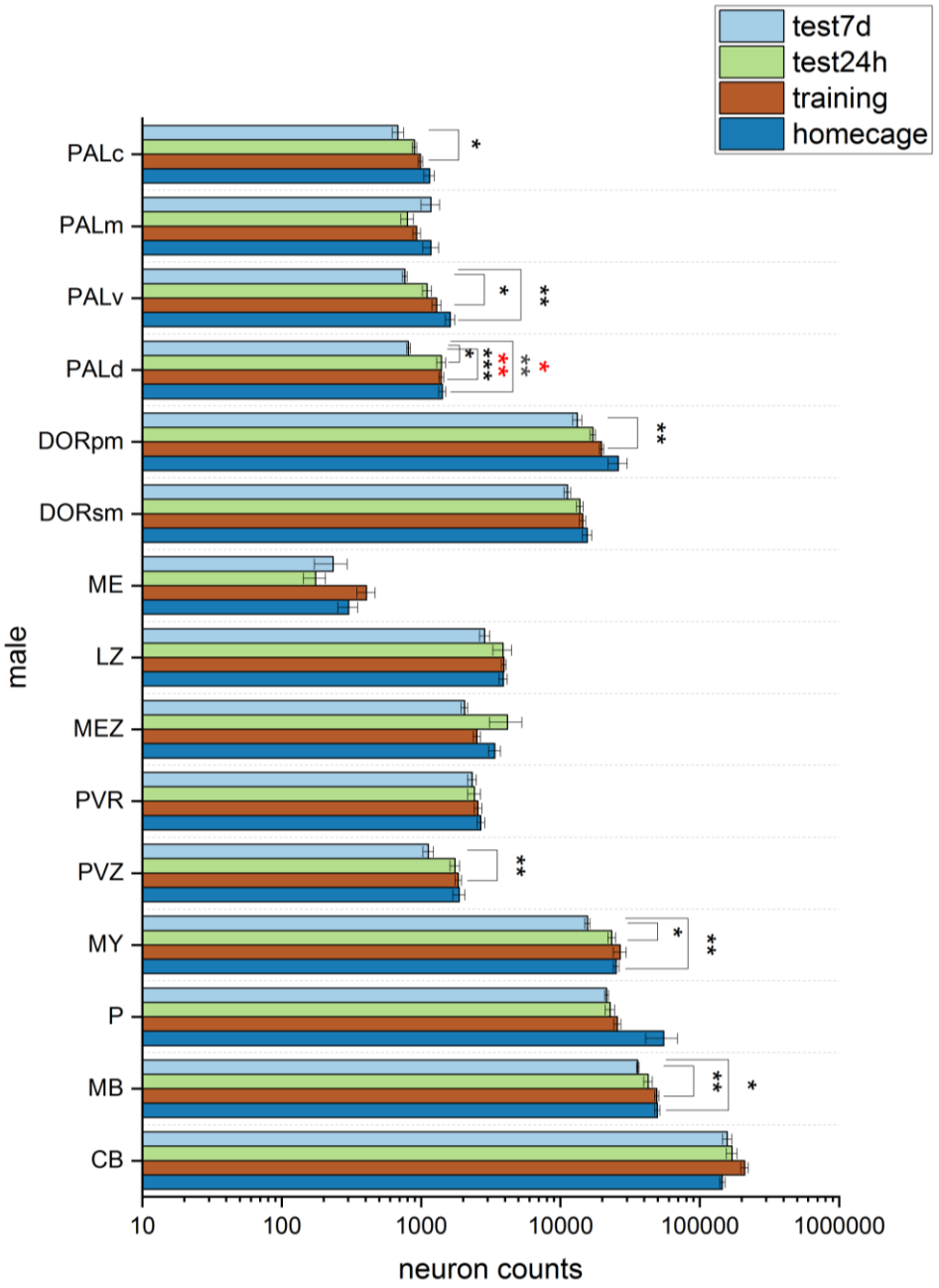

Figure 9.2: Automated quantification of the TRAPed cell between our four experimental classes. Here presented the results from **MALE** mice. All brain regions are listed in the legend above.

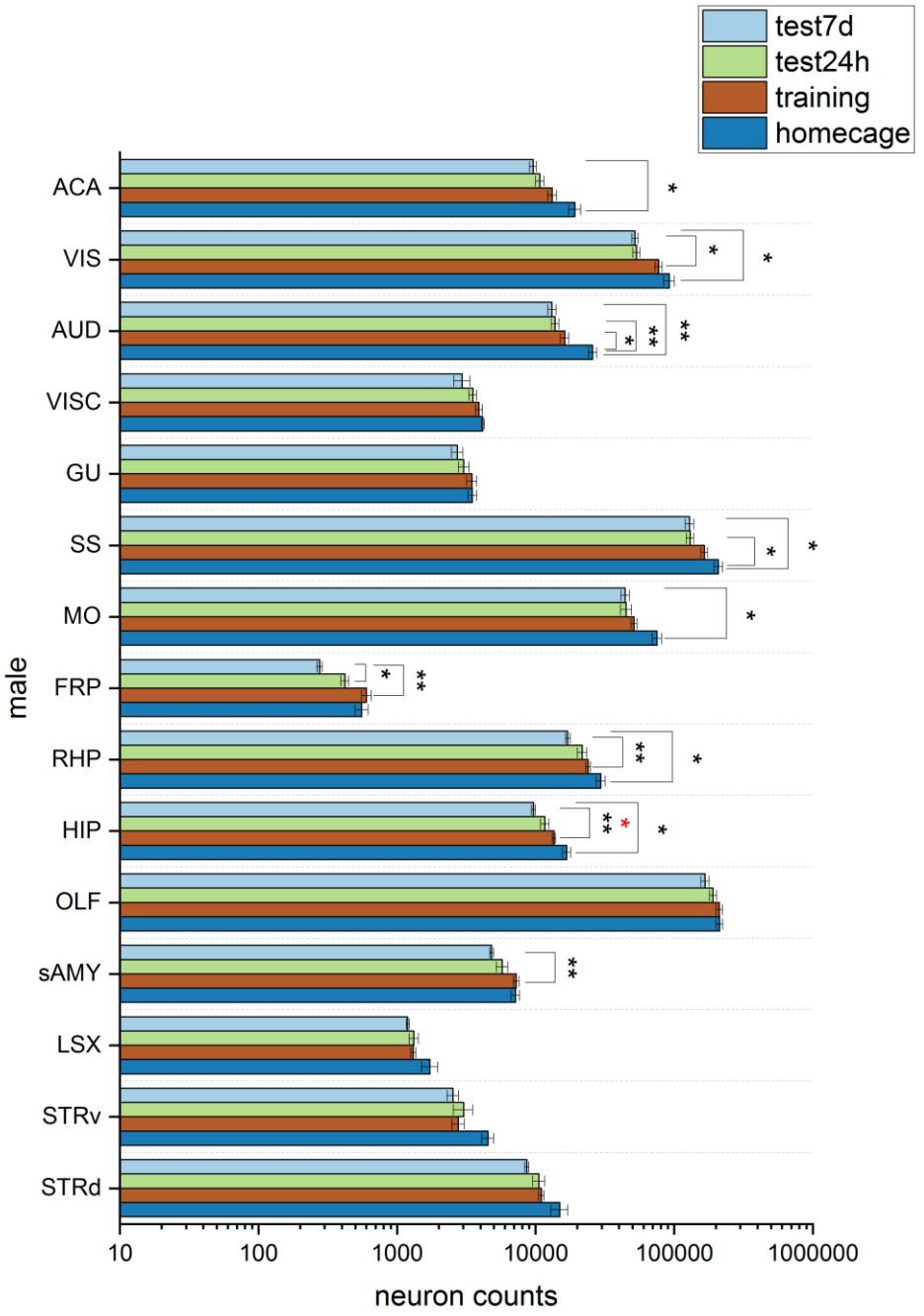

Figure 9.2 (continued): Data are represented as mean ± SEM (***p < 0.01, **p < 0.05, *p < 0.1). FDR approach are used to adjust p values for multiple testing comparison (stars in red)

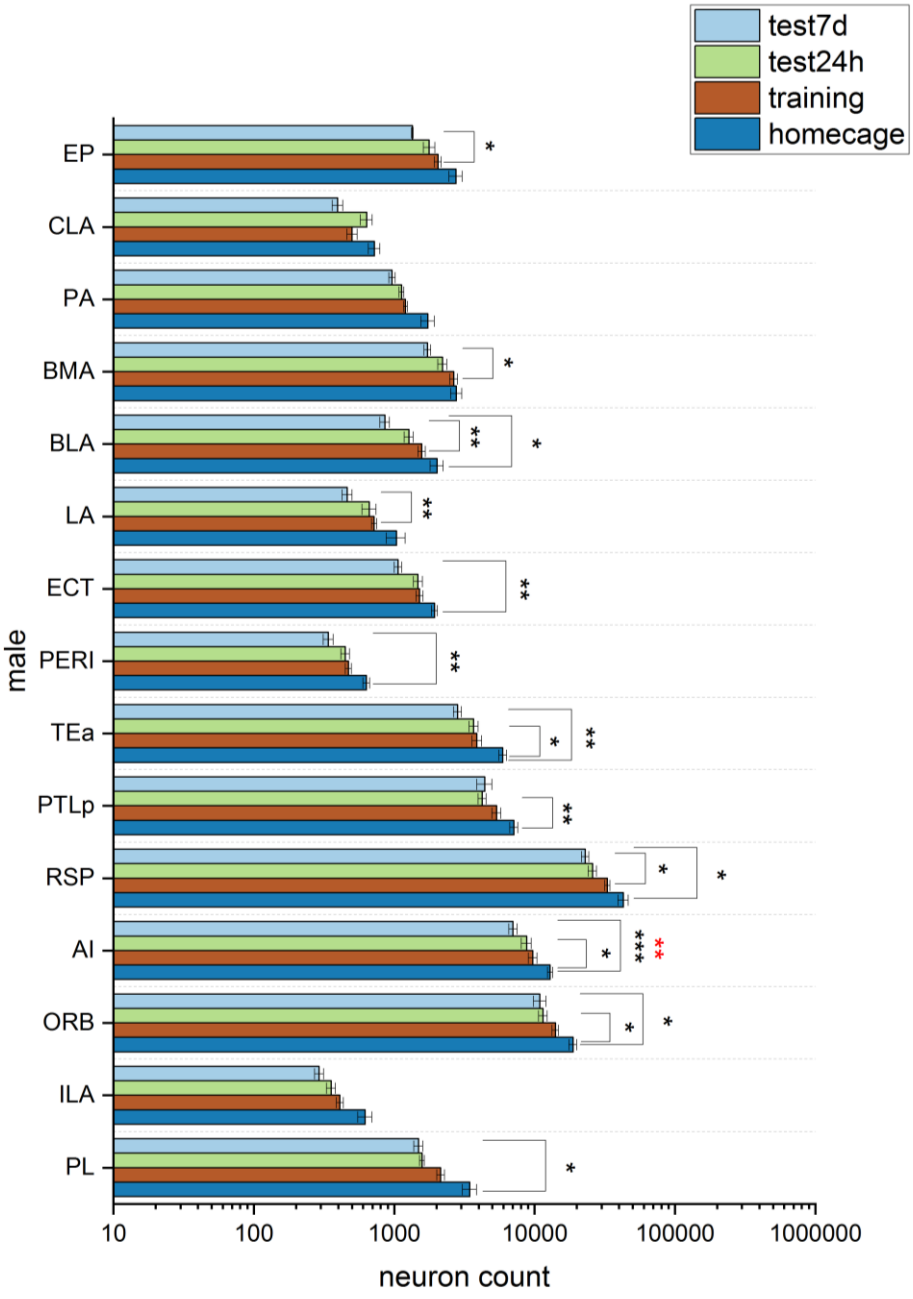

Figure 9.2 (continued)

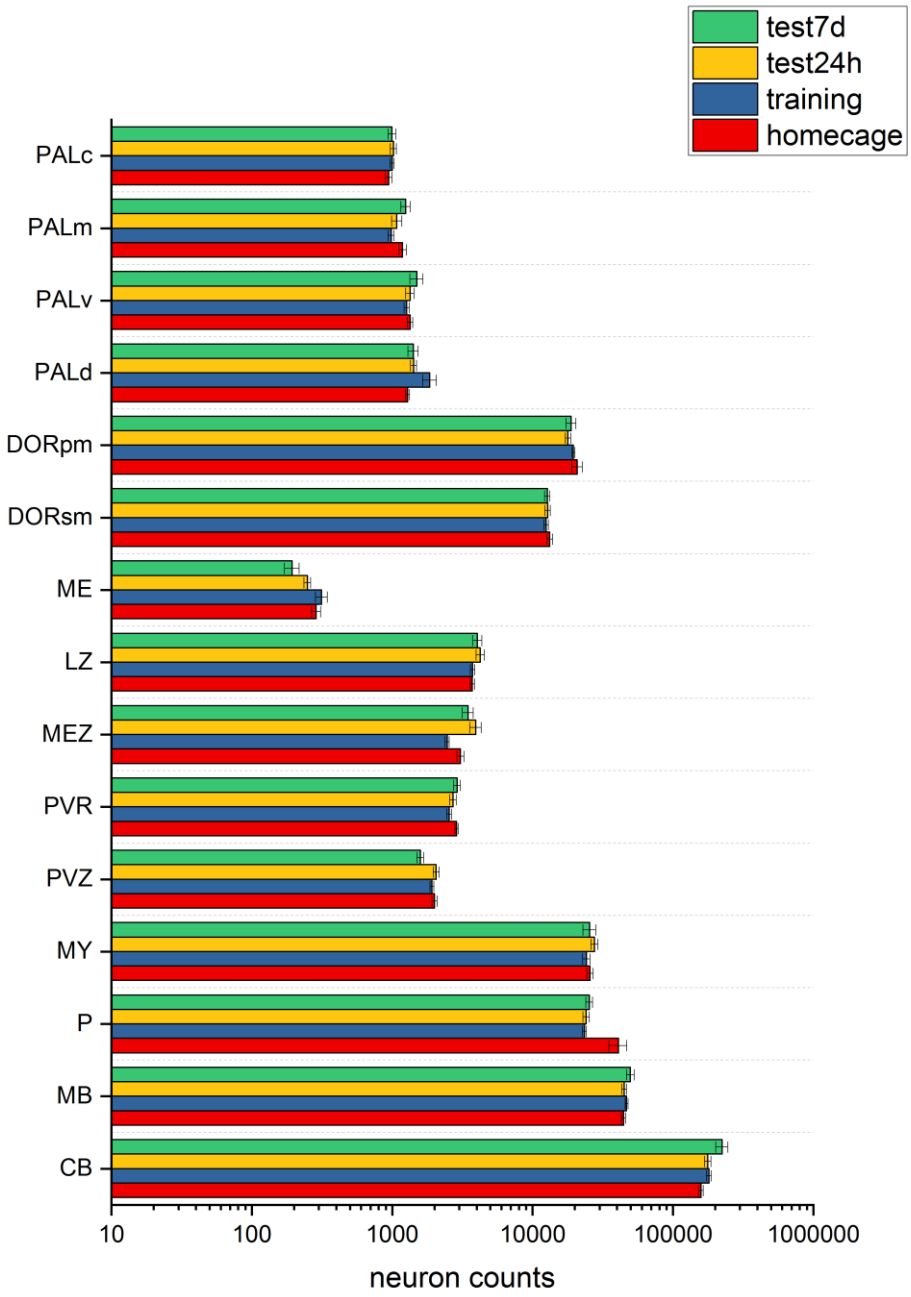

Figure 9.3: Automated quantification of the TRAPed cell between our four experimental classes. Here presented the results from **ALL** mice, independently from sex. All brain regions are listed in the legend above.

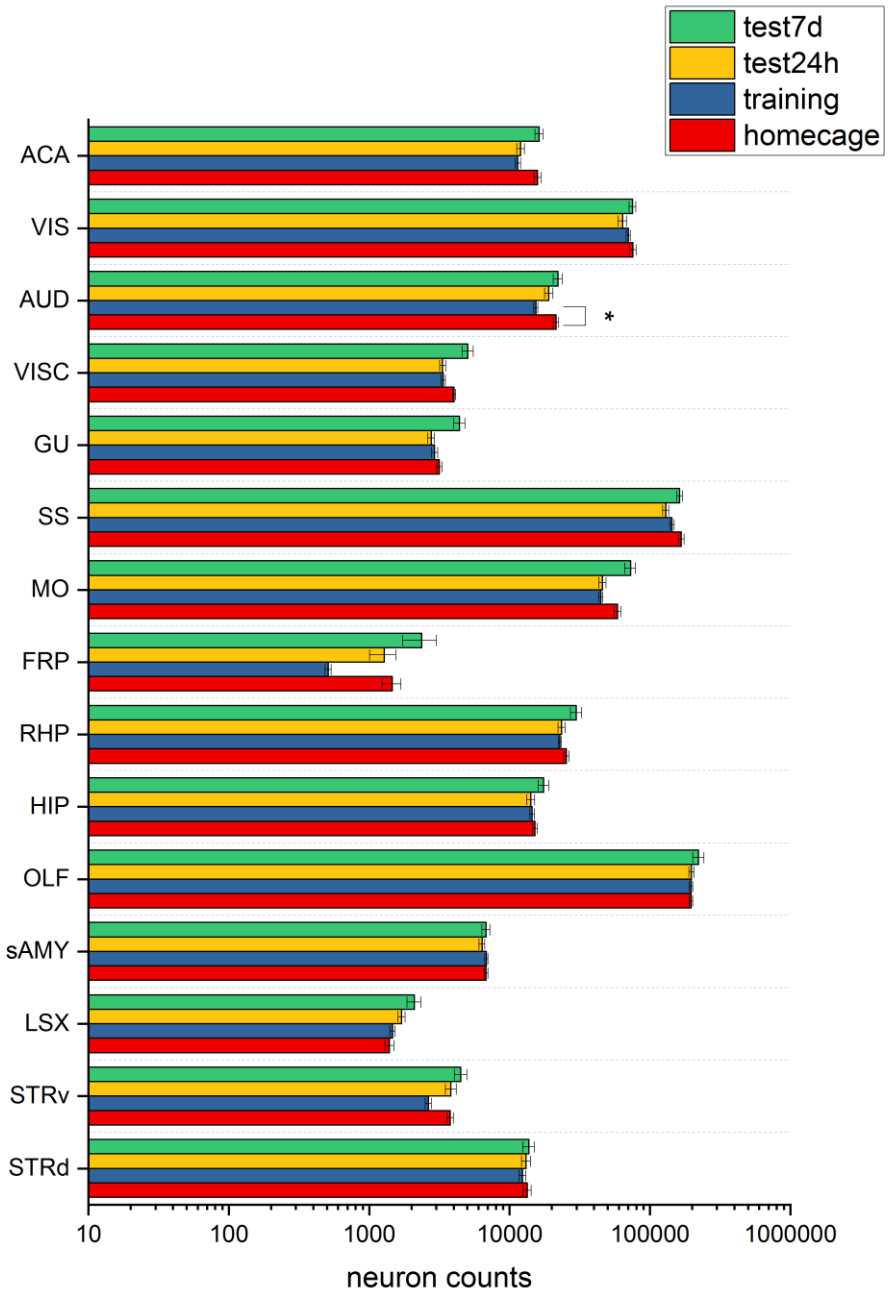

Figure 9.3 (continued): Data are represented as mean ± SEM (***p < 0.01, **p < 0.05, *p < 0.1). FDR approach are used to adjust p values for multiple testing comparison (stars in red)

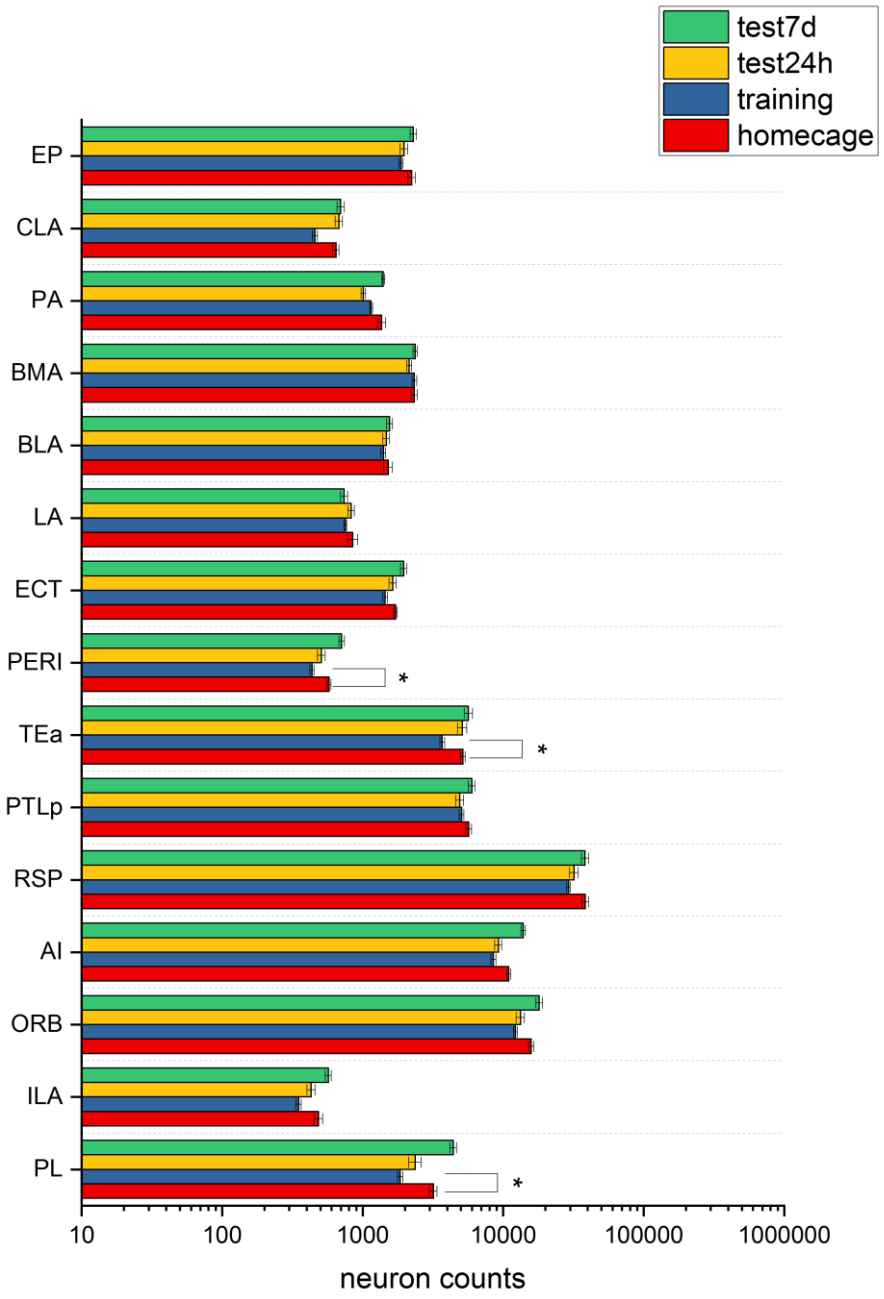

Figure 9.3 (continued)

Further investigations were performed to better understand our data. We focused then on each experimental class to fully explore our data. By analyzing homecage and training groups, I provided evidence that many brain areas were more activated in males rather than females (Figure 9.4, 9.5). Whereas 24 hours after training, activation levels of both genders were similar (Figure 9.6). The trend was totally reversed for the test 7d group where activated neurons were more present in female samples than male ones (Figure 9.7). As proof of these observations, averaged density maps were performed to confirm quantitative data from bar plots (Figure 9.9).

Sex and experimental class were not indipendent variables since they affected each other. In each region there was a variability associated with the class but, according to the graphs, the experimental groups responded differently on the basis of gender. Thus, aiming to better highlight gender differences during learning, consolidation, and retrievial of aversive memory, I performed a two-way ANOVA test, analyzing the separate effect of the single variables (sex and experimental class) and their combined one (Figure 9.8). This statistical test allowed to observed the combined effect, not shown by a simple t-test which was used to compare the means of the two experimental classes. In agreement with the heatmap, these findings suggested that circuitry patterns involved in fear memory are influenced by sexually dimorphic tendency.

Brain regions more affected by this combined effect, were retrohippocampal region, somatomotor areas, visceral areas, auditory areas, anterior cingulate area, prelimbic area, infralimbic area, agranular insular area, basolateral amygdala and posterior amygdalar nucleus. This is coherent with the fact that these regions are among the most implicated in fear responses. This analysis further demonstrates the activation of different neuronal circuits in males and females in response to threats.

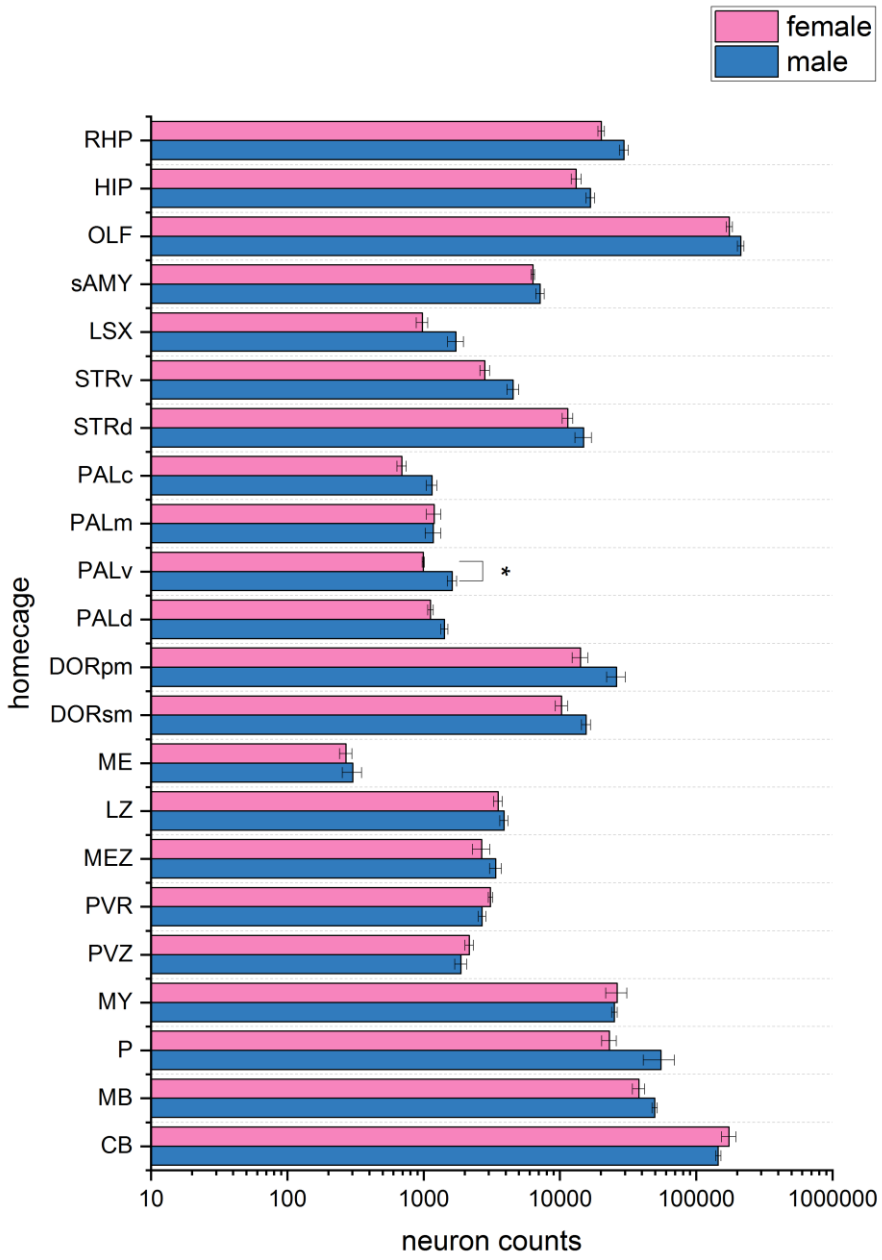

Figure 9.4: Automated quantification of the TRAPed cell between male and female mice. Here presented the results from the **homecage** group. All brain regions are listed in the legend above.

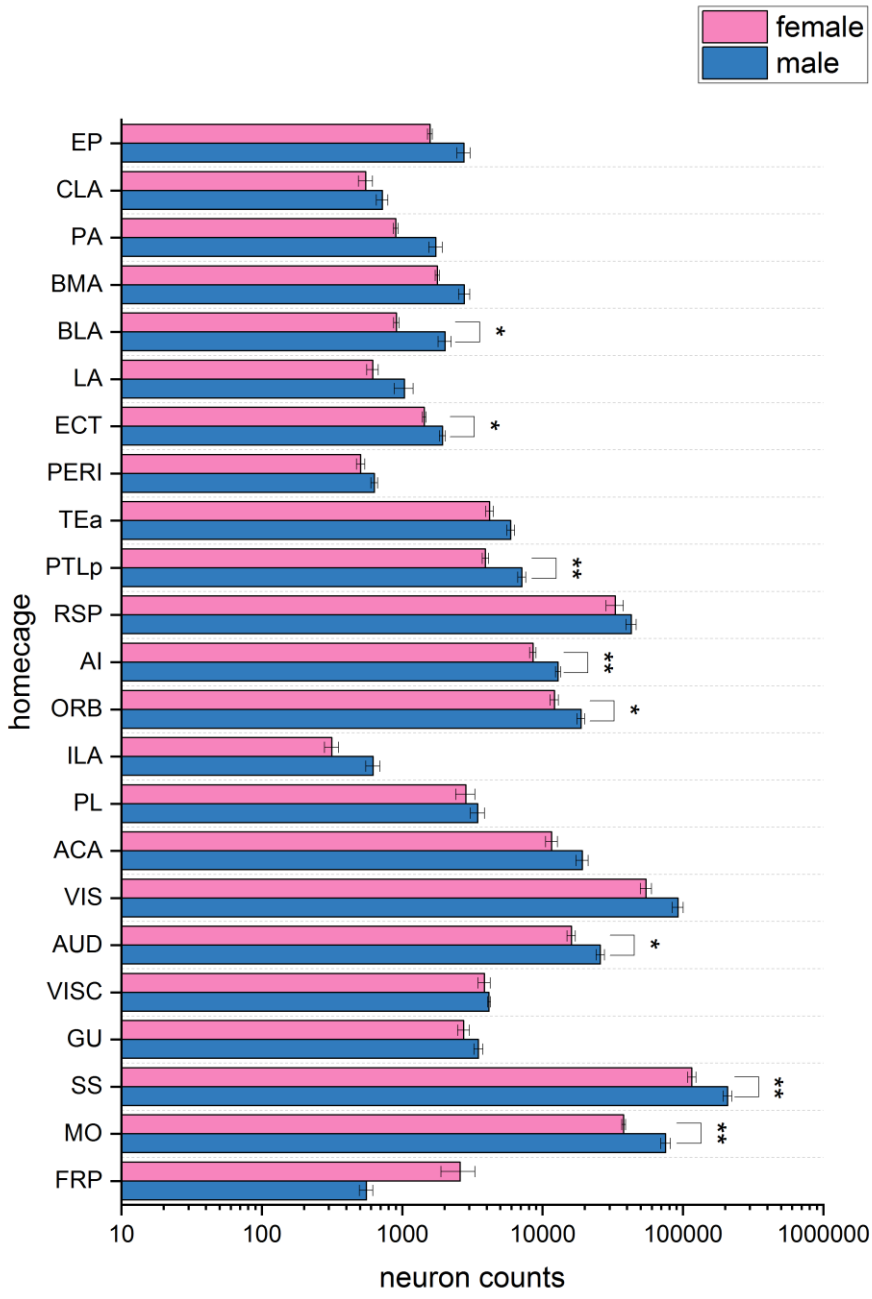

Figure 9.4 (continued): Data are represented as mean ± SEM (***p < 0.01, **p < 0.05, *p < 0.1).

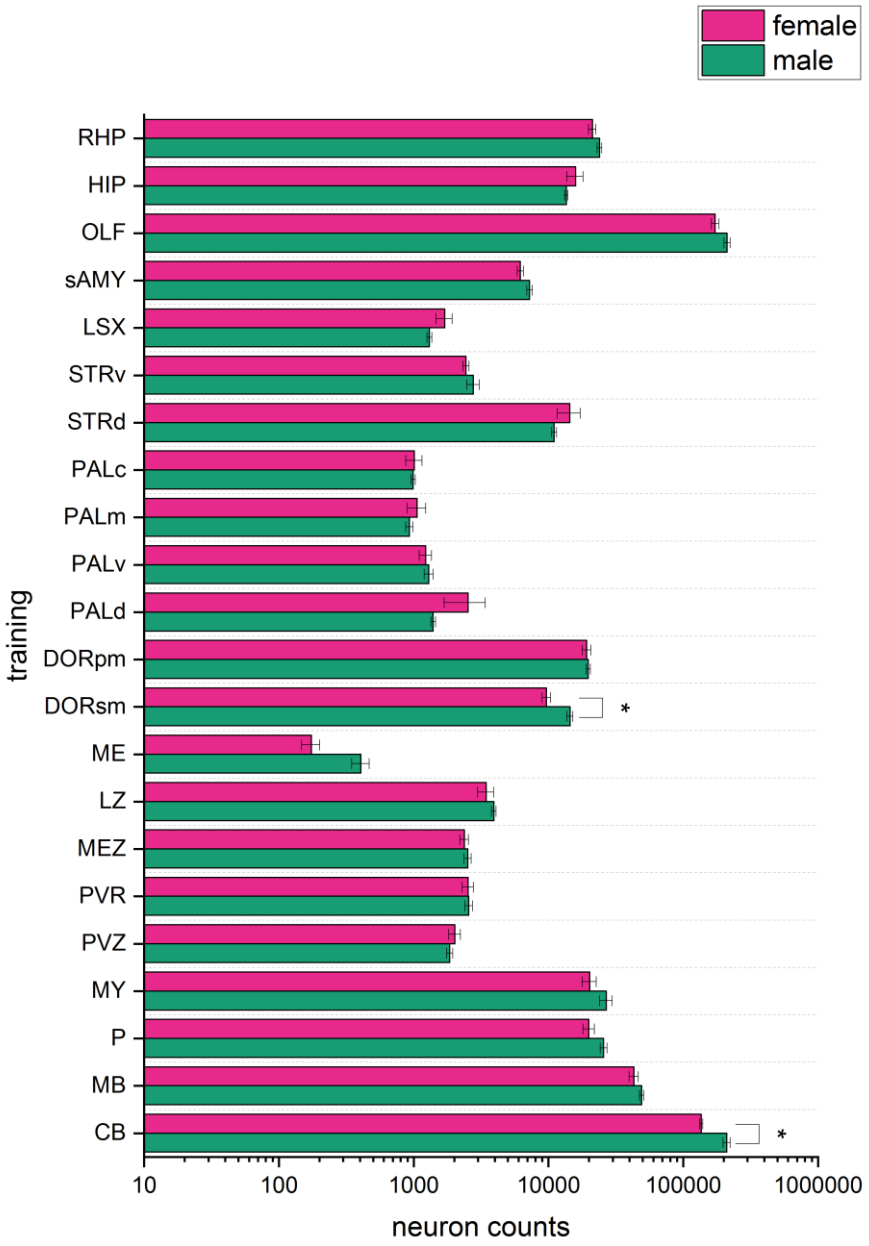

Figure 9.5: Automated quantification of the TRAPed cell between male and female mice. Here presented the results from the **training** group. All brain regions are listed in the legend above.

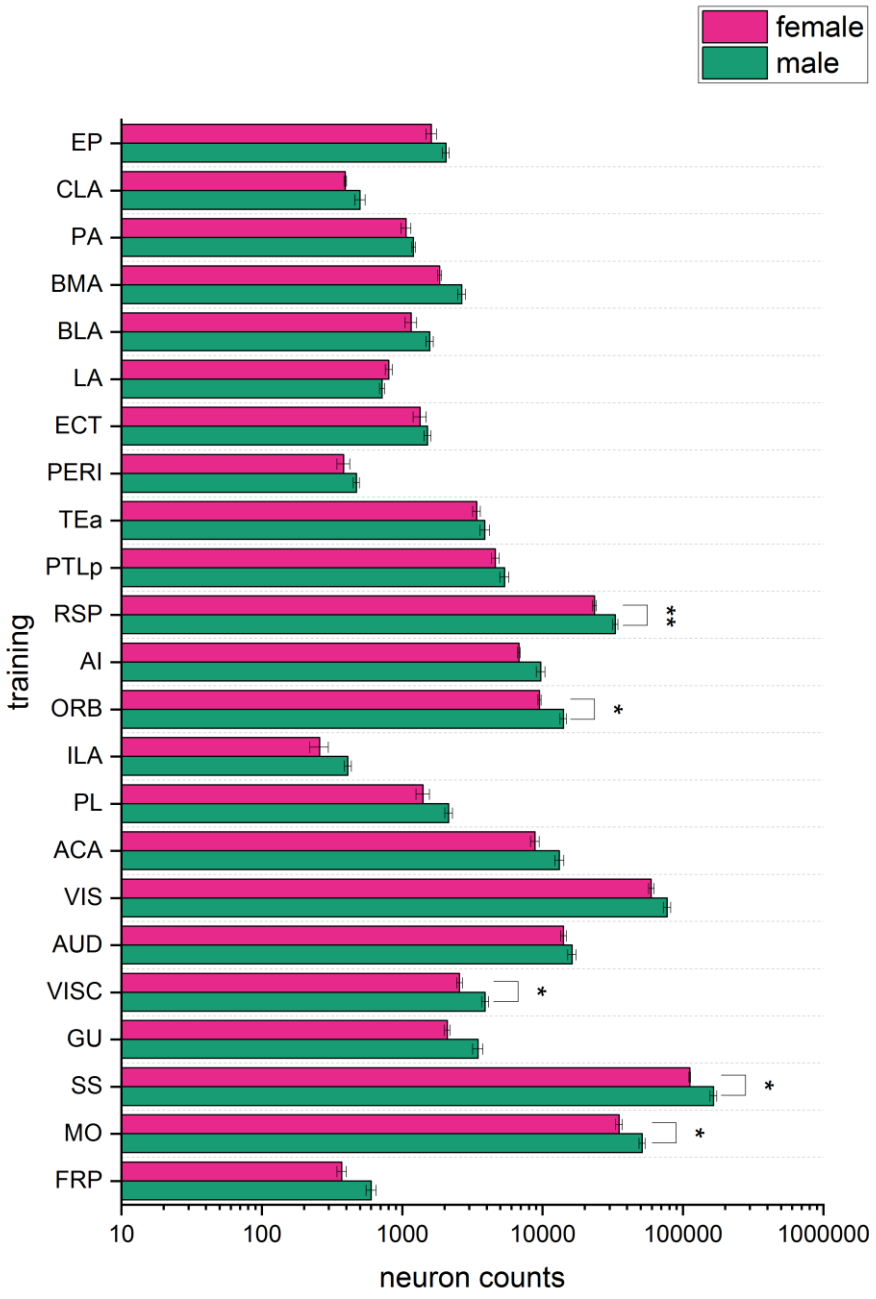

Figure 9.5 (continued): Data are represented as mean ± SEM (***p < 0.01, **p < 0.05, *p < 0.1).

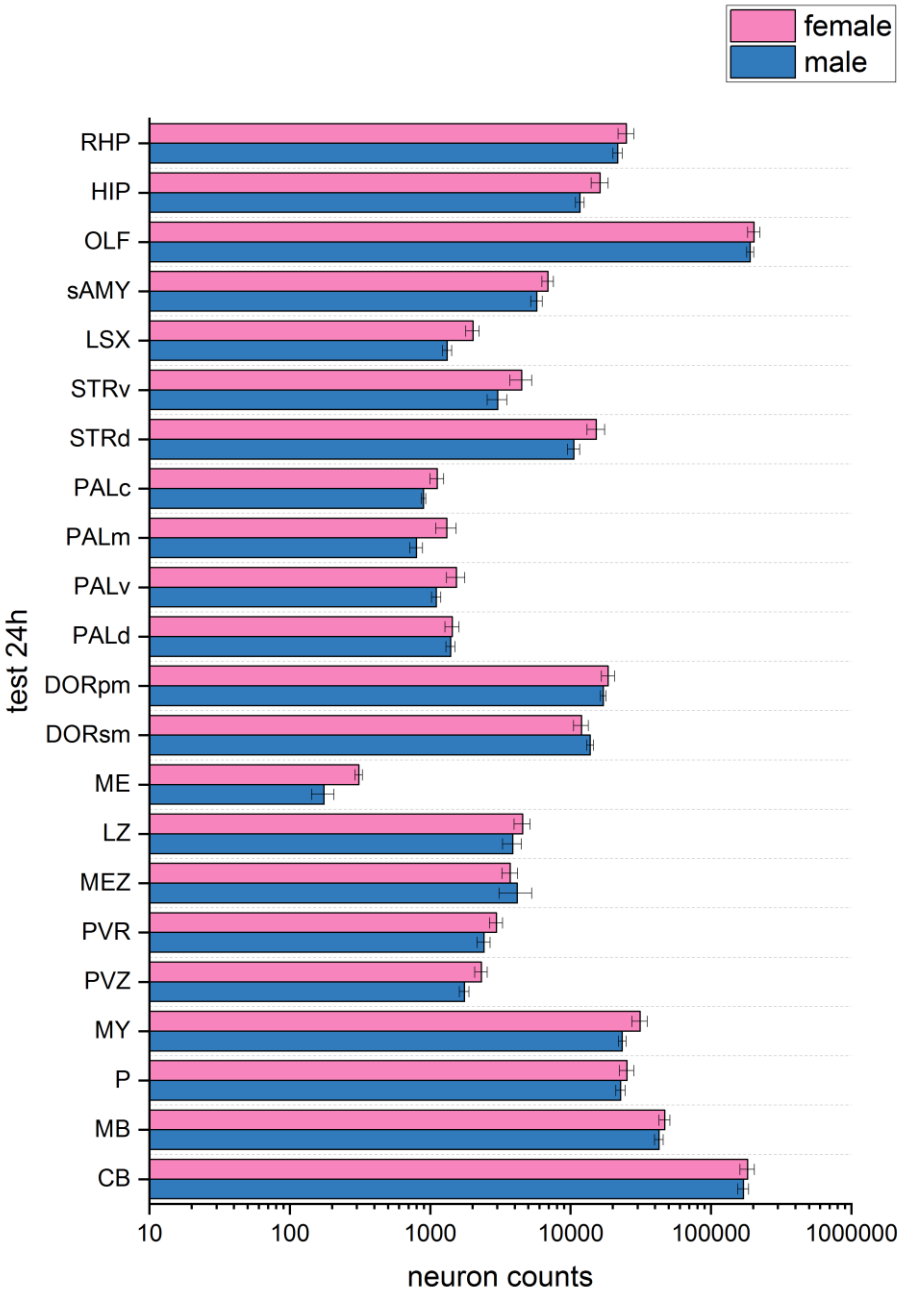

Figure 9.6: Automated quantification of the TRAPed cell between male and female mice. Here presented the results from the **test 24h** group. All brain regions are listed in the legend above.

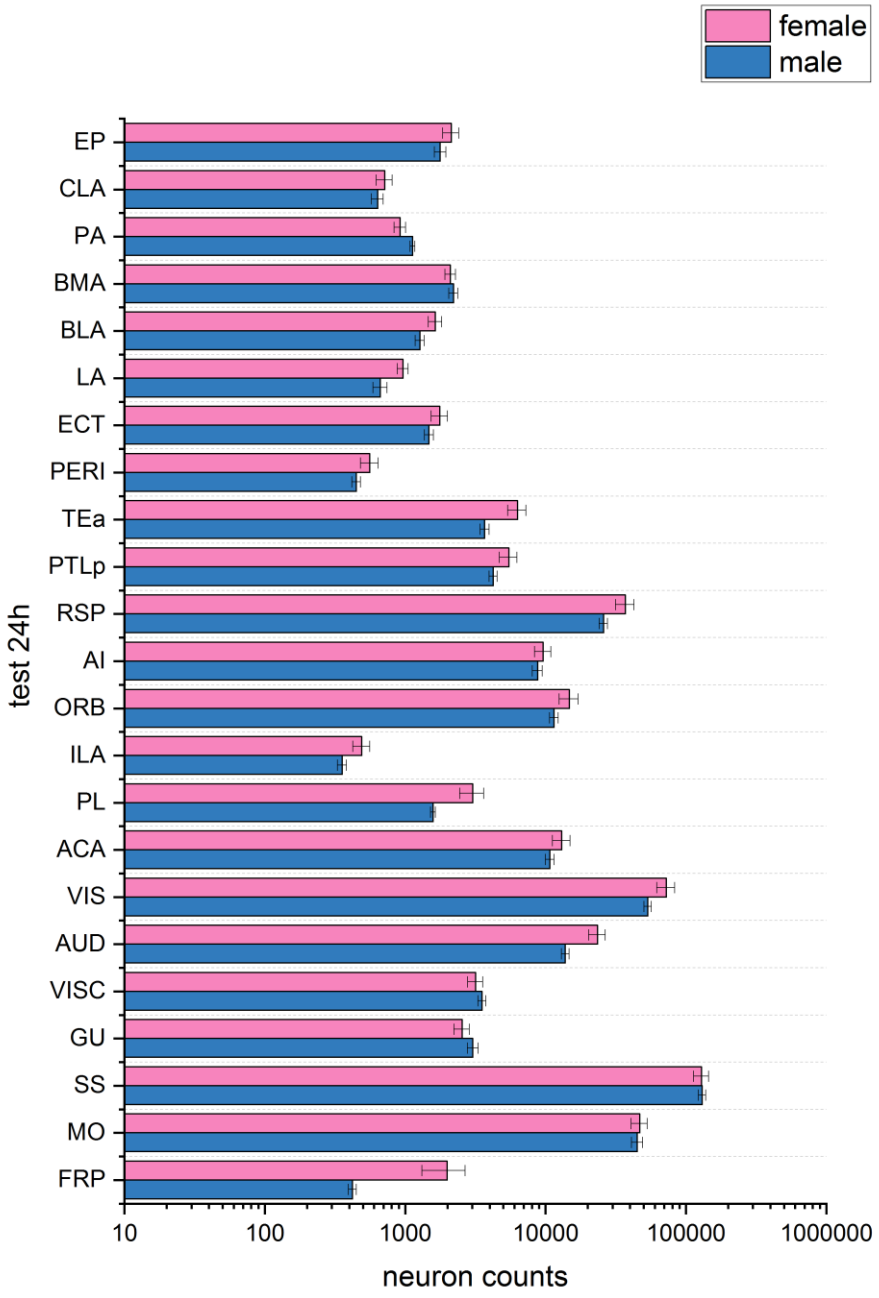

Figure 9.6 (continued): Data are represented as mean ± SEM (***p < 0.01, **p < 0.05, *p < 0.1).

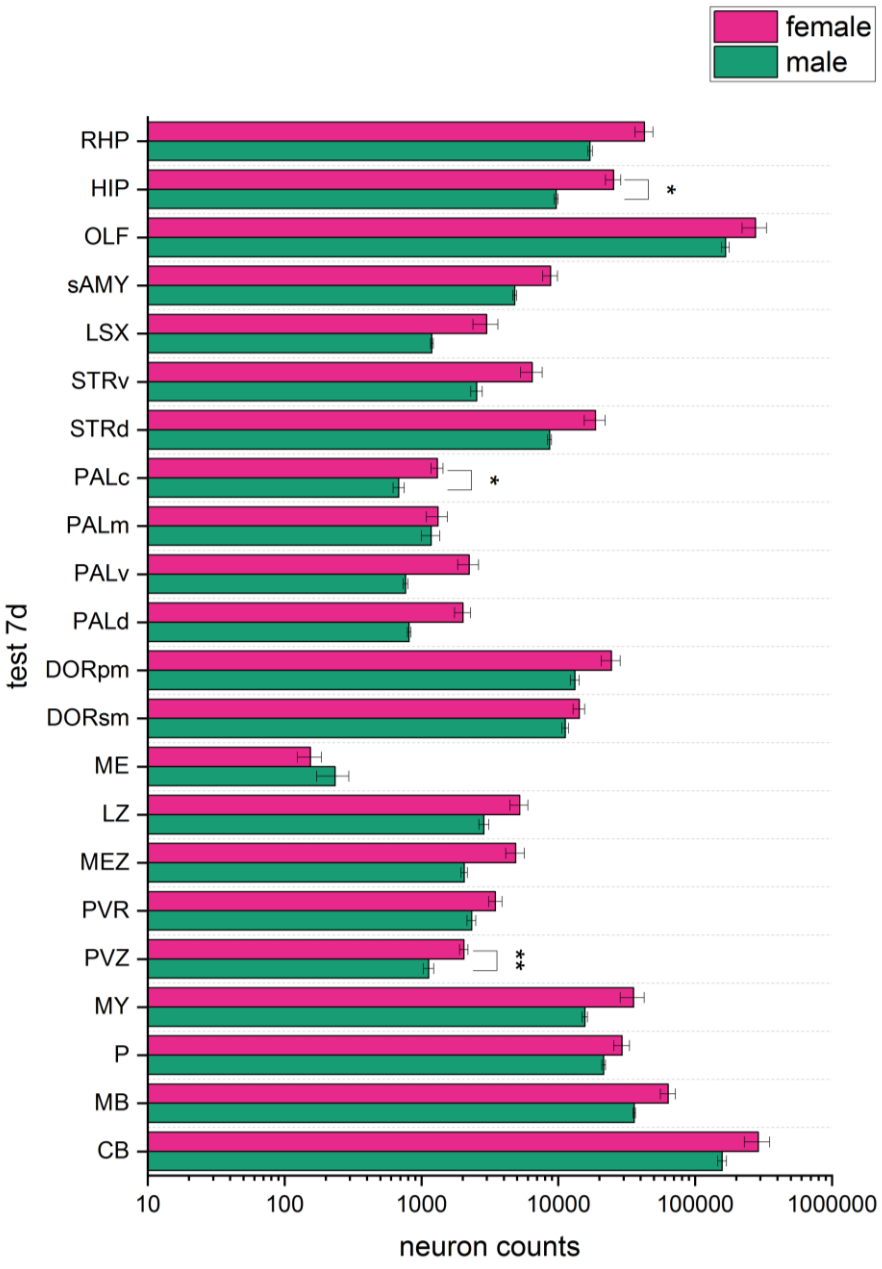

Figure 9.7: Automated quantification of the TRAPed cell between male and female mice. Here presented the results from the **test 7d** group. All brain regions are listed in the legend above.

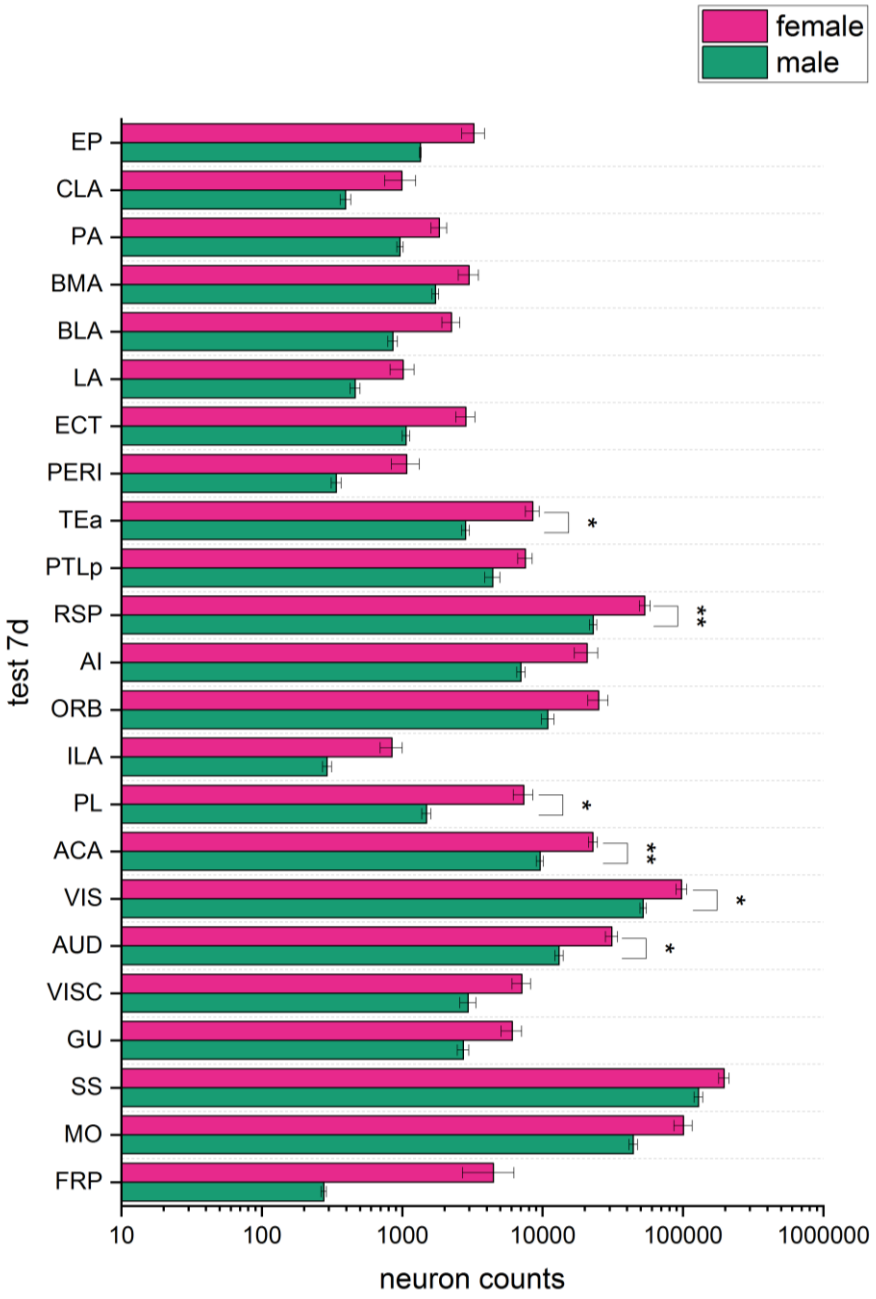

Figure 9.7 (continued): Data are represented as mean ± SEM (***p < 0.01, **p < 0.05, *p < 0.1).

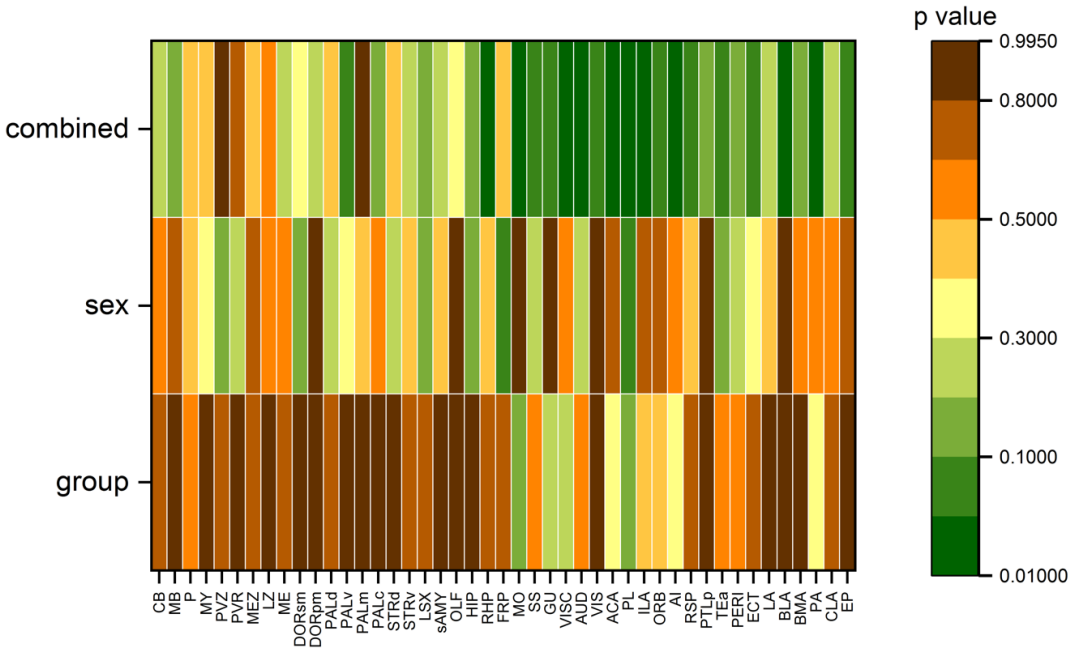

Figure 9.8: A two-way ANOVA analysis that evaluate the effect of a single variable, like sex or experimental group, and the effect of their combination on different brain areas.

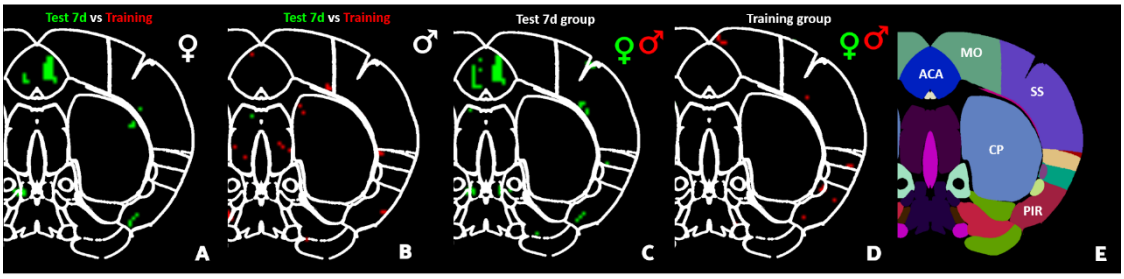

Figure 9.9: Whole-brain network involved in fear memory learning and recall. (A) Comparison between training and test 7d groups in female animals. The image shows regions where there were a significantly greater number of activated neurons in female test 7d mice recalling fear memories (green) compared to the training group (red), $p<0.05$. (B) Comparison between training and test 7d groups in male animals. The image shows regions where there were a significantly greater number of activated

neurons in male training mice learning fear (red) compared to test 7d group (green), $p<0.05$. (C) Comparison between male (red) and female (green) during fear memory recalling and (D) learning, $p<0.05$. (E) The last image shows the corresponding Allen Mouse Brain Atlas reference atlas annotations. Annotation: ACA anterior cingulate cortex, MO motorsensory area, SS somatosensory area, CP caudoputamen, PIR piriform area.

9.2 Effect of behavior on brain region activations

Our pipeline allowed to quantify c-Fos$^+$ cells per brain area, estimating the number of neurons and comparing this density between sex and experimental classes. This first step of analysis suggested that circuitry patterns involved in fear memory are influenced by sexually dimorphic trend. Apart from a quantitative analysis that showed quantitative differences between gender or classes; the behavioral outcomes indicated that all mice formed a trace of memory independently from their sex (Figure 8.4). Therefore, further investigations were performed to understand the correlation between activated areas and differences in latency times, identifying brain regions correlated to specific features of the fearful behaviors (Figure 9.10). Pearson correlation was used to study this brain-behavior association. By using this type of statistical test, new areas involved in learning, consolidation and retrieval of fear memory were discovered. Indeed, the heatmap pointed out to regions of the hindbrain as pons and medulla, not identified by previous quantitative analysis. A strong positive correlation of these areas was exhibited during the acquisition and retrieval of both genders. These parts of the motor system are known to be involved in fear memory, especially in specific motor actions invoked in emotions, as well as in the control of heart rate, respiration, vocalization (Holstege, 2009; Venkatraman et al., 2017).

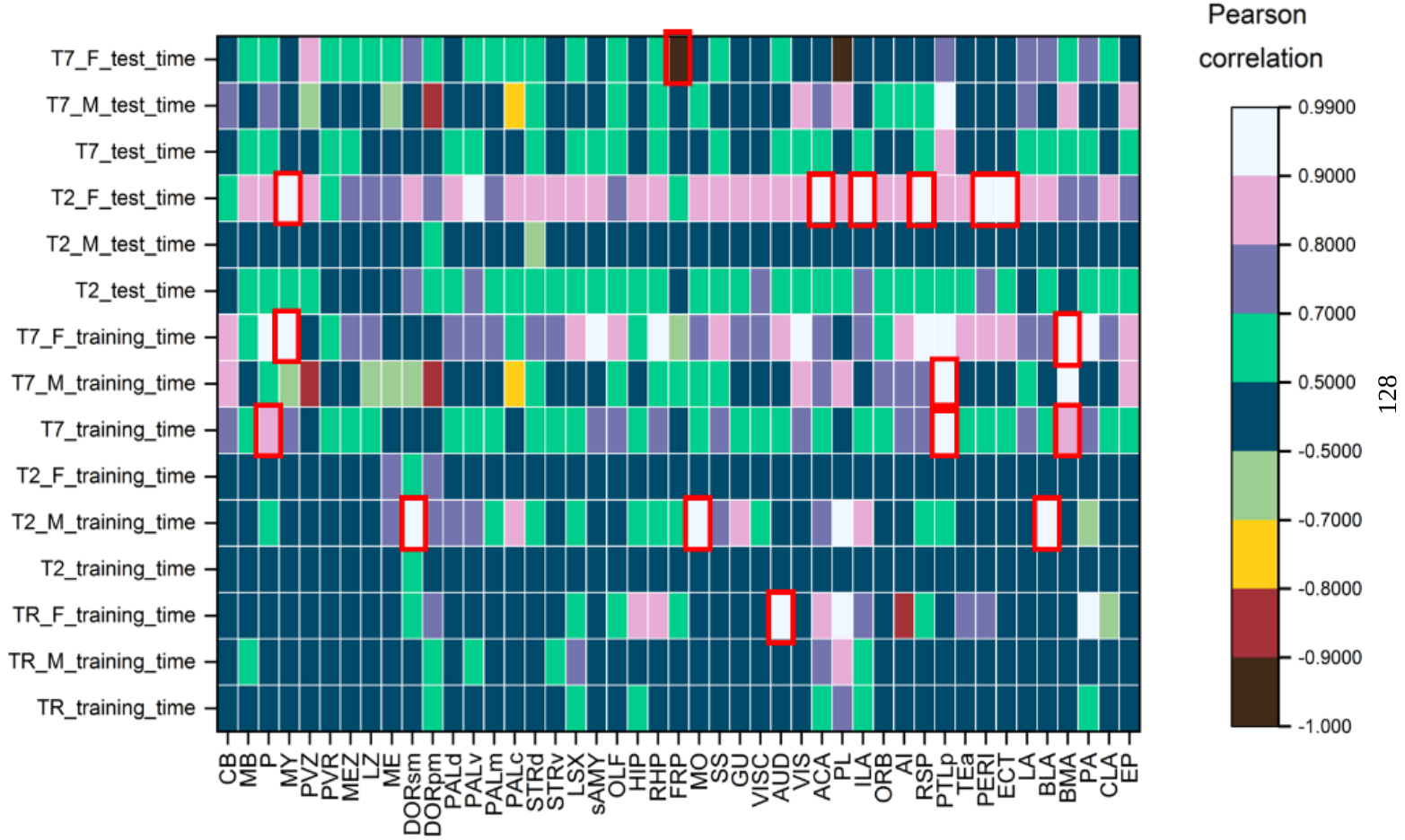
T7_F_test_time
T7_M_test_time
T7_test_time
T2_F_test_time
T2_M_test_time
T2_test_time
T7_F_training_time
T7_M_training_time
T7_training_time
T2_F_training_time
T2_M_training_time
T2_training_time
TR_F_training_time
TR_M_training_time
TR_training_time
CB
MB
P
MY
PVZ
PVR
MEZ
LZ
ME
DORsm
DORpm
PALd
PALv
PALm
PALc
STRd
STRv
LSX
sAMY
OLF
HIP
RHP
FRP
MO
SS
GU
VISC
AUD
VIS
ACA
PL
ILA
ORB
AI
RSP
PTLp
TEa
PERI
ECT
LA
BLA
BMA
PA
CLA
EP
Pearson
correlation
0.9900
0.9000
0.8000
0.7000
0.5000
-0.5000
-0.7000
-0.8000
-0.9000
-1.000
128

Figure 9.10: Pearson correlation analysis that shows the correlation between behavior, referred as latency time and levels of activations in specific brain areas. On the right side of the plot, at each level of the Pearson correlation coefficient (PCC) corresponds with a different color. Red frames highlight the brain region with $p < 0.001$.

Moreover, unlike in histogram showing average activation across different subjects, it was also noted that activation in somatomotor and posterior parietal association areas during training was strongly correlated to behavior in male groups. This outcome would seem interesting since these brain parts are implied in the conversion of sensory information (electric foot shock) to motor commands (escape) (Lyamzin & Benucci, 2019). Conversely, the frontal pole was one of the few parts that showed a negative correlation during fear memory recall in mice. This area is known for its role in fear extinction, therefore its inactivation causes a sustained conditioned freezing (Zimmermann et al., 2018). In conclusion, this correlative analysis revealed regions significantly involved at behavioral level. Differently from the histogram that represented the distribution of activated neurons in a population, Pearson correlation was able to appreciate the distinct activation patterns at the level of a single subject.

Chapter 10

Results III

The developed pipeline proved a strong sexual dimorphism during learning, consolidation and recall of fear memory. The use of a whole-brain scale has also exhibited different activation patterns during behavior in each sample.

The use of high-resolution imaging, in addition to enabling the quantification of all TRAPed neurons, allowed detailed analysis of small brain regions, as TMN, inside the same brain.

10.1 Activation patterns of histaminergic neurons involved in fear memory learning

The comprehension of the neurotransmitter systems involved in memory, and particularly memory related to fear emotions has always aroused great interest. Many studies have demonstrated that biogenic amines, as catecholamines and serotonin, modulate the storage and retrieval of memory information (Fernandez et al., 2017; McGaugh, 2000b; Quartermain & Judge, 1983; Roozendaal & McGaugh, 2011; Zhang & Stackman, 2015). From the 1960s, publications about these neurotransmitters overwhelmed those about histamine, largely due to their easy identification at the brain level (Carlsson et al., 1961). However, recent findings have reasserted the role of histamine in the regulation of memory consolidation, first proposed by Almeida and Izquierdo, using inhibitory avoidance paradigm in rats (Benetti et al., 2015). Up to now, comprehensive studies on mouse models do not exist. To fill this knowledge gap, in this thesis I demonstrated the possibility of using novel technologies to investigate the role of histamine in aversive memory in mice, too.

An important question is related to the inter-individual variability of the sub-population of histaminergic neurons that are activated following an aversive stimulus. As proof of principle, all activated histaminergic neurons, related to four male homecage mice and four male training mice, were quantified. These findings did not reveal any statistical difference in neuron counts. This lack of significance may be attributed to high variability inside the same group (Figure 10.1).

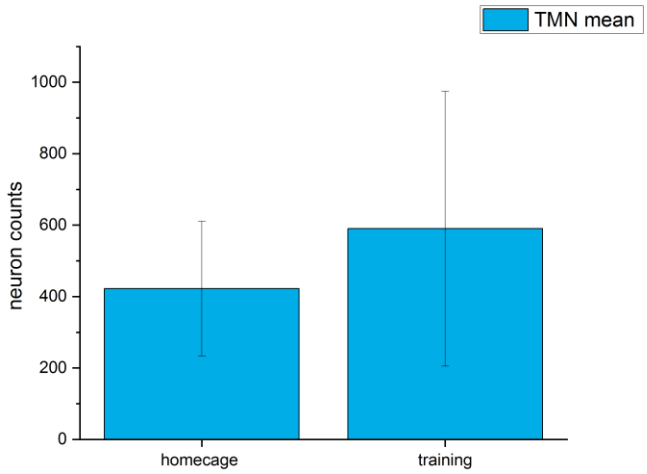

Figure 10.1: Quantification of activated histaminergic neurons in homecage and training male groups. Data are represented as mean ± SEM.

Despite the comparison of these groups did not show any difference in cell counts, the spatial distribution of activated histaminergic neurons changed between the homecage and training group (Figure 10.2). In order to understand how the spatial distribution of these cells varies, the 3D high resolution was exploited to evaluate the distance between each H^+ neuron and the sagittal medial plane (Figure 10.3). As the graph suggests, histaminergic cells regarding the homecage group are more distant from the medial sagittal plane compared to those of the training group (Figures 10.2, 10.4, 10.5). This could indicate a major distribution of these neurons on the ventral part of TMN (Figure 10.4), contrary to neurons related to the training group that showed a more dorsal distribution (Figure 10.5). These results suggest that specific sub-populations of histaminergic cells are recruited after an aversive stimulus. This is coherent with the hypothesis of the histaminergic system composed by multiple functional sub-units.

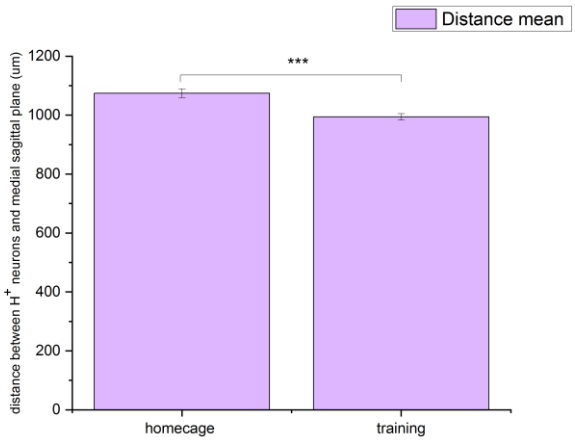

Figure 10.2: The mean of the distances between the activated histaminergic neuron and medial sagittal plane. Data are represented as mean ± SEM (***$p < 0.01$).

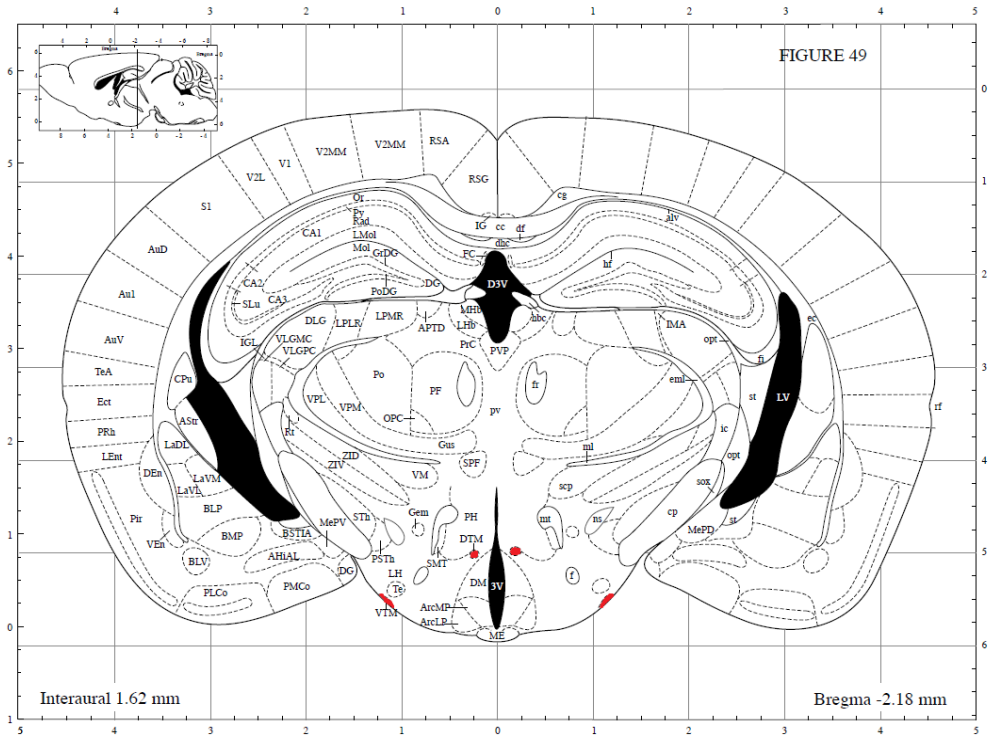

Figure 10.3: Coronal sections showing DTM and VTM, here colored in red, inside the mouse brain. Image are from (Paxinos & Franklin, 2001).

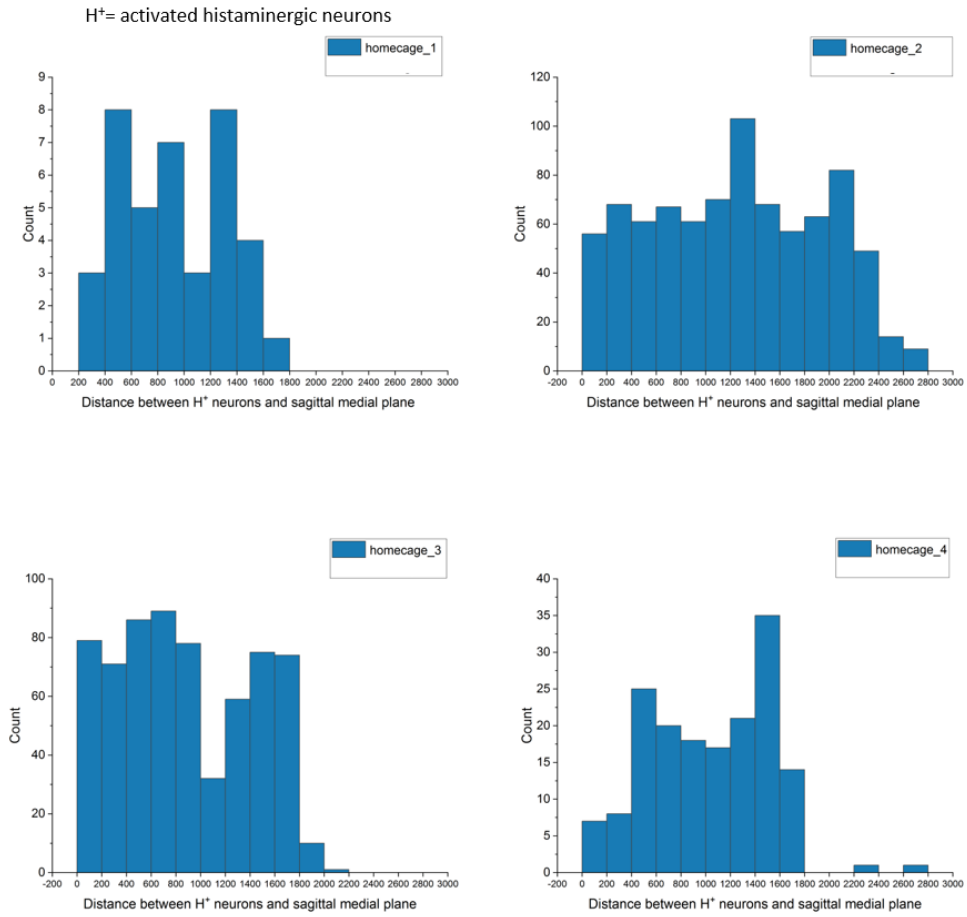

Figure 10.4: Spatial distribution of activated histaminergic neurons inside TMN. The graphs show the number of histaminergic activated neurons that are equidistant from the medial sagittal plane, for the homecage group.

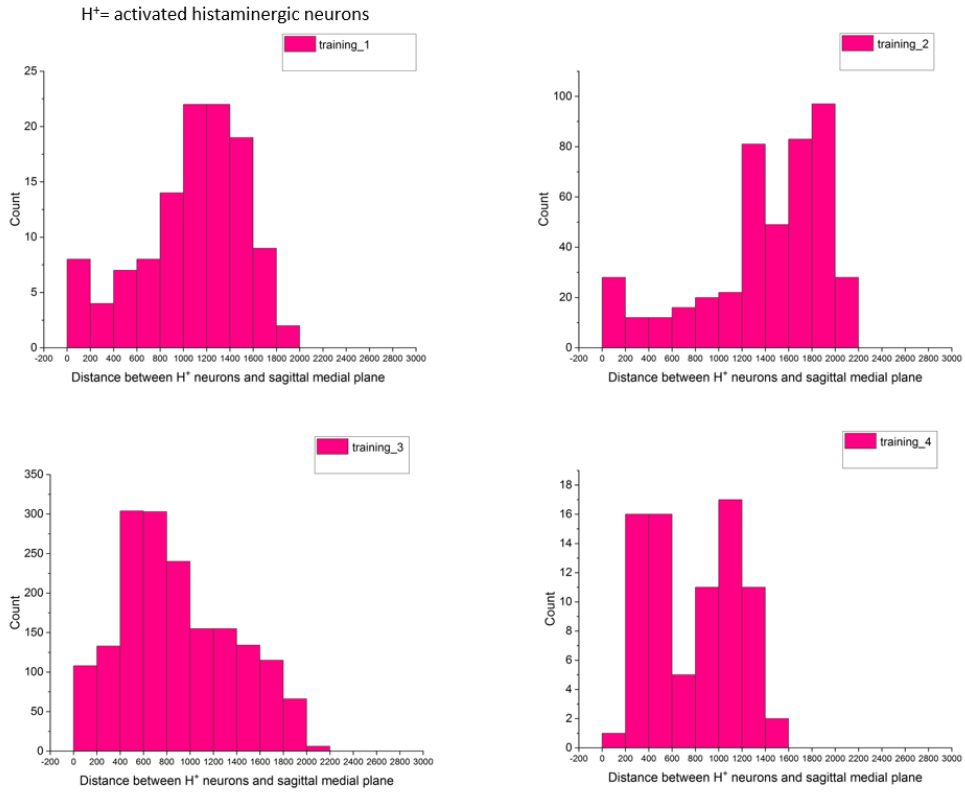

Figure 10.5: Spatial distribution of activated histaminergic neurons inside TMN. The graphs show the number of histaminergic activated neurons that are equidistant from the medial sagittal plane, for the training group.

Part IV

Conclusion

Chapter 11

Discussion

Memory in general, but especially memory related to aversive events, has always received a lot of attention since it triggers many behaviors, crucial for survival (i.e. fight, escape and freeze). The reconstruction of the neuronal circuitry involved in memory is currently one of the major challenges for contemporary neuroscience. Nowadays, although many brain structures involved in fear memory are well-known (Ivan Izquierdo et al., 2016; Silva et al., 2016), the mechanism by which memory is encoded in specific circuits has not been widely investigated. From a methodological point of view, recent technological advancements have made possible to solve this issue. Nevertheless, no 3D technique with a resolution high enough to quantify neurons across the entire brain, including densely labeled areas, has been used up to now. Indeed, if on the one hand high-resolution techniques were limited by selected spatial areas (Hasan et al., 2019), on the other hand, current whole-approaches allowed fast reconstruction of large volumes but at low resolution (Renier et al., 2016b; Ye et al., 2016).

To tackle the question about fear memory engram, an integrated approach that involves brain-wide scale and cellular resolution has proved necessary.

In this thesis, I developed a pipeline for mapping neuronal activation at micron resolution, combining transgenic approach, clearing protocol, high-resolution imaging, atlas registration, and automated 3D image analysis. This method allowed to visually represent a specific phase of aversive memory capturing all activated neurons, as would make a snapshot photo.

The combination of high-resolution imaging and 3D analysis for processing sub-cellular information became the key point of this pipeline, enabling high performance. This synergistic approach also allowed to focus simultaneously on the entire brain and a small region like TMN, known for for its involvement in memory functions. Although the presented intact-brain pipeline could appear complex and long-lasting, it was used on large cohorts of experimental classes, but also and overall, in a routine way. Moreover, this type of approach could bypass some limitations related to physical sectioning. For example, different computational pipelines based on high-resolution exploited STP as 3D optical imaging (Kim et al., 2015; Vousden et al., 2015). In general, the inability to process the intact volume provides a drawback related to selection bias and to the loss of continuity, since only a small percentage of the total volume is actually imaged (Renier et al., 2016b; Ye et al., 2016). Therefore, a complete quantification of TRAPed cells would have not been possible using 2D planes or "sparse sampling reconstructions". Additionally, STP is a destructive technique that leads to sample damage. It is for this reason that the pipeline reported here seemed necessary for integrating whole-brain neuronal activity quantification with further analysis, as immunohistochemical investigations at a later time.

The choice of micron-scale resolution for mapping neuronal activity is paramount in our question. Although the amount of data contained in all reconstructions could be estimated at about 600 TB (15 TB for each brain), our high-throughput method ensured an efficient data handling. Moreover, the option to increase the resolution proved indispensable for automated quantitative analysis since, using the TRAP model, the signal for c-Fos is extended to the entire neurons. As shown in 8.1.5, due to the high expression of TRAP cells in many brain regions, low-resolution imaging was unable to provide an appropriate quantification, limiting the analysis to selected areas (Ye et al., 2016).

Its unique features in terms of micron-scale resolution and automated 3D analysis make this pipeline a rapid and unbiased method to address the question of fear memory engram.

Indeed, this approach allowed us to highlight a strong sexual dimorphism, during fear learning and recall, which was not evident from behavioral tasks, revealing the involvement of brain regions not always related to this type of memory, as temporal association areas, somatosensory areas, perirhinal area or retrosplenial cortex. In this respect, analysis of regional cell counts was the first step of investigation that provided relevant information inside the same experimental group.

However, each animal exhibits its own behavior, which in turn depends on coordinated activity across multiple brain regions. Thus, group-averaged cell quantification is insufficient to investigate the physical trace of memory. To overcome this limitation, brain-behavior correlation analyses were exploited to understand which brain regions are more relevant for the observed inter-individual variability in step-through latency times. The use of high-resolution coupled with high-throughput imaging and image analysis enabled comprehensive whole-brain analysis in TRAP mice, where activated cells are labelled in their entirety, challenging low-resolution analysis (Ye et al., 2016). In turn, TRAP permanent labelling overcame the temporal limits related to IEG kinetics in traditional anti-cfos IHC, allowing to explore more flexibility in experimental design.

The observed outcomes reaffirmed the power and the multifunctional character of the pipeline developed in this thesis, showing its flexibility for numerous aims. As a result, different activity patterns were involved in different phases of fear memory, confirming the elevated fleetingness of the engram. This suggests that the memory physical trace could show inter-individual diversity (Josselyn et al., 2015), in line with the large variability of behavioral responses to the same stimulus.

The study of selected neurotransmitter systems is of fundamental importance to improve the understanding of how the brain remembers fear emotions. Investigations on small nucleus as TMN suggested a precise distribution of activated histaminergic neurons in organized distinct circuits. In this case, the choice of high resolution allowed more accurate analysis of spatial distribution, not limited to cell counts as in standard stereological quantification. These types of analysis, only feasible using a cell-resolution 3D methodology, could demonstrate whether histamine neurons are organized in a heterogeneous population with independent functions.

In conclusion, the pipeline I described here, is readily adaptable for broader applications. The advantage of using micrometer resolution on brain-wide scale for analyzing the entire brain and an interested region, could revolutionize the way of studying brain connectivity and functions.

Chapter 12

Future outlook

The work of this thesis consisted in the development of a pipeline able to represent and analyze different neuronal patterns involved in aversive memory.

The high-resolution and automated 3D analysis pipeline introduced in this thesis allowed whole-brain quantification in behavioral cohorts with a detail that was not accessible to previous approaches, which were limited either to lower resolution or to a small number of samples.

However, to obtain even higher performances, further improvements need be done. The detection and quantification of all c-fos positive neurons was performed using an ANN that worked with F score equal to 0.71. Therefore, in order to bring F score to value closer to 1, we have to enhance its performance increasing the training data set. This improvement could also be achieved by techniques like transfer learning (Finn et al., 2017; Mishra et al., 2018; Pan & Yang, 2010). Furthermore, another critical step is the registration of our data sets to the Allen Mouse Brain Atlas. By segmenting more precise areas and creating a 3D mask for each of these, the Atlas alignment performance would be improved.

The quantitative whole-brain analysis of neuronal activation presented here, used to analyze a selected behavior, paves the way to targeted cell manipulation with chemogenetic or optogenetic tools (DeNardo et al., 2019; Hasan et al., 2019; Sakurai et al., 2016), giving to researchers the possibility to activate or inactivate behaviorally relevant neurons. The activation maps could be used as first step to understand and to know which brain areas are involved in a specific cognitive or behavioral processes. Using these maps as stepping stone for modulating activity of targeted regions or

neuronal populations, we may assess in a causal way whether those regions or populations are related or not to the investigated behavior, then identifying the exact network activated by encoding or recall of a fear memory in mice. The method described in this thesis could be applied to other biological purposes. Indeed, this pipeline is not restricted to the single study of fear memory but it can be also used to investigate preclinical model of diseases or to validate drug treatments. In this context, an implementation of TRAP with viral strategies, as has already exploited by Deisseroth's group (Ye et al., 2016), could facilitate its application on transgenic models of pathologies. Furthermore, the latest AAV.PHP.eB-based systemic labeling may even reveal surprising results on whole-brain scale. In parallel, a promising improvement to our pipeline could include whole-mount IHC, allowing visualizing activity patterns at two different time-point, one labeled with TRAP-based approaches and another with anti-cFos staining (DeNardo et al., 2019).

In conclusion, these results demonstrated that the methodology developed and validated in this thesis could be applied to preclinical translational research in order to improve the knowledge and medical outcomes about many pathologies as anxiety, OCD and PTSD.

Bibliography

Adolphs, R. (2013). The biology of fear. In *Current Biology*. https://doi.org/10.1016/j.cub.2012.11.055

Albo, Z., & Gräff, J. (2018). The mysteries of remote memory. In *Philosophical Transactions of the Royal Society B: Biological Sciences*. https://doi.org/10.1098/rstb.2017.0029

Alonso, M., Bekinschtein, P., Cammarota, M., Vianna, M. R. M., Izquierdo, I., & Medina, J. H. (2005). Endogenous BDNF is required for long-term memory formation in the rat parietal cortex. *Learning and Memory*. https://doi.org/10.1101/lm.27305

Alvarez, E. O. (2009). The role of histamine on cognition. In *Behavioural Brain Research*. https://doi.org/10.1016/j.bbr.2008.12.010

Atkinson, R.C. & Shiffrin, R. M. (1968). "Chapter: Human memory: A proposed system and its control processes". In Spence, K.W.; Spence, J.T. The psychology of learning and motivation (Volume 2). *Psychology of Learning and Motivation*.

Avants, B. B., Epstein, C. L., Grossman, M., & Gee, J. C. (2008). Symmetric diffeomorphic image registration with cross-correlation: Evaluating automated labeling of elderly and neurodegenerative brain. *Medical Image Analysis*. https://doi.org/10.1016/j.media.2007.06.004

Avants, Brian B., Tustison, N. J., Song, G., Cook, P. A., Klein, A., & Gee, J. C. (2011). A reproducible evaluation of ANTs similarity metric performance in brain image registration. *NeuroImage*. https://doi.org/10.1016/j.neuroimage.2010.09.025

Azevedo, H., Ferreira, M., Mascarello, A., Osten, P., & Guimarães, C. R. W. (2020). Brain-wide mapping of c-fos expression in the single prolonged stress model and the effects of pretreatment with ACH-000029 or prazosin. *Neurobiology of Stress*. https://doi.org/10.1016/j.ynstr.2020.100226

Baarendse, P. J. J., Van Grootheest, G., Jansen, R. F., Pieneman, A. W., Ögren, S. O., Verhage, M., & Stiedl, O. (2008). Differential involvement of the dorsal hippocampus in passive avoidance in C57BL/6J and DBA/2J mice. *Hippocampus*. https://doi.org/10.1002/hipo.20356

Barros, D. M., Izquierdo, L. A., Mello E Souza, T., Ardenghi, P. G., Pereira, P., Medina, J. H., & Izquierdo, I. (2000). Molecular signalling pathways in the cerebral cortex are required for retrieval of one-trial avoidance learning in rats. *Behavioural Brain Research*. https://doi.org/10.1016/S0166-4328(00)00226-6

Barros, D. M., Mello e Souza, T., De David, T., Choi, H., Aguzzoli, A., Madche, C., Ardenghi, P., Medina, J. H., & Izquierdo, I. (2001). Simultaneous modulation of retrieval by dopaminergic D1, β-noradrenergic, serotonergic-1A and cholinergic muscarinic receptors in cortical structures of the rat. *Behavioural Brain Research*.

https://doi.org/10.1016/S0166-4328(01)00208-X

Benetti, F., Guerino Furini, C. R., De Carvalho Myskiw, J., Provensi, G., Passani, M. B., Baldi, E., Bucherelli, C., Munari, L., Izquierdo, I., & Blandina, P. (2015). Histamine in the basolateral amygdala promotes inhibitory avoidance learning independently of hippocampus. *Proceedings of the National Academy of Sciences of the United States of America*. https://doi.org/10.1073/pnas.1506109112

Benjamini, Y., & Hochberg, Y. (1995). Controlling the False Discovery Rate: A Practical and Powerful Approach to Multiple Testing. *Journal of the Royal Statistical Society: Series B (Methodological)*. https://doi.org/10.1111/j.2517-6161.1995.tb02031.x

Berry, A., Bellisario, V., Capoccia, S., Tirassa, P., Calza, A., Alleva, E., & Cirulli, F. (2012). Social deprivation stress is a triggering factor for the emergence of anxiety- and depression-like behaviours and leads to reduced brain BDNF levels in C57BL/6J mice. *Psychoneuroendocrinology*. https://doi.org/10.1016/j.psyneuen.2011.09.007

Blandina, P., Munari, L., Provensi, G., & Passani, M. B. (2012). Histamine neurons in the tuberomamillary nucleus: A whole center or distinct subpopulations? In *Frontiers in Systems Neuroscience*. https://doi.org/10.3389/fnsys.2012.00033

Bryan, K. J., Lee, H., Perry, G., Smith, M. A., & Casadesus, G. (2009). Transgenic Mouse Models of Alzheimer's Disease: Behavioral Testing and Considerations. In *Methods of Behavior Analysis in Neuroscience*.

Burwell, R. D., Saddoris, M. P., Bucci, D. J., & Wiig, K. A. (2004). Corticohippocampal Contributions to Spatial and Contextual Learning. *Journal of Neuroscience*. https://doi.org/10.1523/JNEUROSCI.0410-04.2004

Cahill, L., & McGaugh, J. L. (1998). Mechanisms of emotional arousal and lasting declarative memory. *Trends in Neurosciences*. https://doi.org/10.1016/S0166-2236(97)01214-9

CARLSSON, A., FALCK, B., HILLARP, N. A., THIEME, G., & TORP, A. (1961). A new histochemical method for visualization of tissue catechol amines. *Medicina Experimentalis. International Journal of Experimental Medicine*. https://doi.org/10.1159/000135003

Chung, K., Wallace, J., Kim, S. Y., Kalyanasundaram, S., Andalman, A. S., Davidson, T. J., Mirzabekov, J. J., Zalocusky, K. A., Mattis, J., Denisin, A. K., Pak, S., Bernstein, H., Ramakrishnan, C., Grosenick, L., Gradinaru, V., & Deisseroth, K. (2013). Structural and molecular interrogation of intact biological systems. *Nature*, *497*(7449), 332–337. https://doi.org/10.1038/nature12107

Costantini, I., Ghobril, J. P., Di Giovanna, A. P., Allegra Mascaro, A. L., Silvestri, L., Müllenbroich, M. C., Onofri, L., Conti, V., Vanzi, F., Sacconi, L., Guerrini, R., Markram, H., Iannello, G., & Pavone, F. S. (2015). A versatile clearing agent for multi-modal brain imaging. *Scientific Reports*, *5*, 1–9. https://doi.org/10.1038/srep09808

De Almeida, M. A. M. R., & Izquierdo, I. (1986). Memory facilitation by histamine. *Archives Internationales de Pharmacodynamie et de Therapie*.

DeNardo, L. A., Liu, C. D., Allen, W. E., Adams, E. L., Friedmann, D., Fu, L., Guenthner, C. J., Tessier-Lavigne, M., & Luo, L. (2019). Temporal evolution of cortical ensembles promoting remote memory retrieval. *Nature Neuroscience*, *22*(3), 460–469. https://doi.org/10.1038/s41593-018-0318-7

Di Giovanna, A. P., Credi, C., Franceschini, A., Müllenbroich, M. C., Silvestri, L., & Pavone, F. S. (2019). Tailored sample mounting for light-sheet fluorescence microscopy of clarified specimens by polydimethylsiloxane casting. *Frontiers in Neuroanatomy*. https://doi.org/10.3389/fnana.2019.00035

Fendt, M., & Fanselow, M. S. (1999). The neuroanatomical and neurochemical basis of conditioned fear. In *Neuroscience and Biobehavioral Reviews*. https://doi.org/10.1016/S0149-7634(99)00016-0

Fernandez, S. P., Muzerelle, A., Scotto-Lomassese, S., Barik, J., Gruart, A., Delgado-Garciá, J. M., & Gaspar, P. (2017). Constitutive and Acquired Serotonin Deficiency Alters Memory and Hippocampal Synaptic Plasticity. *Neuropsychopharmacology*. https://doi.org/10.1038/npp.2016.134

Finn, C., Abbeel, P., & Levine, S. (2017). Model-agnostic meta-learning for fast adaptation of deep networks. *34th International Conference on Machine Learning, ICML 2017*.

Franceschini, A., Costantini, I., Pavone, F. S., & Silvestri, L. (2020). Dissecting Neuronal Activation on a Brain-Wide Scale With Immediate Early Genes. *Frontiers in Neuroscience*. https://doi.org/10.3389/fnins.2020.569517

Franz, S. I., & Lashley, K. S. (1917). The retention of habits by the rat after destruction of the frontal portion of the cerebrum. *Psychobiology*. https://doi.org/10.1037/h0074177

Frasconi, P., Silvestri, L., Soda, P., Cortini, R., Pavone, F. S., & Iannello, G. (2014). Large-scale automated identification of mouse brain cells in confocal light sheet microscopy images. *Bioinformatics*. https://doi.org/10.1093/bioinformatics/btu469

Gabrieli, J. D. E. (1998). COGNITIVE NEUROSCIENCE OF HUMAN MEMORY. *Annual Review of Psychology*. https://doi.org/10.1146/annurev.psych.49.1.87

Galil, Z. (1983). Efficient algorithms for finding maximal matching in graphs. *Lecture Notes in Computer Science (Including Subseries Lecture Notes in Artificial Intelligence and Lecture Notes in Bioinformatics)*. https://doi.org/10.1007/3-540-12727-5_4

Garner, J. P., Dufour, B., Gregg, L. E., Weisker, S. M., & Mench, J. A. (2004). Social and husbandry factors affecting the prevalence and severity of barbering ("whisker trimming") by laboratory mice. *Applied Animal Behaviour Science*. https://doi.org/10.1016/j.applanim.2004.07.004

Gerrig, R. J., & Zimbardo, P. G. (2005). Psicologia y Vida. *Pearson Educación*.

Gold, P. E. (1986). The use of avoidance training in studies of modulation of memory storage. *Behavioral and Neural Biology*. https://doi.org/10.1016/S0163-1047(86)90927-1

Guenthner, C. J., Miyamichi, K., Yang, H. H., Heller, H. C., & Luo, L. (2013). Permanent genetic access to transiently active neurons via TRAP: Targeted recombination in active populations. *Neuron*, *78*(5), 773–784. https://doi.org/10.1016/j.neuron.2013.03.025

Haas, H. L., Sergeeva, O. A., & Selbach, O. (2008). Histamine in the nervous system. In *Physiological Reviews*. https://doi.org/10.1152/physrev.00043.2007

Hasan, M. T., Althammer, F., Silva da Gouveia, M., Goyon, S., Eliava, M., Lefevre, A., Kerspern, D., Schimmer, J., Raftogianni, A., Wahis, J., Knobloch-Bollmann, H. S., Tang, Y., Liu, X., Jain, A., Chavant, V., Goumon, Y., Weislogel, J. M., Hurlemann, R., Herpertz, S. C., … Grinevich, V. (2019). A Fear Memory Engram and Its Plasticity in the Hypothalamic Oxytocin System. *Neuron*, *103*(1), 133-146.e8. https://doi.org/10.1016/j.neuron.2019.04.029

Holstege, G. (2009). The mesopontine rostromedial tegmental nucleus and the emotional motor system: Role in basic survival behavior. In *Journal of Comparative Neurology*. https://doi.org/10.1002/cne.21990

HUNSPERGER, R. W. (1963). Affective behavior patterns elicited by electrical stimulation of the brain stem and forebrain. *Journal de Physiologie*.

Izquierdo, Iván, Bevilaqua, L. R. M., & Cammarota, M. (2006). A arte de esquecer. In *Estudos Avancados*. https://doi.org/10.1590/s0103-40142006000300024

Izquierdo, Iván, Bevilaqua, L. R. M., Rossato, J. I., Bonini, J. S., Medina, J. H., & Cammarota, M. (2006). Different molecular cascades in different sites of the brain control memory consolidation. *Trends in Neurosciences*. https://doi.org/10.1016/j.tins.2006.07.005

Izquierdo, Ivan, Furini, C. R. G., & Myskiw, J. C. (2016). Fear memory. *Physiological Reviews*. https://doi.org/10.1152/physrev.00018.2015

Izquierdo, Ivan, & Medina, J. H. (1997). Memory formation: The sequence of biochemical events in the hippocampus and its connection to activity in other brain structures. *Neurobiology of Learning and Memory*. https://doi.org/10.1006/nlme.1997.3799

Izquierdo, Iván, Medina, J. H., Vianna, M. R. M., Izquierdo, L. A., & Barros, D. M. (1999). Separate mechanisms for short- and long-term memory. In *Behavioural Brain Research*. https://doi.org/10.1016/S0166-4328(99)00036-4

James, W. (1891). The Principles of Psychology. *The American Journal of Psychology*. https://doi.org/10.2307/1412102

Johansen, J. P., Cain, C. K., Ostroff, L. E., & Ledoux, J. E. (2011). Molecular mechanisms of fear learning and memory. In *Cell*. https://doi.org/10.1016/j.cell.2011.10.009

Johansen, J. P., Tarpley, J. W., Ledoux, J. E., & Blair, H. T. (2010). Neural substrates for expectation-modulated fear learning in the amygdala and periaqueductal gray. *Nature Neuroscience*. https://doi.org/10.1038/nn.2594

Josselyn, S. A., Köhler, S., & Frankland, P. W. (2015). Finding the engram. In *Nature Reviews*

Neuroscience. https://doi.org/10.1038/nrn4000

Kalueff, A. V., Stewart, A. M., Song, C., Berridge, K. C., Graybiel, A. M., & Fentress, J. C. (2016). Neurobiology of rodent self-grooming and its value for translational neuroscience. In *Nature Reviews Neuroscience*. https://doi.org/10.1038/nrn.2015.8

Kappel, S., Hawkins, P., & Mendl, M. T. (2017). To group or not to group? Good practice for housing male laboratory mice. In *Animals*. https://doi.org/10.3390/ani7120088

Kim, Y., Venkataraju, K. U., Pradhan, K., Mende, C., Taranda, J., Turaga, S. C., Arganda-Carreras, I., Ng, L., Hawrylycz, M. J., Rockland, K. S., Seung, H. S., & Osten, P. (2015). Mapping social behavior-induced brain activation at cellular resolution in the mouse. *Cell Reports*. https://doi.org/10.1016/j.celrep.2014.12.014

LeDoux, J. (2012). Rethinking the Emotional Brain. In *Neuron*. https://doi.org/10.1016/j.neuron.2012.02.004

LeDoux, J. E. (2014). Coming to terms with fear. In *Proceedings of the National Academy of Sciences of the United States of America*. https://doi.org/10.1073/pnas.1400335111

LeDoux, J. E., & Hofmann, S. G. (2018). The subjective experience of emotion: a fearful view. In *Current Opinion in Behavioral Sciences*. https://doi.org/10.1016/j.cobeha.2017.09.011

Leurs, R., Hough, L. B., Blandina, P., & Haas, H. L. (2012). Histamine. *Basic Neurochemistry*, 323–341. https://doi.org/10.1016/B978-0-12-374947-5.00016-X

Lopes, D. A., Souza, T. M. O., de Andrade, J. S., Silva, M. F. S., Antunes, H. K. M., Sueur-Maluf, L. Le, Céspedes, I. C., & Viana, M. B. (2018). Environmental enrichment decreases avoidance responses in the elevated T-maze and delta FosB immunoreactivity in anxiety-related brain regions. *Behavioural Brain Research*. https://doi.org/10.1016/j.bbr.2018.02.012

Luft, T., Pereira, G. S., Cammarota, M., & Izquierdo, I. (2004). Different time course for the memory facilitating effect of bicuculline in hippocampus, entorhinal cortex, and posterior parietal cortex of rats. *Neurobiology of Learning and Memory*. https://doi.org/10.1016/j.nlm.2004.03.002

Lyamzin, D., & Benucci, A. (2019). The mouse posterior parietal cortex: Anatomy and functions. In *Neuroscience Research*. https://doi.org/10.1016/j.neures.2018.10.008

McGaugh, J. L. (2000a). Memory - A century of consolidation. *Science*, *287*(5451), 248–251. https://doi.org/10.1126/science.287.5451.248

McGaugh, J. L. (2000b). Memory - A century of consolidation. In *Science*. https://doi.org/10.1126/science.287.5451.248

Milczarek, M. M., Vann, S. D., & Sengpiel, F. (2018). Spatial Memory Engram in the Mouse Retrosplenial Cortex. *Current Biology*. https://doi.org/10.1016/j.cub.2018.05.002

Milner, D. (1998). Cognitive Neuroscience: The Biology of the Mind and Findings and Current Opinion in Cognitive Neuroscience. *Trends in Cognitive Sciences*.

https://doi.org/10.1016/s1364-6613(98)01226-1

Mishra, N., Rohaninejad, M., Chen, X., & Abbeel, P. (2018). A simple neural attentive meta-learner. *6th International Conference on Learning Representations, ICLR 2018 - Conference Track Proceedings*.

Müllenbroich, M. C., Silvestri, L., Onofri, L., Costantini, I., Hoff, M. van't, Sacconi, L., Iannello, G., & Pavone, F. S. (2015). Comprehensive optical and data management infrastructure for high-throughput light-sheet microscopy of whole mouse brains. *Neurophotonics*. https://doi.org/10.1117/1.nph.2.4.041404

Myskiw, J. C., Fiorenza, N. G., Izquierdo, L. A., & Izquierdo, I. (2010). Molecular mechanisms in hippocampus and basolateral amygdala but not in parietal or cingulate cortex are involved in extinction of one-trial avoidance learning. *Neurobiology of Learning and Memory*. https://doi.org/10.1016/j.nlm.2010.06.007

Myskiw, J. C., & Izquierdo, I. (2012). Posterior parietal cortex and long-term memory: Some data from laboratory animals. *Frontiers in Integrative Neuroscience*. https://doi.org/10.3389/fnint.2012.00008

Neurological Disorders: Public Health Challenges. (2008). *Archives of Neurology*. https://doi.org/10.1001/archneurol.2007.19

Pan, S. J., & Yang, Q. (2010). A Survery on Transfer Learning. *IEEE Transactions on Knowledge and Data Engineering*.

Panksepp, J. (1989). The neurobiology of emotions: Of animal brains and human feelings. In *Handbook of social psychophysiology. Wiley handbooks of psychophysiology.*

Paradiso, S. (1998). The Emotional Brain: The Mysterious Underpinnings of Emotional Life. *American Journal of Psychiatry*. https://doi.org/10.1176/ajp.155.4.570

Parmentier, R., Ohtsu, H., Djebbara-Hannas, Z., Valatx, J. L., Watanabe, T., & Lin, J. S. (2002). Anatomical, physiological, and pharmacological characteristics of histidine decarboxylase knock-out mice: Evidence for the role of brain histamine in behavioral and sleep-wake control. *Journal of Neuroscience*. https://doi.org/10.1523/jneurosci.22-17-07695.2002

Parsons, M. E., & Ganellin, C. R. (2006). Histamine and its receptors. In *British Journal of Pharmacology*. https://doi.org/10.1038/sj.bjp.0706440

Paxinos, G., & Franklin, K. B. J. (2001). The Mouse Brain in Stereotaxic Coordinates, 2nd edition. In *Academic Press*.

Quartermain, D., & Judge, M. E. (1983). Recovery of memory following forgetting induced by depletion of biogenic amines. *Pharmacology, Biochemistry and Behavior*. https://doi.org/10.1016/0091-3057(83)90360-X

Raber, J., Arzy, S., Bertolus, J. B., Depue, B., Haas, H. E., Hofmann, S. G., Kangas, M., Kensinger, E., Lowry, C. A., Marusak, H. A., Minnier, J., Mouly, A. M., Mühlberger, A., Norrholm, S. D., Peltonen, K., Pinna, G., Rabinak, C., Shiban, Y., Soreq, H., … Boutros, S. W. (2019).

Current understanding of fear learning and memory in humans and animal models and the value of a linguistic approach for analyzing fear learning and memory in humans. In *Neuroscience and Biobehavioral Reviews*. https://doi.org/10.1016/j.neubiorev.2019.03.015

Ransom, R. C., Foster, D. S., Salhotra, A., Jones, R. E., Marshall, C. D., Leavitt, T., Murphy, M. P., Moore, A. L., Blackshear, C. P., Wan, D. C., & Longaker, M. T. (2018). Genetic dissection of clonal lineage relationships with hydroxytamoxifen liposomes. *Nature Communications*. https://doi.org/10.1038/s41467-018-05436-6

Renier, N., Adams, E. L., Kirst, C., Wu, Z., Azevedo, R., Kohl, J., Autry, A. E., Kadiri, L., Umadevi Venkataraju, K., Zhou, Y., Wang, V. X., Tang, C. Y., Olsen, O., Dulac, C., Osten, P., & Tessier-Lavigne, M. (2016a). Mapping of Brain Activity by Automated Volume Analysis of Immediate Early Genes. *Cell*. https://doi.org/10.1016/j.cell.2016.05.007

Renier, N., Adams, E. L., Kirst, C., Wu, Z., Azevedo, R., Kohl, J., Autry, A. E., Kadiri, L., Umadevi Venkataraju, K., Zhou, Y., Wang, V. X., Tang, C. Y., Olsen, O., Dulac, C., Osten, P., & Tessier-Lavigne, M. (2016b). Mapping of Brain Activity by Automated Volume Analysis of Immediate Early Genes. *Cell*, *165*(7), 1789–1802. https://doi.org/10.1016/j.cell.2016.05.007

RESCORLA, R. A. (1968). PROBABILITY OF SHOCK IN THE PRESENCE AND ABSENCE OF CS IN FEAR CONDITIONING. *Journal of Comparative and Physiological Psychology*. https://doi.org/10.1037/h0025984

Ronneberger, O., Fischer, P., & Brox, T. (2015). U-net: Convolutional networks for biomedical image segmentation. *Lecture Notes in Computer Science (Including Subseries Lecture Notes in Artificial Intelligence and Lecture Notes in Bioinformatics)*. https://doi.org/10.1007/978-3-319-24574-4_28

Roozendaal, B., & McGaugh, J. L. (2011). Memory Modulation. In *Behavioral Neuroscience*. https://doi.org/10.1037/a0026187

Sakurai, K., Zhao, S., Takatoh, J., Rodriguez, E., Lu, J., Leavitt, A. D., Fu, M., Han, B. X., & Wang, F. (2016). Capturing and Manipulating Activated Neuronal Ensembles with CANE Delineates a Hypothalamic Social-Fear Circuit. *Neuron*, *92*(4), 739–753. https://doi.org/10.1016/j.neuron.2016.10.015

Silva, B. A., Gross, C. T., & Gräff, J. (2016). The neural circuits of innate fear: Detection, integration, action, and memorization. In *Learning and Memory*. https://doi.org/10.1101/lm.042812.116

Singewald, N., Schmuckermair, C., Whittle, N., Holmes, A., & Ressler, K. J. (2015). Pharmacology of cognitive enhancers for exposure-based therapy of fear, anxiety and trauma-related disorders. In *Pharmacology and Therapeutics*. https://doi.org/10.1016/j.pharmthera.2014.12.004

Smith, I. M., Pang, K. C. H., Servatius, R. J., Jiao, X., & Beck, K. D. (2016). Paired-housing selectively facilitates within-session extinction of avoidance behavior, and increases c-

Fos expression in the medial prefrontal cortex, in anxiety vulnerable Wistar-Kyoto rats. *Physiology and Behavior*. https://doi.org/10.1016/j.physbeh.2016.05.044

Todd, T. P., & Bucci, D. J. (2015). Retrosplenial Cortex and Long-Term Memory: Molecules to Behavior. In *Neural Plasticity*. https://doi.org/10.1155/2015/414173

Venkatraman, A., Edlow, B. L., & Immordino-Yang, M. H. (2017). The brainstem in emotion: A review. In *Frontiers in Neuroanatomy*. https://doi.org/10.3389/fnana.2017.00015

Vetere, G., Kenney, J. W., Tran, L. M., Xia, F., Steadman, P. E., Parkinson, J., Josselyn, S. A., & Frankland, P. W. (2017). Chemogenetic Interrogation of a Brain-wide Fear Memory Network in Mice. *Neuron*. https://doi.org/10.1016/j.neuron.2017.03.037

Vousden, D. A., Epp, J., Okuno, H., Nieman, B. J., van Eede, M., Dazai, J., Ragan, T., Bito, H., Frankland, P. W., Lerch, J. P., & Henkelman, R. M. (2015). Whole-brain mapping of behaviourally induced neural activation in mice. *Brain Structure and Function*. https://doi.org/10.1007/s00429-014-0774-0

Watson, J. B., & Rayner, R. (1920). Conditioned emotional reactions. *Journal of Experimental Psychology*. https://doi.org/10.1037/h0069608

Weihe, E., & Eiden, L. E. (2000). Chemical neuroanatomy of the vesicular amine transporters. *The FASEB Journal*. https://doi.org/10.1096/fj.00-0202rev

Ye, L., Allen, W. E., Thompson, K. R., Tian, Q., Hsueh, B., Ramakrishnan, C., Wang, A. C., Jennings, J. H., Adhikari, A., Halpern, C. H., Witten, I. B., Barth, A. L., Luo, L., McNab, J. A., & Deisseroth, K. (2016). Wiring and Molecular Features of Prefrontal Ensembles Representing Distinct Experiences. *Cell*. https://doi.org/10.1016/j.cell.2016.05.010

Zanatta, M. S., Schaeffer, E., Schmitz, P. K., Medina, J. H., Quevedo, J., Quillfeldt, J. A., & Izquierdo, I. (1996). Sequential involvement of NMDA receptor-dependent processes in hippocampus, amygdala, entorhinal cortex and parietal cortex in memory processing. *Behavioural Pharmacology*. https://doi.org/10.1097/00008877-199608000-00005

Zhang, G., & Stackman, R. W. (2015). The role of serotonin 5-HT2A receptors in memory and cognition. In *Frontiers in Pharmacology*. https://doi.org/10.3389/fphar.2015.00225

Zimmermann, K. S., Li, C. C., Rainnie, D. G., Ressler, K. J., & Gourley, S. L. (2018). Memory retention involves the ventrolateral orbitofrontal cortex: Comparison with the basolateral amygdala. *Neuropsychopharmacology*. https://doi.org/10.1038/npp.2017.139

Tre anni di dottorato, quattro conferenze a giro per il mondo e una che mi ha permesso di sperimentare la nuova frontiera del virtuale. Un anno di pandemia difficile da scordare, che non solo ha rallentato il ritmo del mio lavoro ma ha fermato il mondo intero. Un progetto interminabile di cui, per molto tempo, non riuscivo a vedere la fine. Un numero indefinito di persone che sono entrate a far parte della mia vita e che mi hanno lasciato qualcosa. Per ogni istante che mi ha arricchito e reso meno sola durante questo dottorato devo ringraziare molte persone. La prima persona è Ludovico, supervisore e amico. Grazie per aver creduto in me prima ancora che io stessa ci credessi. Hai reso questo lavoro una passione, qualcosa che amo fare. Abbiamo iniziato a piccoli passi ma il finale è stato con il botto. Tra le mille cose per cui ti sono grata, ce ne sono due in particolare, il "teorema dello spritz" utile per festeggiare qualsiasi momento e la nostra *playlist* "grandi classici italiani", colonna sonora di tanti pomeriggi, poco sonori, alla SPIM. Ora che abbiamo tagliato questo traguardo, lo posso dire… *To Ludo*. Il secondo grazie è rivolto al Prof. Francesco Pavone, per avermi accolta nel suo gruppo e per aver permesso che tutto questo si realizzasse. Ringrazio di cuore (o come direbbe lei stessa "dolce cuore") anche Irene, forse conosciuta ai più come "Irene cara". Grazie per la fiducia, per il sostegno e per avermi accompagnata nei primi passi di un mondo che a me era sconosciuto.

Come in ogni grande opera che si rispetti, metà del lavoro è svolto dagli uomini dietro le quinte. A Curzio un enorme grazie per essere stato un pilastro portante di questo progetto. Grazie per aver trovato la soluzione a tanti problemi che non sarei mai stata in grado di risolvere da sola. Non preoccuparti, la tua pazienza sarà pagata a peso di birre. Un ringraziamento speciale va a Giacomo, per non confondere i lettori direi il "Mazza", per essere una garanzia e un aiuto costante, in qualsiasi momento.

Non per citare Christiane F. ma *Noi, i ragazzi del pollaio* è un libro di gran lunga superiore. Alla vecchia generazione devo l'iniziazione ad un ufficio che assomiglia più a uno stile di vita. Grazie per avermi fornito gli "strumenti" di cui avevo bisogno. Alla nuova, devo la creazione di un bellissimo gruppo, che tra sorrisi e spensieratezza ha alleggerito pomeriggi che avevano l'odore della pesantezza. A tutti voi grazie per avermi fatto capire che ridere è una parte fondamentale di ogni lavoro. Il lato leggero e sorridente di questo dottorato, siete voi.

Tanto devo anche a tutto il resto dei miei colleghi, che hanno condiviso con me pause pranzo, tavoli da pingpong e laboratori, diventando per me nuovi punti di riferimento e amici.

Alla mia caotica famiglia devo molto, senza il loro sostegno non avrei raggiunto anche questo traguardo. Tra le mille cose che mi hanno insegnato e per le quali ne sono

immensamente grata la più importante è che non è mai troppo tardi per essere ciò che vogliamo. Siete e sarete sempre il mio porto sicuro.

Alle mie migliori amiche va un grazie enorme. Non avrete contribuito direttamente alla stesura di questa tesi ma sicuramente avete contribuito nell'alleggerirla. Come già sapete, siete un pezzo di cuore. Siete entrate nella mia vita, lasciando un po' di voi e portando via un po' di me.

Una promessa è una promessa, e come ogni promessa va rispettata. A Filippo, la prima persona che mi ha sostenuto in tutto questo percorso. Grazie. Anzi, ancora meglio, *ad maiora*.

E infine concludo con Giacomo, il mio Giacomo. Quattro anni fa ti ho conosciuto che eri a pagina "0" della tesi e oggi siamo PhD. Non ci avrei mai creduto. Il primo di tanti traguardi insieme. Questi tre anni sono stato un preludio di ciò che ci aspetterà, ma ti prometto che ne varrà la pena. I grazie che ti devo sono superflui.